Scaling Effects on Damage Development, Strength, and Stress-Rupture Life of Laminated Composites in Tension

J. André Lavoie

Dissertation submitted to the Faculty of the Virginia Polytechnic Institute and State University
in partial fulfillment of the requirements for the degree of

Doctor of Philosophy
in
Engineering Mechanics

John Morton, Chair
William A. Curtin, Co-Chair
Kenneth L. Reifsnider
Karen E. Jackson
Don H. Morris
Mark S. Cramer

April 4th, 1997
Blacksburg, Virginia

Keywords: strength scaling, size effects, microcracking, first-ply failure, delamination, composite material, Weibull statistics, tension testing, flexural testing, carbon/epoxy, glass/epoxy, creep, stress-rupture, creep-rupture, stress relaxation, stress-corrosion cracking, durability, life.

Scaling Effects on Damage Development, Strength, and Stress-Rupture Life of Laminated Composites in Tension

J. André Lavoie

(ABSTRACT)

The damage development and strength of ply-level scaled carbon/epoxy composite laminates having stacking sequence of $[+\theta_n/-\theta_n/90_{2n}]_s$ where constraint ply angle, θ, was 0°, 15°, 30°, 45°, 60°, and 75°, and size was scaled as n=1,2,3, and 4, is reported in Part I. X-radiography was used to monitor damage developments. First-ply failure stress, and tensile strength were recorded. First-ply failure of the midplane 90° plies depended on the stiffness of constraint plies, and size. All 24 cases were predicted using Zhang's shear-lag model and data generated from $[0_2/90_2]_s$ cross-ply tests. Laminate strength was controlled by the initiation of a triangular-shaped local delamination of the surface angle plies. This delamination was predicted using O'Brien's strain energy release rate model for delamination of surface angle plies. For each ply angle, the smallest laminate was used to predict delamination (and strength) of the other sizes.

The in-situ tensile strength of the 0° plies within different cross-ply, and quasi-isotropic laminates of varying size and stacking sequence is reported in Part II. No size effect was observed in the strength of 0° plies for those lay-ups having failure confined to the gauge section. Laminates exhibiting a size-strength relationship, had grip region failures for the larger sizes. A statistically significant set of 3-point bend tests of unidirectional beams were used to provide parameters for a Weibull model, to re-examine relationship between ultimate strength of 0° plies and specimen volume. The maximum stress in the of 0° plies in bending, and the tensile strength of the of 0° plies (from valid tests only) was the same. Weibull theory predicted loss of strength which was not observed in the experiments.

An effort to model the durability and life of quasi-isotropic E-glass/913 epoxy composite laminates under steady load and in an acidic environment is reported in Part III. Stress-rupture tests of unidirectional coupons immersed in a weak hydrochloric acid solution was conducted to determine their stress-life response. Creep tests were conducted on unidirectional coupons parallel and transverse to the fibers, and on ±45° layups to characterize the lamina stress- and time-dependent compliances. These data were used in a composite stress-rupture life model, based on the critical element modeling philosophy of Reifsnider, to predict the life of two ply-level thickness-scaled quasi-isotropic laminates.

Keywords: strength scaling, size effects, microcracking, first-ply failure, delamination, composite material, Weibull statistics, tension testing, flexural testing, carbon/epoxy, glass/epoxy, creep, stress-rupture, creep-rupture, stress relaxation, stress-corrosion cracking, durability, life.

This work was supported by the US Army Research Laboratory under NASA grant NAS1-19610, No. 15, by the U.K. Ministry of Defence, and by the Virginia Institute for Material Systems.

ACKNOWLEDGMENTS

The author acknowledges the financial support of the US Army Research Laboratory for financial support under NASA grant NAS1-19610, No. 15, monitored by Dr. Karen Jackson. Additional financial support from the Virginia Institute for Material Systems, made possible by Prof. Ken Reifsnider, is gratefully acknowledged. Dr. Jackson's careful reading of drafts of my various papers was very helpful. A visit to the Royal Institute of Technology, Stockholm, was undertaken to collaborate with Professor Peter Gudmundson and his student, Erik Adolfsson, and would not have been possible without a tuition waiver. Erik was a pleasure to work with, and gave freely of his time. At the Structural Materials Centre (SMC), Defence Research Agency, in Farnborough, England, the author received support from many people in different groups while working on the stress-rupture project. Prof. Paul Curtis authorized composite plate fabrication, and Dr. Phil Powell arranged financing for Andrew Renshaw, a sandwich student, to help with creep and stress-rupture testing, and Mr. Bill Mitten allowed free access to the creep lab.

The author extends thanks to Dr. Costas Soutis at Imperial College for being a friend and taking special interest in the work. Dr. Paul Smith at the University of Surrey, Prof. Frank Jones at the University of Sheffield, Mr. Micheal G. Phillips at the University of Bath, and Dr. Paul Hogg at Queen Mary and Westfield College made time for helpful discussions. Prof. Kenneth L. Reifsnider provided helpful guidance during the literature review and proposal phase of the research, by steering me toward experimentation. The author is especially grateful to Dr. John Morton, committee chair and Director of the SMC, for providing me opportunities, especially the opportunity to spend one year pursuing my studies at the SMC. Prof. Bill Curtin, co-chair, provided further guidance, and help analyzing data.

The author wishes to thank his wife, Chiara, for her love and support during the long months of their separation while he pursued his research abroad. Her forgiveness is replied with a promise to avoid long separations again.

TABLE OF CONTENTS

Page

LIST OF TABLES

Part I

Part II

Part III

LIST OF FIGURES

Part I.

Part II.

Part III.

Part I

Effects of Size, Constraint and Thickness, on Damage Initiation, Growth, and Strength of $[+\theta_n/-\theta_n/90_{2n}]_s$ Composite Laminates

Abstract

An experimental investigation of damage development and strength was conducted on ply-level scaled carbon/epoxy composite laminates having stacking sequence of $[+\theta_n/-\theta_n/90_{2n}]_s$ where the constraint ply angle, θ, was 0°, 15°, 30°, 45°, 60°, and 75°, and size was scaled as n=1,2,3, and 4. Photomicrography and x-radiography were used to monitor damage development with tensile load. Subcritical damage development before complete failure was dependent upon the constraint ply angle, θ, for their mode, but the size affected the initiation stress, and rate of development. Damage in the form of high density matrix cracking in plies adjacent to plies with a major matrix crack appeared due to thermal residual stress, and after monotonic loading. To highlight the significance of the failure mode on elastic properties of particular damaged lay-ups, the $[(+60/-60/90_2)_2]_s$ lay-up was tested, and its stress-strain response compared to that predicted from Gudmundson's model (Gudmundson, Östlund, and Zang, 1993).

Measurements of first-ply failure stress, and tensile strength were made. First-ply failure of the midplane 90° plies was shown to depend on the level of constraint, and the scale factor, n. The strain energy release rate for matrix microcracking was computed from first-ply failure data of the $[0_2/90_2]_s$ laminate. Then, first-ply failure was predicted from Zhang's model (Zhang, Fan, and Soutis, 1993) for all other lay-ups and sizes, accounting for both constraint and size. Tensile strength was predicted using O'Brien's strain energy release rate model for delamination of surface angle plies. A delamination energy value for each ply angle was calculated from the smallest (n=1) laminates to predict delamination (and strength) of the n=2, 3, and 4 sizes. The predictions were successful because strength was controlled by the initiation of a triangular-shaped local delamination of the surface angle plies.

Keywords: strength scaling, size effect, matrix microcracking, first-ply failure, delamination, carbon/epoxy composite material, laminated composite material.

1. Introduction

The problem of matrix cracking in composite materials is usually not that it is a cause for some impending structural failure, but that these cracks can act as stress raisers, and are initiation sites for more critical damage such as delamination. Cracks can allow ingress of the environment, which is often deleterious. The motivations for the work contained in this report originates with observations that matrix microcracking in the transverse, or 90°, plies of cross-ply composite laminates in tension did not initiate at the same stress as that measured in a transverse tension test. Instead, the stress to crack the 90° plies varies as a function of the constraint imposed by the sandwiching plies, and the thickness of both constraint and constrained plies.

A 2-D elasticity analysis of a three ply laminate for the case of a single crack in the middle ply was given by Vasil'ev (1970). Each ply could be orthotropic, and a saturation crack spacing could be predicted. An equilibrium element approach (1-D shear-lag model) was used by Reifsnider (1977) and Highsmith and Reifsnider (1982), to analyze the role of the constraining plies on the development of cracks in the interior constrained plies, to predict the saturation crack spacing, and to give information on stress concentration in the constraint plies. Parvizi, Garrett, and Bailey (1978) tested cross-ply laminates of the form $[0/90_n]_s$ where n=1,2,3,... They modeled the crack initiation using a 1-D shear lag model and a Griffith energy balance concept extended from the theory of Aveston and Kelly. Flaggs and Kural (1982) tested $[0_2/90_n]_s$, $[\pm 30/90_n]_s$, and $[\pm 60/90_n]_s$, where n=1,2,4, and 8, to investigate the effect of constraint on cracking. They showed that the models of the time had difficulty predicting the onset of cracking except in the most constrained cases. They also showed that the material system could not be characterized as a simple Weibull material. Fukunaga *et al.* (1984) used a statistical strength analysis together with a shear-lag analysis to predict first ply failure of the $[\pm\theta/90_n]_s$ laminates described by Flaggs and Kural. Kistner, Whitney, and Browning (1985) confirmed that the "in situ" strength variation of the transverse plies was real in the sense that the orientation of the constraining plies affected the strain at which cracking initiates. They tested unidirectional laminates ranging in thickness from four to sixteen plies in transverse tension, and showed that the thickness, in and of itself, had no effect on transverse strength. However, O'Brien and Salpekar (1993) found that the transverse tensile strength did obey a Weibull volumetric scaling law. Crossman and Wang (1982) studied damage initiation and growth in $[\pm 25/90_n]_s$ laminates where n=1,...,8. The first damage to initiate depended upon n. A finite element energy analysis could predict onset of transverse cracking. Dvorak and Laws (1987) attempted to predict the growth of a transverse crack within the ply, parallel to the fibers, and toward the ply interfaces. Zhang, Fan, and Soutis (1992) presented a model based on classical fracture mechanics and assuming a through-thickness flaw. The model used a modified 2-D shear-lag analysis wherein shear stresses were allowed to vary linearly within the constraining plies and cracked 90° plies. Hashin (1985) used variational methods to account for crack interaction and predicted changes in axial Young's modulus, and Poisson's ratio. Varna and Berglund (1991, 1993) found unacceptably large errors in Hashin's analysis for Poisson's

ratio prediction, due to the approximate stress field chosen, improved upon his work, and resolved the problem of accurate stress field determination. Gudmundson and coworkers (1992, 1993) have developed a general model for estimating the thermoelastic properties of arbitrary composite laminates having cracks in any ply, and any crack density. The model depends upon a closed form solution for the crack opening displacements in an infinite isotropic medium. Most elastic properties, thermal expansion coefficients, and elastic coupling coefficients are computed. The model does not predict crack initiation, but must be given the strain energy release rate for cracking and resistance curve for progressive cracking. Talreja (1985a,b) developed a continuum damage mechanics modeling approach, where the mechanical response of a damaged composite material is characterized by a set of vector fields each representing a damage mode. Recently, Talreja (1996) proposed a combined approach to structural analysis in which the strengths of micromechanics to compute accurate local displacements in damaged materials is combined with continuum damage mechanics useful to compute laminate level thermoelastic property changes.

Several types of delamination were encountered during the course of this work, and have all been studied previously. These are gross edge delamination, crack-tip induced interply delamination, and triangular-shaped local delaminations in off-axis plies. The large edge delamination characterized by interply separation along the length of the gauge section of a composite coupon specimen, for example, often involves a substantial portion of the width. This kind of delamination has received much attention, and some works are by O'Brien (1982a,b), Kim and Soni (1984), and Lagace (1987). Not to be neglected are works which look at the conditions which favor the development of edge delamination. Edge stresses and edge effects were studied by Pipes and Pagano (1970, 1973), Pipes and Daniel (1971), Pagano and Pipes (1973), Oplinger, Parker, and Chiang (1974), Hsu and Herakovich (1977), Rodini and Eisenmann (1978), Curtis (1980), Herakovich, Post, Buczek, and Czarnek, (1985), and Herakovich (1981,1982).

The development of delamination at the interface of the cracked and the constraining plies is described by Reifsnider, Henneke, Stinchcomb, and Duke (1983), Jamison, Schulte, Reifsnider, and Stinchcomb (1984), and Crossman and Wang (1982), among others. Talreja (1986) employed continuum damage mechanics to model the property changes that result. Zhang, Soutis, and Fan (1994a,b) use a combined fracture mechanics and finite element model to compute the total strain energy associated with this form of delamination at the edge. Wang and Karihaloo (1994) solved for the stress intensity factor to cause delamination due to a matrix crack. The triangular delamination was observed by Herakovich (1982), and O'Brien and Hooper (1993). A model to predict the onset of the triangular delamination was developed by O'Brien (1993).

In the current work, damage development, and ultimate strength of composite laminates was studied from the scaling viewpoint. Specifically, the dimensions were varied in length, width, and most importantly, thickness. Thickness was usually scaled in two ways: ply-level scaling in

which plies of the same orientation are clustered together, and sublaminate-level scaling in which a stacking sequence is repeated any number of times to build up the laminate thickness. Some works which consider thickness scaling are by Rodini and Eisenmann (1978), Crossman and Wang (1982), Herakovich (1982), Kellas and Morton (1990,1992), Kellas, Johnson, Morton, and Jackson (1993), and Jackson and Kellas (1993).

The work of Jackson and Kellas (1993) was an experimental investigation of damage development and strength of ply-level scaled carbon/epoxy composite laminates having stacking sequence of $[+\theta_n/-\theta_n/90_{2n}]_s$ where constraint ply angle, θ, was 0°, 15°, 30°, 45°, 60°, and 75°, and size was scaled as n=1,2,3, and 4. In addition, they tested the sublaminated-level scaled $[(+\theta/-\theta/90_2)_2]_s$ layup, where θ varied as before. The results reported were on initial modulus and ultimate strength. The purpose of their work was to investigate the effect of outer ply constraint (the $[+\theta_n/-\theta_n$ ply group) on the initial modulus and tensile strength of the coupons. Strength was shown to vary markedly as a function of thickness, n. The current paper is a continuation of the work begun by Jackson and Kellas (1993). The focus here, was to characterize the nature and sequence of the damages developed, such as those described previously, to isolate the mechanism(s) governing strength and to attempt to model the onset of various damage modes and strength, especially accounting for the effect of size. Furthermore, the $[(+60/-60/90_2)_2]_s$ layup was singled out for added attention because of its remarkable plastic-like stress-strain response.

2. Materials and Specimens

2.1. MATERIALS AND LAMINATES

The material used for this study was a commonly available 0.125 mm thick unidirectional graphite/epoxy prepreg: Hercules Magnamite AS-4/3502. Laminates were cured at 177°C. A range of laminates were fabricated. They were ply-level scaled laminates having the stacking sequence $[+\theta_n/-\theta_n/90_{2n}]_s$, where θ varied from 0° to 75° in 15° steps. Laminate thickness, width, and length was changed by varying "n" from 1 to 4. There was also a 16-ply laminate having stacking sequence of $[(+60/-60/90_2)_2]_s$. Specimen dimensions appear in Table 1.

2.2. SPECIMEN PREPARATION

Specimens were machined from flat panels using a high speed diamond saw with liquid cooling. This machining operation resulted in very smooth, square cuts. One edge of each specimen was polished so that cracks and delaminations could be readily discerned. A special polishing procedure was needed to polish the entire specimen's edge. First, to help keep the specimen edge flat against the grinding surface, three to five specimens were clamped together. It was possible to begin the wet grinding with #400 grit silicon carbide paper because the edges were

cut very square and flat during the machining operation. Flatness had to be maintained at each step in the grinding process for the final polish to result in a high quality finish. To ensure flatness, the block of specimens was ground by hand against a large flat surface using a fore and aft motion with the specimens aligned to the grinding direction. Grit and debris were flushed out with running water, followed by immersion in an ultrasonic bath. The second step was carried out using an Engis Corporation Hyprez lapping system. A copper lapping platen, 38 centimeters in diameter, and turning at 50 revolutions per minute (rpm), was sprayed with a 3 μm diamond slurry (formula 3(S4305-6) STD-MA). The diamond was carried in a low viscosity petroleum distillate, having a texture of light oil, but with the property of evaporating away within minutes. Polishing took about 3 minutes when the platen's surface was freshly prepared. Final polish was on a polishing wheel covered with a hard and flat cloth, such as Kempad "Pan-W" PSA. The polishing compound was a 0.3 μm alumina suspension, such as Struers code SDALOC-.3. Polishing took about a minute, when a wheel speed of about 150 rpm was used.

Mechanical Testing These laminates did not suffer from grip region stress concentration which might adversely affect strength, and so end tabs were not needed. Specimen ends were covered with a #100 grit cloth, which was sufficient to protect the fibers from damage by the grip face, yet still provide the needed traction. All data reported are for specimens from the same batch of material. Each panel yielded twelve specimens. Six specimens per panel were used to determine strength and initial elastic modulus, by Jackson and Kellas (1993). Their data was used here, and appears in Table 2. The remaining specimens were used to study damage development. To verify that there was not a significant difference in the test methods used, one specimen each from the remaining six specimens, was tested to failure. For those tests the test conditions were as follows. The test machine was a screw driven Instron. Specimens were gripped in Instron hand-tightened wedge-action grips. The crosshead speeds were chosen according to the specimen size to give a constant strain rate of 0.5% strain per minute, which translated to 2.54 x n mm/minute (where n = 1, 2, 3, or 4). The elastic modulus data presented was determined by Jackson and Kellas (1993) using back-to-back strain gages located at the geometric center of the specimen.

First-ply failure was determined by listening for the onset of matrix microcracking in the 90° plies, striking the "unload" button on the test machine, and recording the peak load from the test machine's memory. For this study, first-ply failure was the stress to initiate a 90° matrix crack, regardless of whether there were pre-existing cracks. To characterize damage developments beyond first ply failure, specimens were loaded to intermediate stress levels below failure, and x-rays were taken to observe the damage developed. Damage was monitored by occasionally removing the specimen and inspecting the polished edge for cracks and delamination. Dye penetrant enhanced x-radiography was used to peer inside the laminate to determine the extent of delamination and the nature of the matrix cracking. The recipe for the x-ray dye penetrant was to dissolve 60 grams of zinc iodide in 10 ml each of water, ethanol, and Kodak Photo-Flo 200.

Two methods were used for taking x-rays after loading specimens to the desired stress level. The first method involved removing the specimen from the tensile test machine, submerging it in the dye penetrant for at least 1/2 hour, then carefully cleaning the entire specimen. Failure to completely clean the specimen resulted in clouded or foggy x-rays. Specimens were then arranged on a sheet of Kodak Industrex SR5, or Industrex M5 x-ray film inside an Hewlett Packard Faxitron series 43805N x-ray cabinet. The film was processed using Kodak GBX developer and fixer. Besides being time consuming and messy, this method had the drawback that when the specimen was unloaded the cracks would close. Even with a long soak time, dye penetration may have been incomplete. The second method of obtaining x-radiographs had the advantage of speed, cleanliness, and assured penetration of the dye. The specimen was loaded to the desired stress level, then unloaded slightly (about 20%) to ensure that failure would not occur while preparing the specimen for x-ray, or during the x-ray exposure. Dye penetrant was introduced to both edges of the specimen using a syringe and a bead of penetrant was allowed to drip along the specimen length. Immediately after, a sheet of Polaroid Type 52 (ISO 400), or Type 55 (ISO 50), black and white film was taped to the specimen and exposed using a portable x-ray system. The convenience of the Polaroid film was undermined by its low resolution for this task. Resolution was adequate to reveal all damage except for very fine cracks having the appearance of stitches. X-rays were repeated, as needed, using the Kodak Industrex film described earlier, to highlight the missing details.

3. Analysis

The topics of matrix cracking and delamination, both investigated in this study, were two areas that have had a great deal of attention from the modeling community, therefore it would have been unwise to spend additional time on model development. Even reproducing the models from the literature, in order to test them against the experimental results, was highly time consuming. Of the three models eventually used, only O'Brien's (1993) had a simple closed-form solution that was easily implemented. The other two models were complex computer models that would have been prohibitively time consuming to reconstruct. Therefore, gaining direct access to the models was well worth the effort involved. The author was fortunate to have been given the computer code for the model of Zhang, Fan and Soutis (1992) and was provided with the resources for an on-site visit to use the model of Gudmundson, Östlund, and Zang (1992).

3.1. MODEL FOR FIRST-PLY FAILURE

The equivalent constraint model (ECM) is a 2-D shear-lag model used to predict in-plane stiffness properties for laminates of the general type $[\pm\theta_m/90_n]_s$ which contain 90° matrix cracks, Zhang, Fan and Soutis (1992). In the current study, the ECM was used to predict first-ply failure as a function of constraint ply angle and laminate size. The ECM allowed for out-of-plane shear

deformation in the constraining plies. In contrast, the 1-D shear-lag models assumed constant in-plane displacements across the thickness of the constraint plies, and confined shear stress transfer to a resin-rich interply layer. This distinction between the 1-D and 2-D models becomes increasingly significant when the constraint plies are oriented off-axis. As the constraint ply angle, θ, increases, the out-of-plane shear modulus, G_{23} (on the order of 50 to 60% that of G_{12}) becomes the dominant shear modulus, in preference to G_{12}. Hence, as the shear moduli of constraint layers and constrained layers converges, the assumption of constant in-plane displacements becomes increasingly inaccurate. Another refinement to the model was to allow partial linear variation of the shear stresses across the constraining plies. This approach was more realistic than using the entire constraint ply group thickness because stress perturbations are generally thought to dissipate within a typical ply thickness. Here, the model was set to confine the shear stress in the constraining plies to vary linearly over a single ply thickness for all sizes of laminates.

In order to predict the initiation of first-ply failure, the model needed the material elastic properties, residual thermal stresses, and the strain energy release rate, G, for transverse matrix cracking. Obtaining elastic properties was not difficult. However, the residual stress state was unknown because there was substantial stress relaxation, especially immediately after fabrication. Use of the difference between the cure and room temperature would give an overly high estimate of residual stress. For that reason, model predictions assuming no stress relaxation, and complete stress relaxation, were included.

The $[0_2/90_2]_s$ cross-ply lay-up (n=1) was chosen to determine the strain energy release rate, G. Then, the model was used to predict first-ply failure stress as a function of constraint ply angle, θ, and laminate size, n.

3.2. MODEL FOR STRESS-STRAIN RESPONSE WHILE LAMINATE IS CRACKING

Gudmundson and coworkers have produced a model capable of predicting the onset and growth of matrix cracking in each and every ply of an arbitrary composite laminate, and the thermoelastic property changes as a consequence. The general nature of the model made it the best available choice for the task of modeling the stress-strain response of laminates which exhibit matrix cracking in arbitrary layers. The response of the $[(+60/-60/90_2)_2]_s$ lay-up was highly nonlinear due to the development of dense matrix cracking. The purpose of modeling the stress-strain response of this laminate was twofold. First, this lay-up would provide a harsh test of the model, and second, to highlight the effect of a particularly dense form of microcracking on laminate stiffness.

The model was given an initial strain energy release rate for matrix microcracking, G, of 100 J/m^2. Past research which investigates crack multiplication, has shown that there is an

increasing resistance to continued cracking as the matrix crack density increases. A resistance curve was used for G(r) and was assumed to be:

$$G(r) = 100\left(1 + \sqrt{r}\right). \tag{1}$$

The variable, r, is crack density normalized by the thickness of the cracked layer. The form chosen for G(r) was based upon that of similar carbon/epoxy materials. Attention was given to forcing the onset of matrix cracking in the midplane 90° plies of the model to coincide with that of the experimental data. The value for G was assumed to be the same for all plies in the laminate, regardless of their orientation or thickness.

3.3. MODEL FOR STRENGTH OF ANGLE-PLY LAMINATES

Catastrophic failure of $[+\theta_n/-\theta_n/90_{2n}]_s$ laminates was identified to occur upon initiation of a triangular-shaped delamination of the surface +θ° angle plies from a +θ° matrix crack at the free edge. The analysis of O'Brien (1993) gives an expression for the strain energy release rate, G, for such local delaminations growing from an arbitrary angle ply matrix crack as:

$$G = \frac{P^2}{2mw^2}\left(\frac{1}{t_{LD}E_{LD}} - \frac{1}{tE_{LAM}}\right) \tag{2}$$

Here, m=1 because delamination initiates from one +θ° crack on one side of the laminate, not on both sides simultaneously. The expression in Equation 2 can be rewritten as:

$$G = \frac{N_x^2}{2h}\left(\frac{1}{(N-n)E_{LD}} - \frac{1}{NE_{LAM}}\right) \tag{3}$$

symbols, definitions, and units:
G = strain energy release rate for local delamination, J/m^2
N_x = tensile force resultant on the laminate, N/m
h = ply thickness, m
N = number of plies in the laminate
n = number of plies in the locally delaminated region
E_{LAM} = modulus of the laminate, Pa
E_{LD} = modulus of the locally delaminated region, Pa

The general expression for E_{LD} given by O'Brien handles unsymmetric delaminated sublaminates and is:

$$E_{LD} = \frac{2}{(N-n)h}\left[A_{11} - \left(\frac{A_{12}D_{22} - B_{12}B_{22}}{A_{22}D_{22} - B_{22}^2}\right)A_{12} + \left(\frac{A_{12}B_{22} - A_{22}B_{12}}{A_{22}D_{22} - B_{22}^2}\right)B_{12}\right] \quad (4)$$

The laminates in this study all had symmetric delaminated sublaminates, and as a consequence there is no bend extension coupling, therefore the B_{ij} terms are all zero and the expression for E_{LD} in Equation 4 simplifies to:

$$E_{LD} = \frac{2}{(N-n)h}\left(A_{11} - \frac{A_{12}^2}{A_{22}}\right) \quad (5)$$

The strain energy release rate, G, is computed using the average tensile force resultant, N_x, at failure of the 8-ply (n=1) laminate for each value of θ. The force resultant to cause failure of the thicker laminates (n increasing) is predicted by rearranging Equation 3 as:

$$N_x(n) = \sqrt{2hG\left(\frac{1}{(N-n)E_{LD}} - \frac{1}{NE_{LAM}}\right)^{-1}} \quad (6)$$

4. Results

In the following subsections the various forms of damage development are described, and related to the constraint ply angle and laminate size (scale factor, n). Damage due to residual thermal stress is the topic of Section 4.1. The obvious differences in the stress-strain response as a function of laminate size and constraint ply angle are presented in Section 4.2. In Section 4.3, transverse matrix cracking and first-ply failure data, as a function of constraint and size, was modeled. In Section 4.4, the development of damage after first-ply failure, as affected by the constraint ply angle and laminate size was examined with the aid of detailed x-ray and edge photomicrographs. In Section 4.5, the elastic/plastic-like stress-strain response of the $[(+60/-60/90_2)_2]_S$ lay-up was examined specifically because its response was highly sensitive to the effect of dense localized cracking not accounted for in most models available. In Section 4.6, the strength-controlling delamination of +θ° plies was predicted. The delamination of the midplane, along the -θ/90 interface, which had a strong effect on stiffness, was not examined. This decision was made because the relationship between delamination initiation and growth, for ply-level scaling of a quasi-isotropic lay-up, was successfully modeled by O'Brien (1993).

4.1. THERMAL STRESS-INDUCED MATRIX CRACKING

Thermal stress-induced cracking appeared spontaneously in the $[+\theta_n/-\theta_n/90_{2n}]_s$ laminates having high constraint (low θ angle), and thick blocks of plies (n increasing). The cracks in the

90° and +θ° or -θ° plies existed throughout the panel. It was likely that these cracks formed during cooling of the laminate from cure, though they may have formed when the first edge of the panel was trimmed. It was certain that they were not a result of cutting individual specimens, as was verified by marking the location of each crack on each specimen and piecing the panels together again to see that cracks were continuous from one specimen to the next. A summary of the thermal stress-induced crack density in the 90° plies of each $[+\theta_n/-\theta_n/90_{2n}]_s$ laminate is given in Table 3. In the columns labeled "r" the crack spacing *a* is divided by the thickness, *d*, of the 90° ply block. For +θ° ply cracking, the crack count along the length of the specimen at the top and bottom surface plies is given in Table 4.

The n=1 size laminates had no thermal stress-induced matrix cracks, nor were there cracks in any lay-up having +60° or +75° constraint plies. The n=2, 3, and 4 size lay-ups had 90° cracks, for constraint ply angles of θ = 0°, +15°, +30°, or +45°. For the n=3 size lay-up, additional cracking appeared in the top surface plies for θ = +15° and +30°. The n=4 size lay-up also had cracks in the top surface plies for θ = +45°. There was a tendency toward large numbers of cracks in the top surface plies, but few in the bottom surface plies. Finally, all of the coupon specimens had a small concave down curvature, as measured between the middle of the coupon and a flat surface. The consistent appearance, in all 24 composite panels, of convex curvature toward the underside of each coupon, indicated unbalanced resin content of the upper and lower surfaces, rather than error in orienting the plies during the hand lay-up. This phenomenon was expected from the fabrication process, because the laminate was cured against a caul plate, which is impenetrable to fluids, while excess resin was bled through the bleeder ply at the top. The warpage due to the fabrication process was studied by Radford (1993). He measured the fiber volume fraction across the thickness, and found that resin content was fairly uniform throughout the laminate thickness, but rose sharply in the ply against the caul plate, and dropped sharply in the ply against the bleeder cloth. The resin content gradient was likely responsible for the different crack counts of the +θ° ply groupings at the top and bottom surfaces.

The angle, θ, of the constraint plies relative to the 90° plies, and also the angle of the constraint plies to each other, affected whether or not stitch-like cracks formed in the -θ° plies. An x-ray of a $[+15_4/-15_4/90_8]_s$ laminate appears in Figure 1, and shows the presence of -15° stitch cracks due to a neighboring +15° crack. Constraint ply angles of 30° resulted in very few stitch cracks, but -30° cracks were much longer, see Figure 2. In Figure 3, there is a return of stitch crack formation, but now in the -45° plies due to a 90° matrix crack.

4.2. MECHANICAL TESTING: STRESS-STRAIN RESPONSE

Six representative plots of the stress-strain response of $[+\theta_n/-\theta_n/90_{2n}]_s$ laminates, for θ=0°, 15°, 30°, 45°, 60°, and 75°, appears in Figure 4. Each plot contains four curves, one for each size tested, n=1,2,3, and 4. The initial elastic modulus, strength, and strain to failure was given in Table 2. There was no size effect on the initial elastic modulus. However, it was clear that upon tensile loading, differences in damage onset stress, and development rate, resulted in early loss of stiffness, and strength, as size, n, was increased. For θ=0°, 15°, 60°, and 75°, the most obvious effect was a reduction in strength. The lay-ups having constraint plies at 30° and 45° had substantial change in the stiffness, due to midplane delamination.

4.3. FIRST-PLY FAILURE: EFFECTS OF CONSTRAINT AND THICKNESS

First-ply failure (fpf) was recorded for each $[+\theta_n/-\theta_n/90_{2n}]_s$ laminate for n=1 to 4, and for θ=0°, 15°, 30°, 45°, 60°, and 75°. The experimental data, along with predictions of the ECM, appear in Figure 5. The model was used to predict fpf for various levels of constraint, as indicated by the constraint ply angle, θ, and for the four different scales, as indicated by n. All predictions were based upon experimental data from the $[0_2/90_2]_s$ cross-ply lay-up. To maintain clarity, each plot contains the data and predictions for one size of laminate (marked on the plot as n=1, n=2, n=3, and n=4).

The residual stress state was unknown, because the lamina stress-relaxation response was not characterized. Therefore, an attempt was made to bound the possible predictions. The two extremes are full residual stress (no stress relaxation), represented as a solid curve; and no residual stress (full stress relaxation) represented as the dashed curve. Note that the value for strain energy release rate, G, computed by the model from the $[0_2/90_2]_s$ cross-ply data, was very different depending upon the residual stress that was input to it.

Examine first the plot labeled “n=1” in Figure 5. The experimental data suggested an immediate drop in the fpf stress as the constraint ply angle, θ, was increased, while the model predicted a gradual drop initially. The level of residual stress had little effect on the predictions. The plot “n=2”, corresponds to 16-ply laminates. The solid curve follows the data best, but underpredicts fpf of the cross-ply (which has a 0° constraint angle) more than the dashed curve. For both the “n=3” and “n=4” plots, corresponding to 24-ply and 32-ply laminates, respectively, there are similar trends: the solid curve follows the data best, but consistently underpredicts fpf stress of the cross-plies. On the other extreme, the dashed curve predicts the cross-ply’s dependence of fpf on n well, or is slightly nonconservative. For constraint angles up to 35 or 40° the prediction was highly nonconservative.

4.4. EFFECTS OF CONSTRAINT PLY ORIENTATION ON INTERLAMINAR AND INTRALAMINAR MATRIX CRACKING DUE TO TENSILE LOADING

In this section, damage development in the constrained 90° plies, the constraining -θ° plies, and the -θ/90 interface of $[+\theta_n/-\theta_n/90_{2n}]_s$ laminates is covered. It was found that the type of damage sustained by the respective plies depended on the angle, θ, of the constraint plies. The thickness of the ply groupings, controlled by n, affected the stress for onset of damage, and rate of damage growth.

4.4.1. Damage Progression for Constraint Plies at ±15°

The -15° plies were not damaged due to stress redistribution around the 90° cracks. Instead, the -15/90 interface delaminated from the tips of the 90° cracks, see Figure 6. Subsequent damage to the 90° plies was in the form of inclined secondary cracks near the 90° crack, see right side of Figure 7. The inclined cracks coalesce with the 90° crack-tip delaminations to form a continuous -15/90 delamination at the edge, see left side of Figure 7. The -15/90 delamination progressed deeply into the laminate, running preferentially along the 90° crack, see the magnified portion of the x-ray in Figure 8. Edge delamination was also evident, but did not penetrate with the same readiness as for constraint plies at ±30°.

4.4.2. Damage Progression for Constraint Plies at ±30°

The progression of damage was similar to that of the laminates having ±15° plies just described. After formation of 90° cracks, there was delamination of the -30/90 interface, starting from the tips of the 90° cracks, see Figure 9. Additional damage to the 90° plies appeared as inclined secondary cracks near the 90° crack, also Figure 9. The 90° crack-tip delamination penetrated deeply into the laminate interior, though 90° matrix cracks were still sparse, see Figure 10.

Only one edge of each specimen had been polished, and in this lay-up the effect was marked. The unpolished edge (right edge in Figure 11) exhibits rapid coalescence of the localized delaminations to form a continuous -30/90 delamination that penetrated from the edge toward the interior. Though polishing suppressed delamination along the left edge, it did not forestall cracking in the -30° plies, and may have encouraged it. The -30° ply cracks initiated from the tips of the 90° cracks, see magnified area of Figure 11. The -30° cracks appear fuzzy because they were inclined, as shown in Figure 12.

4.4.3. Damage Progression for Constraint Plies at ±45°

As discussed previously in Section 4.1, the appearance of 90° cracks caused stitch cracks in -45° constraint plies. When stitch cracks formed due to thermal stresses alone, little interfacial damage was found. The exception was the thickest, n=4 size, $[+45_4/-45_4/90_8]_s$ laminate. In a few instances, barely discernible -45/90 delamination along the 90° crack could be found, as shown in

the magnified portion of Figure 3. A cut was made perpendicular to the 90° crack, and the plane of the laminate, at the interior of the specimen, see Figure 13. In this highly magnified view, the -45° and 90° cracks are in close proximity, but the interface is intact.

After tensile loading, both the n=3 and n=4 sizes of laminates had clearly developed the -45/90 interfacial delamination, look ahead to Figure 22. For the n=1 and n=2 sizes, no delaminations had formed at the tips of the 90° cracks either from thermal residual stresses or after loading to failure. To be more certain, sections were taken from a failed n=1 size coupon perpendicular to the 90° crack, as shown in Figure 14. The -45° and 90° cracks were in close proximity, but no delamination was visible. From an n=2 size coupon loaded to failure, a section was taken parallel to the 90° crack, with the crack just under the polished surface, see Figure 15. An inclined -45° crack was visible, which ran across the two ply thickness up to the +45/-45 interface and the -45/90 interface. There was no sign of delamination at either interface.

4.4.4. Damage Progression for Constraint Plies at ±60°

For the n=1 size laminate loaded to 66 MPa, formation of 90° cracks was accompanied by stitch cracks in the -60° plies, see Figure 16. There existed -60/90 delaminations along the 90° crack. Immediately, a +60° crack formed at the intersection of the 90° crack with the edge. From Figure 17, observe that with little additional loading (68 MPa), more 90° cracks formed, which were confined to within a length of about 11 mm, or that defined by the coupon's width x Cos60°. The +60° cracks induced -60° stitch cracks. For the larger sizes, n=2, 3, and 4, the initiation of the first 90° crack triggered complete laminate failure.

4.5. DAMAGE AND THE RESPONSE OF $[(+60/-60/90_2)_2]_S$ LAY-UP

Earlier, it was shown that dense cracking occurs in the $-\theta°$ plies, due to a neighboring 90° crack, for θ values of 45° and 60°. The length and density of the cracks in the $-\theta°$ plies of several laminates is given in Table 5. Damage in the $[(+60/-60/90_2)_2]_s$ lay-up proceeded as follows. First, midplane 90° plies developed matrix cracks. These cracks induced short, densely spaced, cracks in the adjacent -60° plies. Delamination at the -60/90 interface was absent, in preference to forming the -60° cracks. A photomicrograph of the polished edge showing a 90° crack and the cracks induced in the -60° plies, appears in Figure 18(a). Second, matrix cracks form in the off-center 90° plies, accompanied by the same short, densely spaced, cracks in adjacent +60° and -60° plies, see Figure 18(b). As the laminate strain was increased, +60° cracks appear in the surface plies. The profusion of cracks can be seen in the x-ray of Figure 19.

Actual and modeled stress-strain responses are shown in Figure 20. The stages at which damage initiates in the various plies are indicated. The model predicts a four stage stress-strain response, as indicated by the solid line. There was the crack-free linear-elastic stage, then cracking

began first in the midplane 90° plies, next in off-center 90° plies, and lastly in all 60° plies. The actual response was similar to a linear-elastic/ perfectly plastic response.

There were three stages to the experimental stress-strain response, shown as the dashed curve in Figure 20. After the initial linear-elastic stage, the onset of cracking in the midplane 90° plies was accompanied by cracking in neighboring -60° plies. Next, cracking in the off-center 90° plies was accompanied by cracking in neighboring +60° and -60° plies. Lastly, ply scissoring at nearly 1.5% strain causes stiffening of the laminate.

4.6. DELAMINATION OF SURFACE +θ° PLIES AND PREDICTION OF STRENGTH

Ultimate strength of the $[+\theta_n/-\theta_n/90_{2n}]_s$ laminate class was controlled by the initiation of a local delamination of the surface $+\theta_n$ block of plies at the free edge, from a +θ° matrix crack. Typically, the +θ° delamination grew catastrophically when θ=15°, 30°, 60°, and 75°. For θ=45°, growth of the delamination often arrested. If delamination growth was not catastrophic, it was certainly very close to the ultimate strength. The +15° local delamination, for a $[+15/-15/90_2]_s$ laminate, was captured because of its proximity to the grip, and is shown in the x-ray of Figure 21(a). The damage sequence was 90° matrix cracking first, then a +15° matrix crack, immediately followed by -15° stitch cracking, and the initiation of the local delamination. In Figure 21(b) the n=3 size $[+15_3/-15_3/90_6]_s$ lay-up has two sites of +15° ply delamination from the +15° matrix crack. The $[+45_n/-45_n/90_{2n}]_s$ laminate class could develop several +45° surface delaminations before complete laminate failure, though they were still very close to ultimate failure, as shown in Figure 22.

In Figure 23 a photograph of the failed specimens of the size n=3, for each constraint ply angle, θ, is shown. The common characteristic of all ply angles (and sizes), is the delamination of +θ° plies from the -θ° plies. In consequence, it was possible to predict the critical load to cause failure of each.

The strength of each $[+\theta_n/-\theta_n/90_{2n}]_s$ laminate for n>1 was predicted from the strain energy release rate, G=G(θ, n=1), of the n=1 size laminate, for θ=15°, 30°, 45°, 60°, and 75°. The needed values for E_{LAM}, the modulus of the laminate, and E_{LD}, the modulus of the locally delaminated region, were computed from the lamina elastic properties using classical lamination theory, and are tabulated in Table 6. Corresponding values for G(θ, n=1) were computed using the average ultimate force resultant, N_x, of the n=1 size specimens, and Equation 3, and are shown in Table 6. The force resultant, N_x, to initiate a +θ° delamination in the n=2, 3, and 4 size laminates was predicted using the corresponding G value, and Equation 6. The results are given in Table 7, and include the percent error between the predicted and measured values. Plots of the experimental data along with the predictions are given in Figure 24. In most cases, the data scatter was greater than the error between the average experimental value and the prediction. Agreement

between the data and the model was quite good for all, with the exception of the $[+75_n/-75_n/90_{2n}]_s$ lay-up, which failed upon initiation of a 90° crack.

5. Discussion

5.1. FIRST-PLY FAILURE

In Figure 5, the equivalent constraint model was used to predict the first-ply failure of the laminates from sizes of n=2,3, and 4, and gradations of constraint from θ=0°, 15°, 30°, 45°, 60°, and 75° in the $[+\theta_n/-\theta_n/90_{2n}]_s$ layups, based on the first-ply failure stress of the $[0_2/90_2]_s$ cross-ply (n=1 size). Necessarily, the model was tuned to the material's strain energy release rate, G. Clearly, the model has captured the essence of the mechanics of first ply failure as affected by both scaling and constraint.

A problem that appeared while using this model was that it could give unexpectedly high values for G. Specifically, when the residual stress was assumed to be zero, the computed G was 250 J/m^2, a value that is within the range generally reported for graphite/epoxies, see O'Brien (1997), and was close to that reported by Bradley and Cohen (1985) for the same material. When the residual stress was at a maximum (or -138°C, the difference between fabrication and use temperatures) the computed G was 675 J/m^2, well above anything reported for carbon/epoxy, see O'Brien (1997). Thus, when stress relaxation was manipulated using the model, a large effect on fpf was predicted. Perhaps stress relaxation is the change that affects the load at which cracking will initiate. An observation that suggests the importance of stress relaxation in determining the mechanical load to initiate cracking follows.

Laminates with cracks due to thermal residual stress do not immediately resume cracking when loaded mechanically. For example, the n=3 size cross-ply cracks at about 225 MPa, which is more than 50% of the stress to cause cracking in the n=1 size. This is a lot of stress considering that the expectation is to resume cracking immediately upon application of tensile mechanical load. Moore and Dillard (1990) showed that matrix cracking appears during long-term tensile loading of cross-ply laminates. Their work shows that time-dependent change in the ability of the matrix to support load causes delayed appearance of matrix cracking. Their work lends support to the argument that a laminate containing residual fabrication stresses will also experience time-dependent changes in the matrix. It appears that to test the model more rigorously, the stress relaxation behavior of the lamina should be determined as part of a complete materials characterization process, which would include the usual measurements of elastic properties, as well as thermal and moisture expansion coefficients.

5.2. "STITCH" CRACK FORMATION

The cracks in the -θ° ply block which formed because of stress redistribution around a 90° crack were called "stitch" cracks because their length and proximity to each other resembled a stitched incision. Stitch cracks appeared in the -θ° plies due to 90° cracks when θ=-45°, see Figure 3, and in -60° plies after monotonic loading, see Figure 16. Stitch cracks were not observed in laminates having constraint ply angles at ±75°, probably because total laminate failure always occurred upon initiation of the first 90° crack. The -15° stitch cracks followed the cracks in +15° plies, not 90° plies, see Figure 1. When the constraint plies were oriented at ±30° then stitch cracks did not appear, except for a very few, see Figure 2. Tensile loading did not appear to increase the stitch crack density or change their length, see Table 5.

Stitch cracks were first described by Jamison, Schulte, Reifsnider, and Stinchcomb (1984). They considered a 1 mm thick $[0/90/+45/-45]_s$ laminate which apparently did not develop these cracks until after 50,000 tension-tension fatigue cycles at 62% of ultimate tensile load. In the present work, stitch cracks appeared due to thermal stresses, or after monotonic tensile loading. The existence of stitch cracking suggests an additional damage mechanism resulting from stress redistribution around cracks. The local delamination mechanism reported in the literature is more familiar, probably because the laminates studied were cross-plied, where constraint plies are oriented at 0° to the load direction.

In two previous studies, stitch cracks likely existed, but were overlooked. Flaggs and Kural (1982) considered T300/934 (a material having similar elastic and thermal properties to AS4/3502), with stacking sequences of $[\pm 30/90_n]_s$ and $[\pm 60/90_n]_s$, where n=1,2,4, and 8. Dye penetrant enhanced x-radiography had been used, but stitch cracks in -60° plies were not reported. Kistner, Whitney, and Browning (1985) considered AS4/3502 having stacking sequences of

$$\left[+\theta/-\theta/+\theta/-\theta/90_3/\overline{90}\right]_s, \text{ and } \left[+\theta/90/-\theta/90/+\theta/90/-\theta/\overline{90}\right]_s,$$

where θ=45° and θ=60°. Because x-radiographs were not taken, the stitch cracking was missed. In the current work, even when x-radiographs were made, the stitch cracks were fine enough that they were not visible unless the film resolution was sufficiently high. Stitch cracks were overlooked when both the fast Polaroid Type 52 (ISO 400), and finer grain Type 55 (ISO 50) films were used. Finely detailed x-radiographs were made using Kodak Industrex SR5, or Industrex M5. The development of the stitch cracks has been shown to occur in all thicknesses tested, and only required the presence of a matrix microcrack in the neighboring ply. Furthermore, the stitch cracks appeared in great numbers in plies oriented by as much as 45° from the cracked 90° ply, but were few in number for the 30° plies (oriented 60° from the cracked 90° ply). Stitch cracks are a damage form which can appear early in the service life, if not immediately after fabrication, and as such should be considered during design. State-of-the-art models can design to

avoid matrix cracking and subsequent crack-tip delamination (see Wang and Karihaloo, 1996a,b) but stitch cracks are not yet considered.

5.3. STRESS-STRAIN RESPONSE OF THE $[(+60/-60/90_2)_2]_s$ LAY-UP

The same plastic-like stress-strain response observed in the $[(+60/-60/90_2)_2]_s$ lay-up, Figure 20, was observed earlier by Kistner, Whitney, and Browning (1985) in their tests of a similar lay-up. The plastic-like stress-strain response was explained from observation (by edge inspection) that cracks appeared in all plies simultaneously. However, without high resolution x-radiographs it would not have been clear that the cracks in the interior +60° and -60° plies were actually short and stitch-like, and not cracks that ran across the laminate. Talreja (1985b) commented that the elastic/plastic-like response was expected of laminates having transverse plies with low constraint. The immediate effect of the stitch crack was to radically reduce the stiffness. Certainly, structural lay-ups will have plies oriented in the major loading directions, so the effect may not be very noticeable. However, shear stiffness may be more strongly affected.

5.4. STRENGTH OF $[+\theta_n/-\theta_n/90_{2n}]_s$ LAMINATES

The tensile strength of the $[+\theta_n/-\theta_n/90_{2n}]_s$ family of scaled angle-ply laminates was found to closely coincide with initiation of a local delamination in the $+\theta°$ plies, see Figure 24. Because of this fact, the dependence of laminate tensile strength on size was predicted successfully using O'Brien's 1993 model for predicting local delamination of this type. Damage in the form of matrix cracks and -θ/90 delamination served as favored soft zones for initiation of the $+\theta°$ crack and critical strength-controlling $+\theta°$ delamination. This is overlooked when using the model, because the modulus, E_{LAM}, of an undamaged laminate was used. Perhaps the G value computed from the n=1 size experiments is compensating for the fact that the laminate is actually locally softer than E_{LAM} suggests.

6. Conclusions

The scaling effect observed for first-ply failure of 90° plies, in $[+\theta_n/-\theta_n/90_{2n}]_s$ laminates having varying levels of constraint and varying ply thickness, has been shown to follow that predicted by a mechanics-based model. The cause for deviation of the model from the experiment may lay with the model, but certainly contributing factors must be the pre-existence of cracks in thicker laminates with high constraint, and the unknown level of residual stress.

The laminate strength was controlled by delamination of the surface $+\theta°$ ply block in the presence of a $+\theta°$ crack. Damage development before final failure, particularly the midplane delamination of layups with 30° constraint plies, governed the location of final failure. Even so,

the strength scaling effect could be predicted by use of a model customized for the $+\theta°$ ply block delamination just described.

The formation of dense numbers of short, stitch-like cracks in constraint plies of various orientation, but separated by as much as 45°, was found to occur under monotonic tensile loading or thermal stress, not only after high cycle fatigue. Furthermore, this damage mode was shown to be the cause of enormous stiffness loss in the $[(+60/-60/90_2)_2]_S$ lay-up, and not extension of long cracks in the interior +60° and -60° plies.

7. References

Aveston, J., and Kelly, A. (1973). Theory of Multiple Fracture of Fibrous Composites. Journal of Materials Science, Vol. 8, pp. 352.

Bradley, W.L. and Cohen, R.N. (1985). Matrix Deformation and Fracture in Graphite Reinforced Epoxies. In Delamination and Debonding of Materials, ASTM STP 876, October, pp. 389-410.

Crossman, F. W., and Wang, A.S.D. (1982). The Dependence of Transverse Cracking and Delamination on Ply-Thickness in Graphite/Epoxy Laminates. American Society for Testing and Materials.

Curtis, P.T. (1980). The Effect of Edge Stresses on the Failure of (0°,45°,90°) CFRP Laminates. Royal Aircraft Establishment Technical Report TR 80054.

Dvorak, G.J., and Laws, N. (1987). Analysis of Progressive Matrix Cracking in Composite Laminates II. First Ply Failure. Journal of Composite Materials, Vol. 21, April, pp. 309-329.

Flaggs, D.L., and Kural, M.H. (1982). Experimental Determination of the In Situ Transverse Lamina Strength in Graphite/Epoxy Laminates. Journal of Composite Materials, Vol. 16, March, pp. 103-116.

Fukunaga, H., Chou, T.-W., Schulte, K., Peters, P. W. M. (1984). Probabilistic Initial Failure Strength Of Hybrid And Non Hybrid Laminates. Journal of Materials Science, Vol. 19, No.11, pp. 3546-3553.

Gudmundson, P., Östlund, S., and Zang, W. (1992). Local Stresses and Thermoelastic Properties of Composite Laminates Containing Micro Cracks. Local Mechanics Concepts for Composite Material Systems (edited by J.N. Reddy and K.L. Reifsnider), Springer, Berlin, pp. 283-308.

Gudmundson, P., and Zang, W. (1993). An Analytic Model for Thermoelastic Properties of Composite Laminates Containing Transverse Matrix Cracks. International Journal of Solids and Structures, Vol. 30, No. 23, pp. 3211-3231.

Hashin, Z. (1985). Analysis of Cracked Laminates: A Variational Approach. Mechanics of Materials, Vol. 4, pp. 121-136.

Herakovich, C.T. (1981). On the Relationship Between Engineering Properties and Delamination of Composite Materials. Journal of Composite Materials, Vol. 15, pp. 336-348.

Herakovich, C.T. (1982). Influence of Layer Thickness on the Strength of Angle-Ply Laminates. Journal of Composite Materials, Vol. 16, May, pp. 216-227.

Herakovich, C.T., Post, D., Buczek, M.B., Czarnek, R. (1985). Free Edge Strain Concentrations in Real Composite Laminates: Experimental-Theoretical Correlation. Journal of Applied Mechanics, Vol. 52, No. 4, pp. 787-793.

Highsmith, A.L. and Reifsnider, K.L. (1982). Stiffness-Reduction Mechanisms in Composite Laminates. Damage in Composite Materials, ASTM STP 775, K.L. Reifsnider, Ed., American Society for Testing and Materials, pp. 103-117.

Hsu, P. W. and Herakovich., C.T. (1977). Edge Effects in Angle-Ply Composite Laminates. Journal of Composite Materials, Vol. 11, pp. 422-428.

Jackson, K.E., and Kellas, S. (1993). Effect of Specimen Size on the Tensile Strength of Geometrically Scaled $[+\theta_n/-\theta_n/90_{2n}]_s$ Composite Laminates. Army Symposium on Solid Mechanics, August 17-19, Plymouth, MA.

Jamison, R.D., Schulte, K., Reifsnider, K.L., and Stinchcomb, W.W. (1984). Characterization and Analysis of Damage Mechanisms in Tension-Tension Fatigue of Graphite/Epoxy Laminates. Effects of Defects in Composite Materials, ASTM STP 836, American Society for Testing and Materials, Philadelphia, pp. 21-55.

Kellas, S., and Morton, J. (1990). Strength Scaling in Fiber Composites. NASA Contractor Report 4335, November.

Kellas, S., and Morton, J. (1992). Scaling Effects in Angle-Ply Laminates. NASA Contractor Report 4423, February.

Kellas, S., Johnson, D.P., Morton, J., and Jackson, K.E. (1993). Scaling Effects in Sublaminate-Scaled Composite Laminates. 34th AIAA/ASME/ASCE/AHS/ASC Structures, Structural Dynamics and Materials Conference, AIAA/ASME Adaptive Structures Forum, April 19-22, La Jolla, CA, Part 6, pp. 3715-3725.

Kim, R. Y., Soni, S.R. (1984). Experimental and Analytical Studies On the Onset of Delamination in Laminated Composites. Journal of Composite Materials, Vol. 18, pp. 70-80.

Kistner, M.D., Whitney, J.M., and Browning, C.E. (1985). First-Ply Failure of Graphite/Epoxy Laminates. Recent Advances in Composites in the United States and Japan, ASTM STP 864, J.R. Vinson and M. Taya, Eds., American Society for Testing and Materials, Philadelphia, pp. 44-61.

Lagace, P., Brewer, J., and Kassapoglou, C. (1987). The Effect of Thickness on Interlaminar Stresses and Delamination in Straight-Edged Laminates. Journal of Composites Technology and Research, JCTRER, Vol. 9, No. 3, pp. 81-87.

Moore, R.H., and Dillard, D.A. (1990). Time-dependent Matrix Cracking in Cross-ply Laminates. Composites Science and Technology, Vol. 39, pp. 1-12.

O'Brien, T.K. (1982a). The Effect of Delamination on the Tensile Strength of Unnotched, Quasi-Isotropic, Graphite/Epoxy Laminates. Proceedings of the 1982 Joint Conference on Experimental Mechanics, Oahu-Maui, Hawaii, May 23-28, pp. 236-243.

O'Brien, T. K. (1982b). Characterization of Delamination Onset and Growth in a Composite Laminate. Damage in Composite Materials, ASTM STP 775, American Society for Testing and Materials, Philadelphia, pp. 140-167.

O'Brien, T.K., and Salpekar, S.A. (1993). Scale Effects on the Transverse Tensile Strength of Graphite/Epoxy Composites. Composite Materials: Testing and Design (Eleventh Volume), ASTM STP 1206, E.T. Camponeschi, Jr., Ed., American Society for Testing and Materials, Philadelphia, pp. 23-52.

O'Brien, T.K., and Hooper, S.J. (1993). Local Delaminations in Laminates with Angle Ply Matrix Cracks, Part I: Tension Tests and Stress Analysis. Composite Materials: Fatigue and Fracture, Fourth Volume, ASTM STP 1156, W.W. Stinchcomb and N.E. Ashbaugh, Eds., American Society for Testing and Materials, Philadelphia, pp. 491-506.

O'Brien, T.K. (1993). Local Delaminations in Laminates with Angle Ply Matrix Cracks, Part II: Delamination Fracture Analysis and Fatigue Characterization. Composite Materials: Fatigue and Fracture, Fourth Volume, ASTM STP 1156, W.W. Stinchcomb and N.E. Ashbaugh, Eds., American Society for Testing and Materials, Philadelphia, pp. 407-538.

O'Brien, T.K. (1997). Composite Interlaminar Shear Fracture Toughness, G_{IIc}: Shear Measurement or Sheer Myth? NASA Technical Memorandum 110280, February.

Oplinger, D.W., Parker, B.S., and Chiang, F.P. (1974). Edge-Effect Studies in Fiber-Reinforced Laminates. Experimental Mechanics, Vol. 14, No. 9, pp. 347-354.

Pagano, N.J., and Pipes, R.B. (1973). Some Observations on the Interlaminar Strength of Composite Laminates. International Journal of Mechanical Sciences, Vol. 15, pp. 679-688.

Parvizi, A., Garrett, K.W., Bailey, J.E. (1978). Constrained Cracking in Glass Fibre-Reinforced Epoxy Cross-Ply Laminates. Journal of Materials Science, Vol. 13, pp. 195-201.

Pipes, R.B., and Pagano, N.J. (1970). Interlaminar Stresses in Composite Laminates Under Uniform Axial Extension. Journal of Composite Materials, Vol. 4, October, pp. 538-548.

Pipes, R.B., and Daniel, I.M. (1971). Moiré Analysis of Interlaminar Shear Edge Effect in Laminated Composites. Journal of Composite Materials, Vol. 5, pp. 255-259.

Radford, D.W. (1993). Cure Shrinkage Induced Warpage in Flat Uni-Axial Composites, Journal of Composites Technology and Research, JCTRER, Vol. 15, No. 4, pp. 290-296.

Reifsnider, K.L. (1977). Some Fundamental Aspects of the Fatigue and Fracture Response of Composite Materials. Proceedings of the 14th Annual Meeting, Society of Engineering Science, G.C. Sih, Ed., Lehigh University, Bethlehem, PA, Nov. 14-16. Recent Advances in Engineering Science, pp. 373-384.

Rodini, B.T., and Eisenmann, J.R. (1978). An Analytical and Experimental Investigation of Edge Delamination in Composite Laminates. Fibrous Composites in Structural Design. New York, Plenum Press. 441-457.

Talreja, R. (1985a). A Continuum Mechanics Characterization of Damage in Composite Materials. Proceedings of the Royal Society of London, A399, pp. 195-216.

Talreja, R. (1985b). Transverse Cracking and Stiffness Reduction in Composite Laminates. Journal of Composite Materials, Vol. 19, July, pp. 355-375.

Talreja, R. (1986). Stiffness Properties of Composite Laminates with Matrix Cracking and Interior Delaminations. Engineering Fracture Mechanics, Vol. 25, No. 5/6, pp. 751-762.

Talreja, R. (1996). A Synergistic Damage Mechanics Approach to Durability of Composite Material. Progress in Durability Analysis of Composite Systems. Cardon, Fukuda and Reifsnider, Eds. Balkema, Rotterdam, ISBN: 90 5410 809 6, pp. 117-129.

Varna, J., and Berglund, L.A. (1991). Multiple Transverse Cracking and Stiffness Reduction in Cross-Ply Laminates. Journal of Composites Technology and Research, Vol. 13, pp. 97-106.

Varna, J., Berglund, L.A., Talreja, R., and Jacovics, A. (1993). A Study of the Opening Displacement of Transverse Cracks in Cross-Ply Laminates. International Journal of Damage Mechanics, Vol. 2, pp. 272-289.

Vasil'ev, V.V., Dudchenko, and A.A., Elpat'evskii, A.N. (1970). Analysis of the Tensile Deformation of Glass-Reinforced Plastics. Mekhanika Polimerov, Vol. 1, pp. 144-147.

Wang, J., and Karihaloo, B.L. (1994). Cracked Composite Laminates Least Prone to Delamination. Proc. of the Royal Society London, Vol. 444, pp. 17-35.

Wang, J., and Karihaloo, B.L. (1996a). Optimum in Situ Strength Design of Composite Laminates Part I: In Situ Strength Parameters. Journal of Composite Materials, Vol. 30, No. 6, pp. 1314-1337.

Wang, J., and Karihaloo, B.L. (1996b). Optimum in Situ Strength Design of Composite Laminates Part II: Optimum Design. Journal of Composite Materials, Vol. 30, No. 12, pp. 1338-1358.

Zhang, J., Fan, J., and Soutis, C. (1992). Analysis of Multiple Matrix Cracking in $[\pm\theta_m/90_n]_s$ Composite Laminates, Part 2: Development of Transverse Ply Cracks. Composites, Vol. 23, No. 5, September 1992, pp. 299-304.

Zhang, J., Soutis, C., and Fan, J. (1994a). Strain Energy Release Rate Associated with Local Delaminations in Cracked Composite Laminates. Composites, Vol. 25, No. 9, pp. 851-862.

Zhang, J., Soutis, C., and Fan, J. (1994b). Effects of Matrix Cracking and Hygrothermal Stresses on the Strain Energy Release Rate for Edge Delamination in Composite Laminates. Composites, Vol. 25, No.1, pp. 27-35.

Table 1. Specimen sizes and dimensions.

scale	n	plies	length (mm)	width (mm)	thickness (mm)
1/4	1	8	146.1	12.7	1.092
1/2	2	16	292.1	25.4	2.159
3/4	3	24	438.2	38.1	3.302
Full	4	32	584.2	50.8	4.394

Table 2. Mechanical properties of $[+\theta_n/-\theta_n/90_{2n}]_s$ laminates for differing size, n.

θ	n=1			n=2			n=3			n=4		
degrees	modulus GPa	strength MPa	strain %	modulus GPa	strength MPa	strain %	modulus GPa	strength MPa	strain %	modulus GPa	strength MPa	strain %
0	74.3	843.2	1.24	71.5	814.5	1.11	70.5	796.6	1.08	73.8	764.7	1.02
15	65.5	449.6	0.726	63.3	324.7	0.541	62.6	271.9	0.446	61.0	234.5	0.393
30	42.1	270.2	0.824	–	173.2	–	41.7	156.9	0.441	40.3	139.6	0.395
45	22.5	140.5	0.843	–	84.7	–	20.8	79.4	0.577	19.7	79.3	0.503
60	13.3	65.9	0.521	12.2	53.0	0.443	12.4	44.9	0.357	12.9	33.7	0.287
75	10.9	43.9	0.417	10.2	42.6	0.513	10.4	35.7	0.334	10.2	31.1	0.303
90	10.8	39.3	0.366	10.1	38.3	0.383	10.2	38.2	0.377	10.2	37.0	0.846

Table 3. Thermal Stress Induced 90° Crack Density of $[+\theta_n/-\theta_n/90_{2n}]_s$

		constraint ply angle							
		0°		15°		30°		45°	
scale	n	$d^{(1)}$ (cm)	$r^{(2)}$	d (cm)	r	d (cm)	r	d (cm)	r
1/4	1	∞	0	∞	0	∞	0	∞	0
1/2	2	1.02	0.10	0.37	0.27	0.33	0.30	4.17	0.02
3/4	3	0.42	0.36	0.34	0.45	0.87	0.17	0.64	0.24
Full	4	0.39	0.51	0.45	0.44	1.00	0.20	0.67	0.30

(1) d is the average crack spacing in the 90° plies.
(2) r is the micro crack density, where $r=a/d$, and a = the 90° ply block thickness.

Table 4. Count of Thermal Stress-Induced Cracks in +θ° Plies

gauge length, mm	n	+θ° constraint ply angle							
		0°		15°		30°		45°	
		top	bottom	top	bottom	top	bottom	top	bottom
146.1	1	0	0	0	0	0	0	0	0
292.1	2	0	0	0	0	0	0	0	0
438.2	3	0	0	11	0	50	0	0	0
279.4	4	4	4	4	0	0	1	28	0

Table 5. Length and Density of Cracks in -θ° Plies

scale	specimen no.	θ° ply	tensile stress (MPa)	crack density[(1)] (cracks/cm)	crack length, (mm)	
					min.,max.	mean (st.dev.)
3/4	3-15-9*	-15	thermal stress	33,34,31	0.15, 1.95	0.82 (0.71)
Full	4-15-1*	-15	thermal stress	8,6,7.3,8,9.3, 7.3		
1/4	1-45-11	-45	134.7	72,62,64	0.10, 0.50	0.32 (0.11)
1/4	1-45-12	-45	140.4	60,64,60	0.10, 1.50	0.32 (0.11)
1/2	2-45-9	-45	413.4	56,58,44,50,56	0.10, 0.95	0.65 (0.22)
1/2	2-45-11	-45	thermal stress	52,48,60,52		
1/2	2-45-10	-45	406.3		0.25, 1.00	0.65 (0.19)
3/4	3-45-1	-45	thermal stress	12,6,0,0,0,2,2,3, 10	0.40, 1.50	1.13 (0.35)
3/4	3-45-11	-45	92.9	25,28,42,30	0.20, 2.00	1.12 (0.45)
Full	4-45-1	-45	thermal stress	8,9,11,16		
Full	4-45-?	-45				
1/4	1-60-9	-60	68.0	46,42,56,38	0.15, 0.50	0.35 (0.11)
1/4	1-60-11	-60	66.1	50,44,48	0.25, 0.70	0.44 (0.14)
1/2	2-60-11	-60	60.0	33,28,28	0.30, 0.90	0.58 (0.16)

* these -15° cracks follow the +15° crack

(1) The crack density includes cracks counted in both -θ° layers.

Table 6. Stiffnesses and Strain Energy Release Rate for Delamination of +θ° Plies

θ	E_{LAM} (GPa)	E_{LD} (GPa)	G (J/m^2)
15	66.3	32.2	2058
30	44.9	14.3	2110
45	24.0	5.4	1694
60	13.7	3.4	567
75	11.2	3.2	263

Table 7. Experimental results for strength of $[+\theta_n/-\theta_n/90_{2n}]_s$ laminates. Predictions are for initiation of delamination of the surface $+\theta_n$ ply block. Error numbers indicate how closely strength was controlled by the start of delamination.

θ=15° n	σ_{ult} (MPa) (experiment)	N_x (kN/m) (experiment)	N_x (kN/m) (prediction)	% error
1	449.6	449.6	--	--
2	324.7	649.6	635.8	-2.1
3	271.9	815.6	778.6	-4.5
4	234.5	938.0	899.1	-4.2

θ=30° n	σ_{ult} (MPa) (experiment)	N_x (kN/m) (experiment)	N_x (kN/m) (prediction)	% error
1	270.2	270.2	--	--
2	173.2	346.4	382.1	+10.3
3	156.9	470.7	468.0	-0.6
4	139.6	558.4	540.4	-3.2

θ=45° n	σ_{ult} (MPa) (experiment)	N_x (kN/m) (experiment)	N_x (kN/m) (prediction)	% error
1	140.5	140.5	--	--
2	84.7	169.4	198.7	+17.3
3	79.4	238.2	243.4	+2.2
4	79.3	317.2	281.0	-11.4

θ=60° n	σ_{ult} (MPa) (experiment)	N_x (kN/m) (experiment)	N_x (kN/m) (prediction)	% error
1	65.9	65.9	--	--
2	53.0	106.0	93.2	-12.1
3	44.9	134.7	114.1	-15.3
4	33.7	134.8	131.8	-2.2

θ=75° n	σ_{ult} (MPa) (experiment)	N_x (kN/m) (experiment)	N_x (kN/m) (prediction)	% error
1	43.9	43.9	--	--
2	42.6	85.2	62.0	-27.2
3	35.7	107.1	76.0	-29.0
4	31.1	124.4	87.0	-30.1

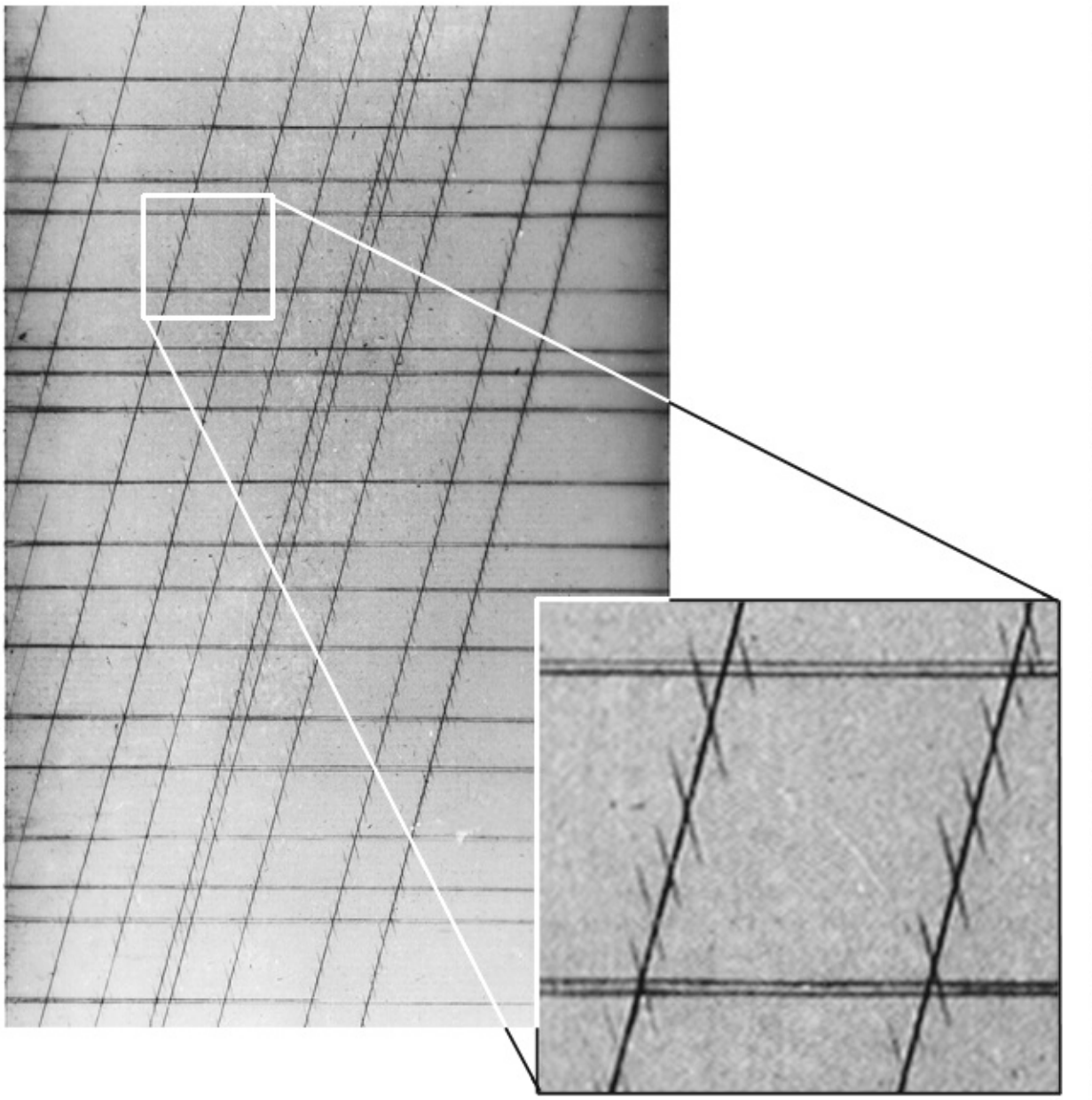

Figure 1. X-radiograph of thermal stress-induced matrix microcracks in the n=4 size layup $[+15_4/-15_4/90_8]_s$. The 90° ply matrix cracks run from left to right. Stress redistribution around the +15° ply matrix cracks induce formation of short, stich-like, -15° ply matrix cracks.

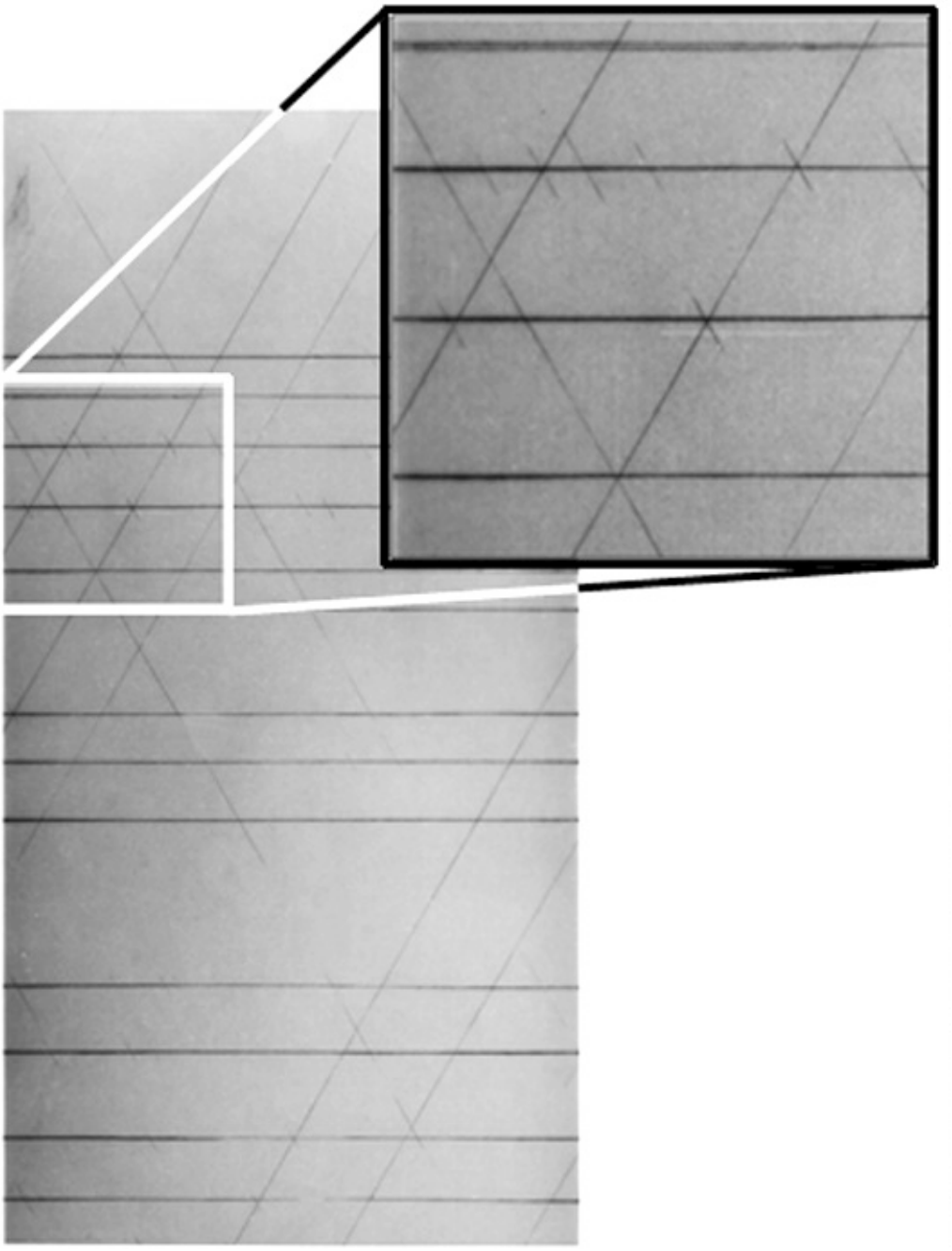

Figure 2. X-radiograph of thermal stress-induced matrix microcracks in the n=4 size layup $[+30_4/-30_4/90_8]_s$. The 90° ply matrix cracks run from left to right, and trigger formation of a few short, stich-like, -30° ply matrix cracks. This layup exhibits long -30° ply matrix cracks, in addition to +30° ply matrix cracks.

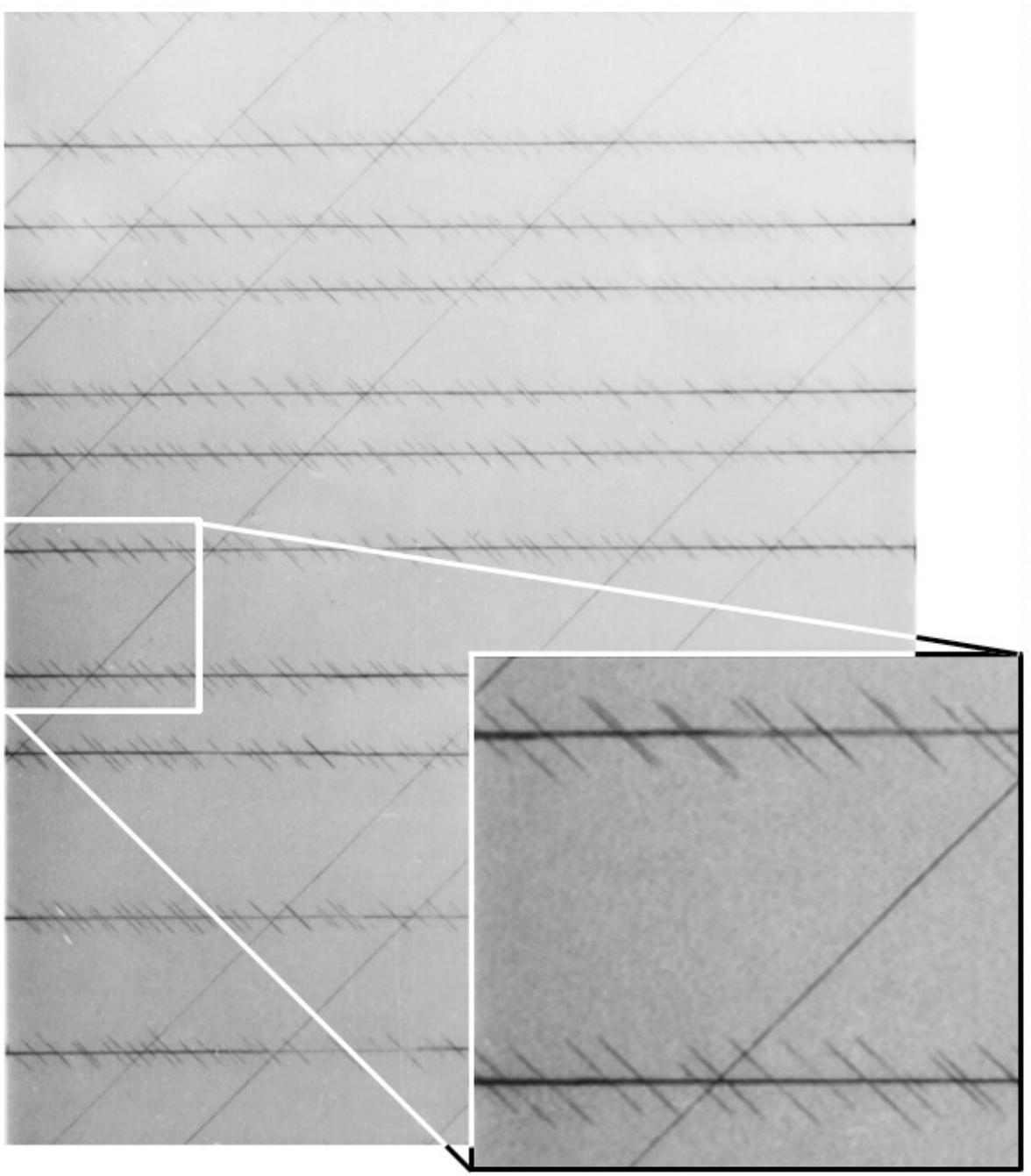

Figure 3. X-radiograph of thermal stress-induced matrix microcracks in the ply-level scaled, (n=4) layup $[+45_4/-45_4/90_8]_s$. The 90° ply matrix cracks run from left to right, and trigger formation of a many short, stich-like, -45° ply matrix cracks. Long +45° ply matrix cracks appear.

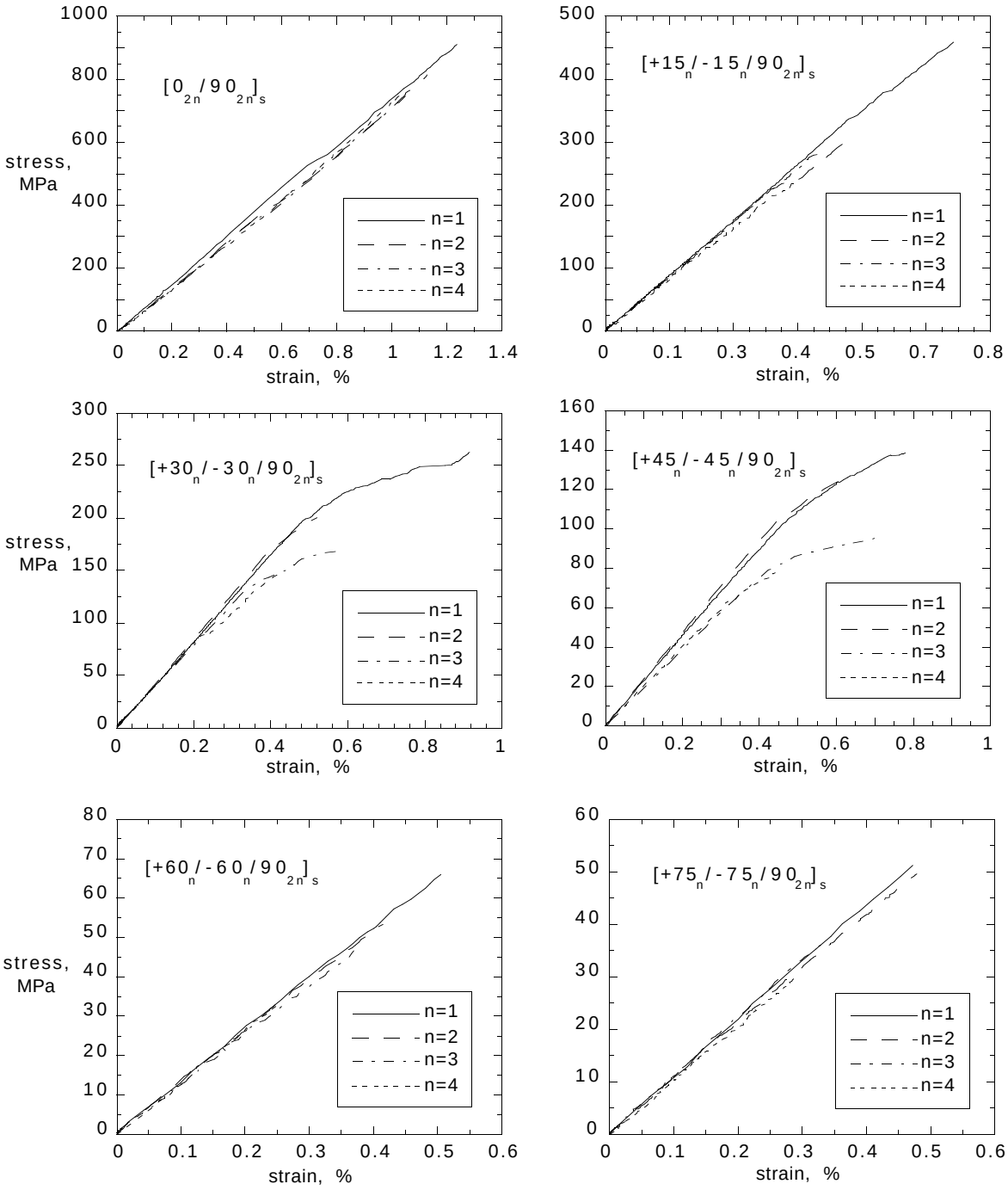

Figure 4. Typical stress versus strain plots for $[+\theta_n/-\theta_n/90_{2n}]_s$ laminates.

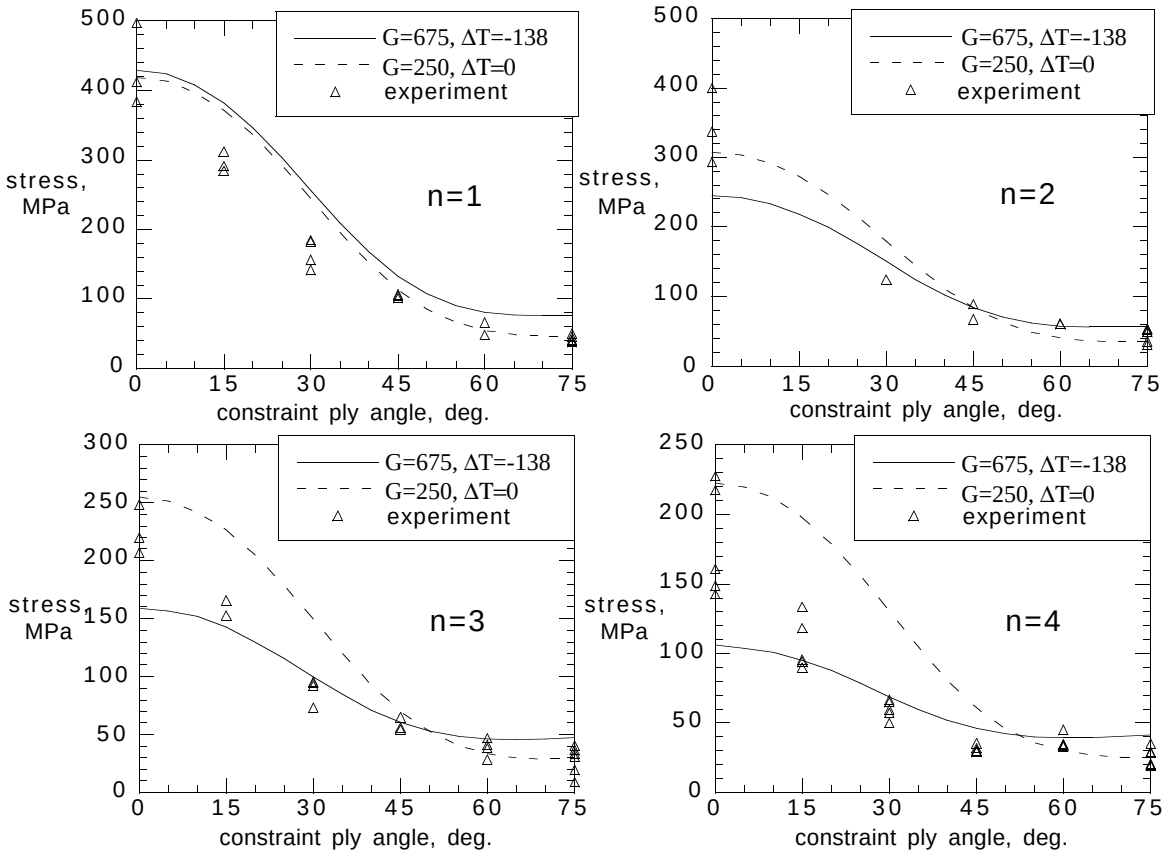

Figure 5. First-ply failure of $[+\theta_n/-\theta_n/90_{2n}]_s$ in the central block of 90° plies as a funtion of both the angle of the constraining plies, and the thickness of the laminate, as governed by *n*. The predictions are made using the "Equivalent Constraint Model" Zhang and Soutis (1992). All predictions are based upon first-ply failure tests of the $[0_2/90_2]_s$ (n=1) size cross-ply laminate. Model parameters were: G=675 J/m^2, ΔT=-138°C (solid line), and G=250 J/m^2, ΔT=0°C (dashed line).

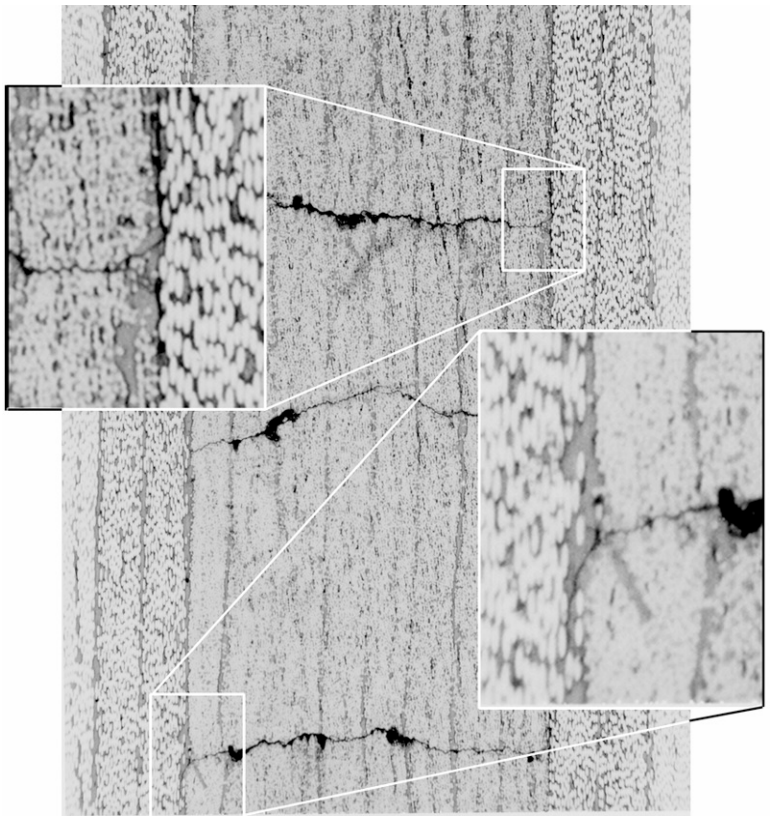

Figure 6. Development of -15/90 interface failure at 90° crack tips as a consequence of stress redistribution around the 90° cracks. Shown is a $[+15_2/-15_2/90_4]_s$ laminate, loaded to 283 MPa.

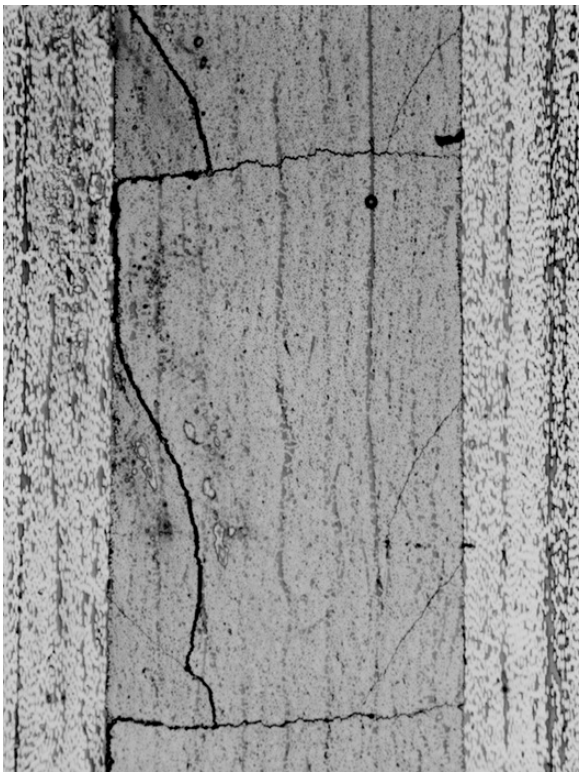

Figure 7. Coalescence of inclined secondary cracks in the 90° plies with 90° crack-tip delaminations into a continuous -15/90 interface delamination. Shown is a $[+15_2/-15_2/90_4]_s$ laminate, loaded to 339 MPa.

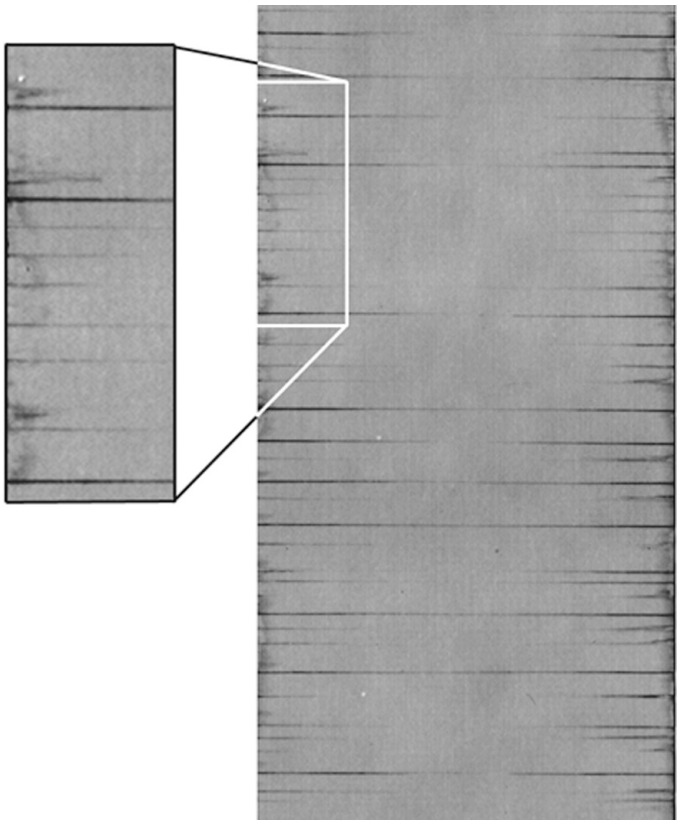

Figure 8. Comparatively high loading did not produce a general edge delamination. Delaminations were very localized and associated with 90° crack-tip delamination. Shown is a $[+15_2/-15_2/90_4]_s$ laminate, loaded to 311 MPa.

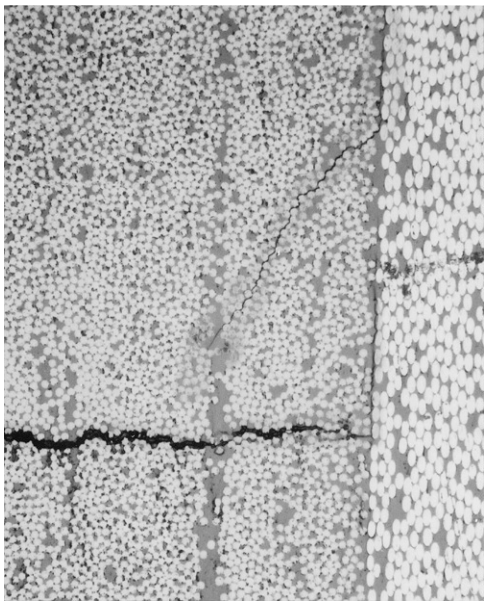

Figure 9. Development of -30/90 delamination from the tip of the 90° crack. Further development of inclined cracking in the 90° plies. Shown is a $[+30_2/-30_2/90_4]_s$ layup, loaded to 124 MPa.

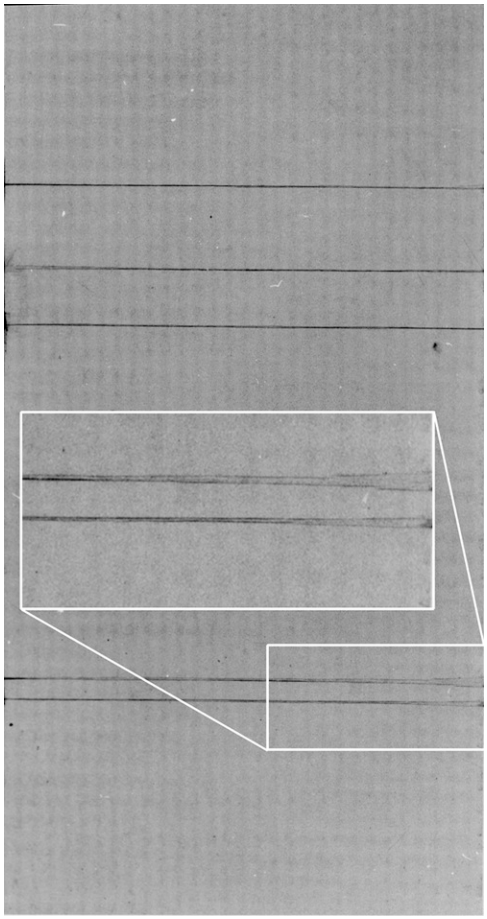

Figure 10. Delamination of the -30/90 interface from 90° crack tips ran deeply into the laminate, before 90° matrix cracking became well developed. Shown is a $[+30/-30/90_2]_s$ layup, loaded to 209 MPa.

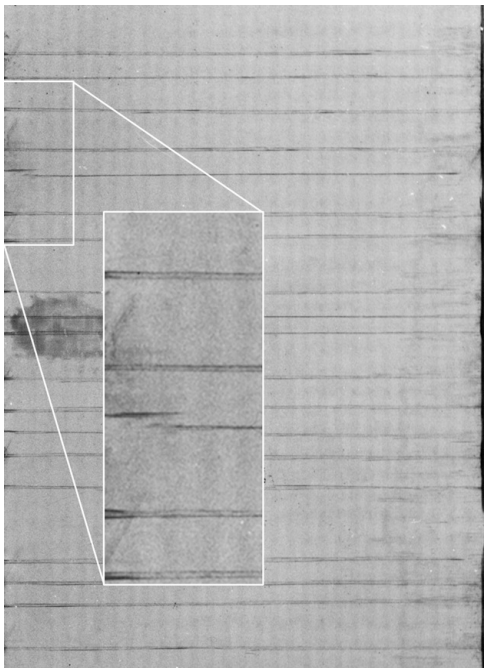

Figure 11. Progress of damage in a $[+30/-30/90_2]_s$ layup loaded to 227 MPa. Right edge, unpolished, shows rapid coalescence of -30/90 local delaminations had formed one large edge delamination. Left edge shows that polishing suppressed the edge delamination, but that -30° cracks formed instead.

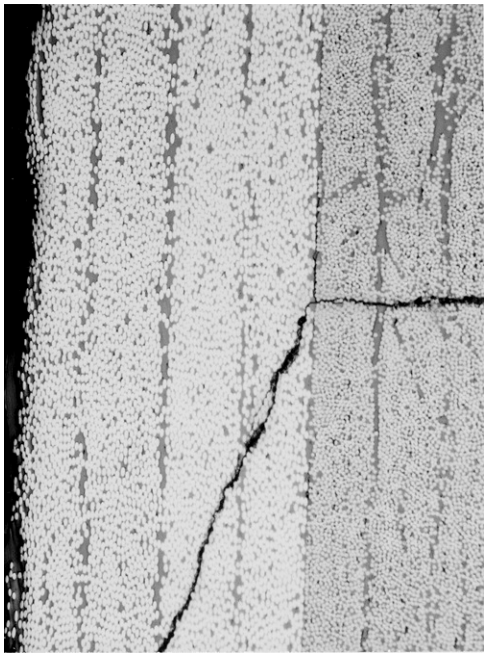

Figure 12. Growth of a -30° crack from the tip of a 90° crack at the -30/90 interface. Shown is a $[+30_2/-30_2/90_4]_s$ laminate, loaded to 160 MPa.

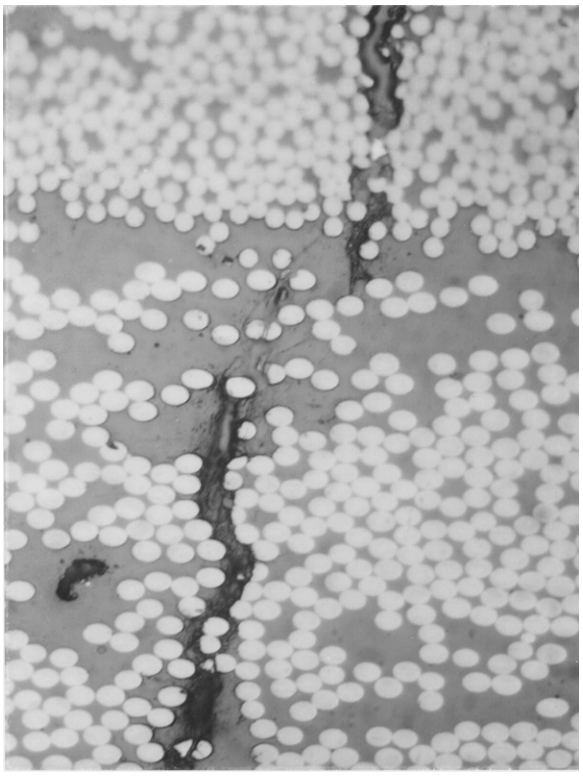

Figure 13. Internal view, perpendicular to the 90° plies, close to the intersection of a -45° stitch crack and a 90° crack. There was no -45/90 delamination. Specimen was an n=4 size, $[+45_4/-45_4/90_8]_s$ laminate, not yet loaded. Magnification is 400X.

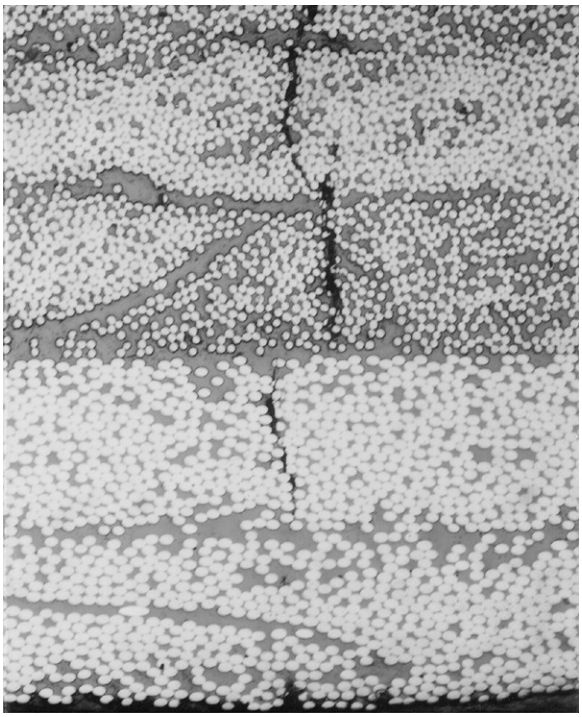

Figure 14. An interior section, close to the intersection of the -45° and 90° cracks, cut and polished perpendicular to the 90° plies. Shown is a $[+45/-45/90_2]_s$ laminate which had been loaded to failure. No -45/90 delamination can be observed.

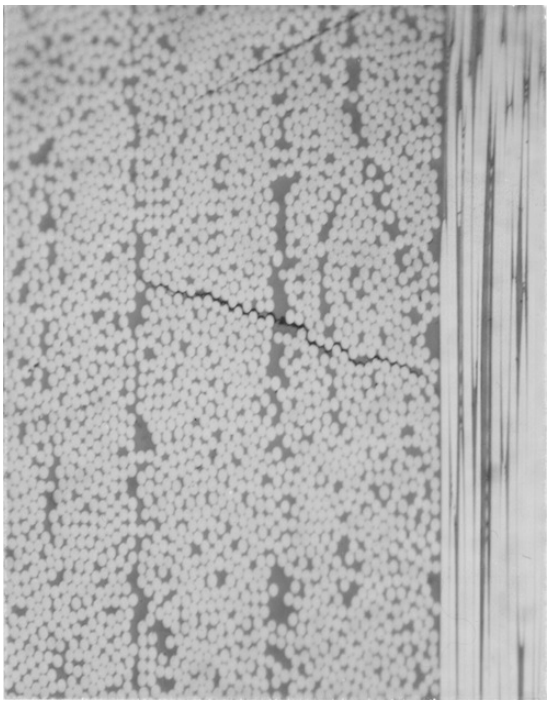

Figure 15. An interior section, cut and polished parallel to the 90° plies, and close to the 90° crack. A -45° stitch crack is evident, but -45/90 delamination cannot be seen. Specimen was a $[+45_2/-45_2/90_4]_s$ loaded to 101 MPa.

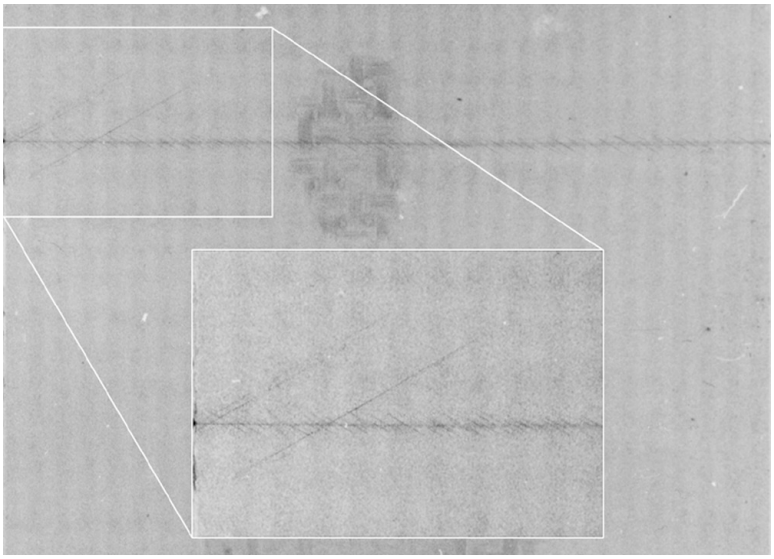

Figure 16. Formation of 90° cracks results in -60° stitch cracks. The +60° cracks initiate from -60° cracks, and prefer to start near 90° cracks. Specimen is a $[+60/-60/90_2]_s$ layup, loaded to 66 MPa.

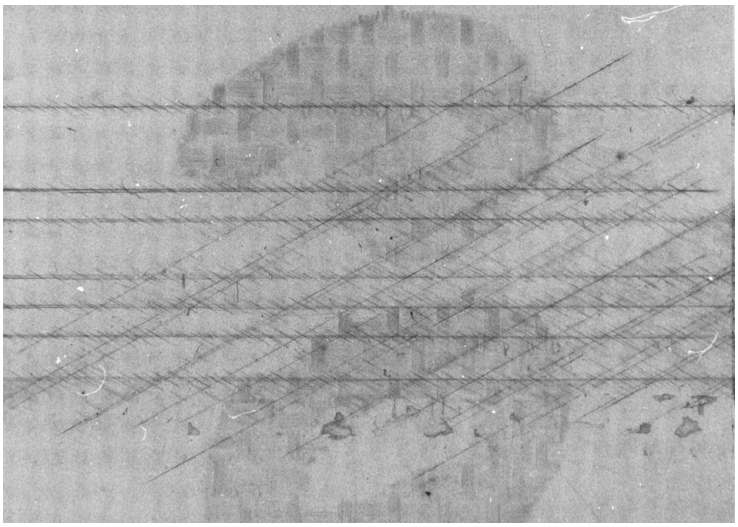

Figure 17. Additional 90° cracks formed, but under the +60° cracks. Stitch cracks in the -60° plies formed due to +60° cracks. Specimen is a $[+60/-60/90_2]_s$ layup, loaded to 68 MPa. Failure was imminent.

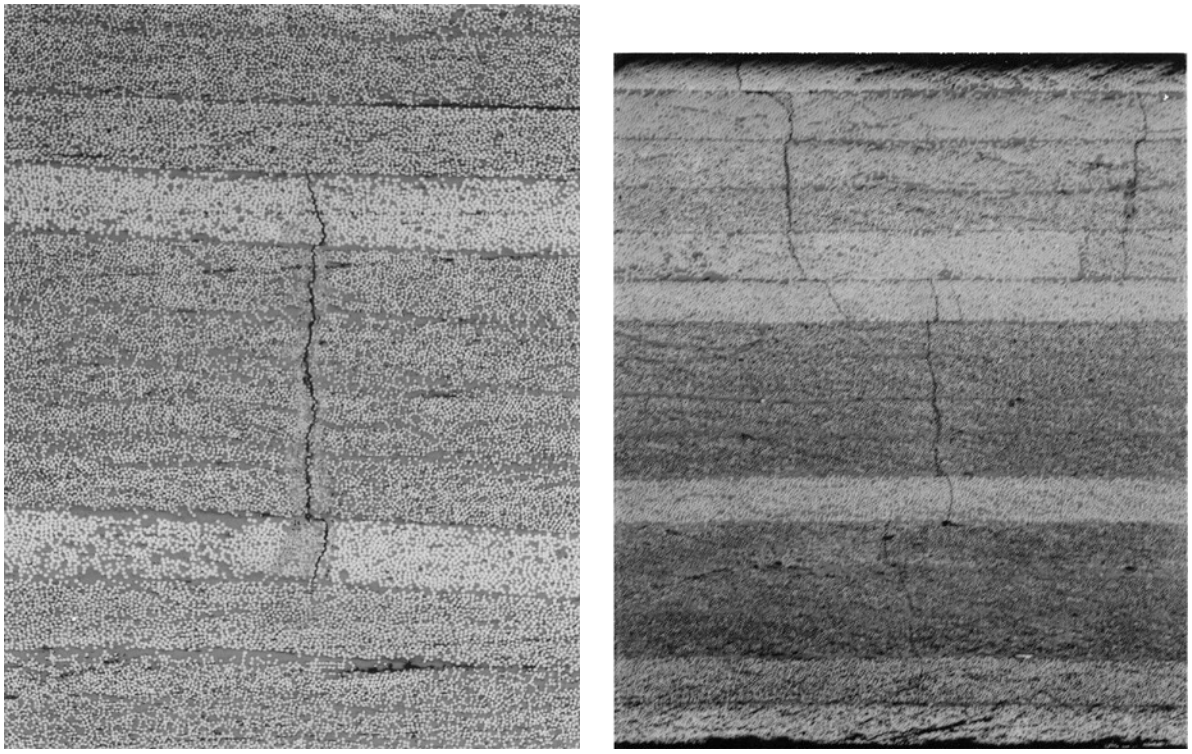

(a) first failure (b) second failure

Figure 18. Micrographs of the polished edge of the sublaminate-level scaled $[(+60/-60/90_2)_2]_s$ layup. The first failure event (a) occurs at 63 MPa, and consists of midplane 90° ply matrix cracks and immediate formation of short, stich-like, -60° ply matrix cracks. The second failure event (b) occurs at 75 MPa, and consists of off-center 90° ply matrix cracks and immediate formation of short, stich-like, -60° and +60° ply matrix cracks in all remaining 60° plies.

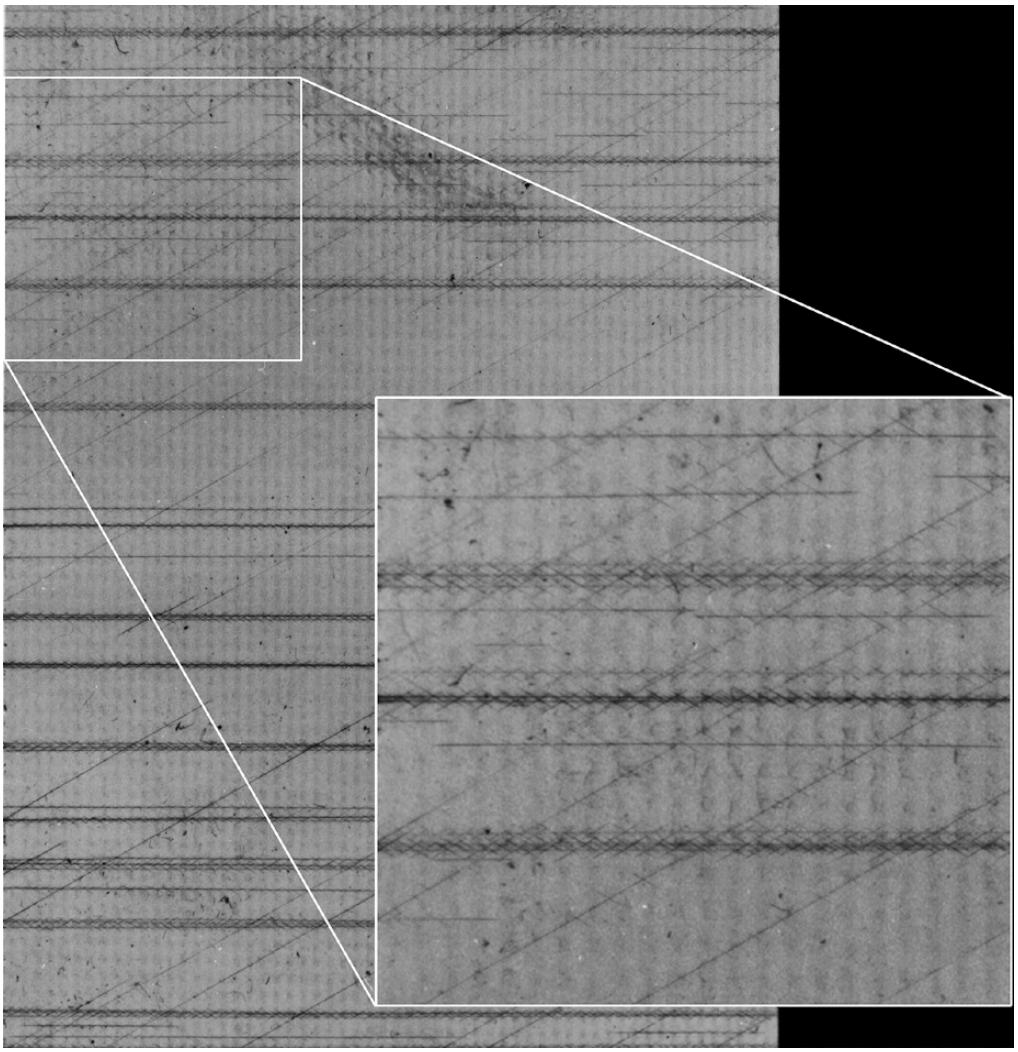

Figure 19. X-radiograph of the sublaminate-level scaled $[(+60/-60/90_2)_2]_s$ layup. Applied stress was 75 MPa. Damage consists of 90° ply matrix cracks and immediate formation of short, stich-like, -60° and +60° ply matrix cracks in all remaining 60° plies. The very long cracks are at the surface in the +60° plies.

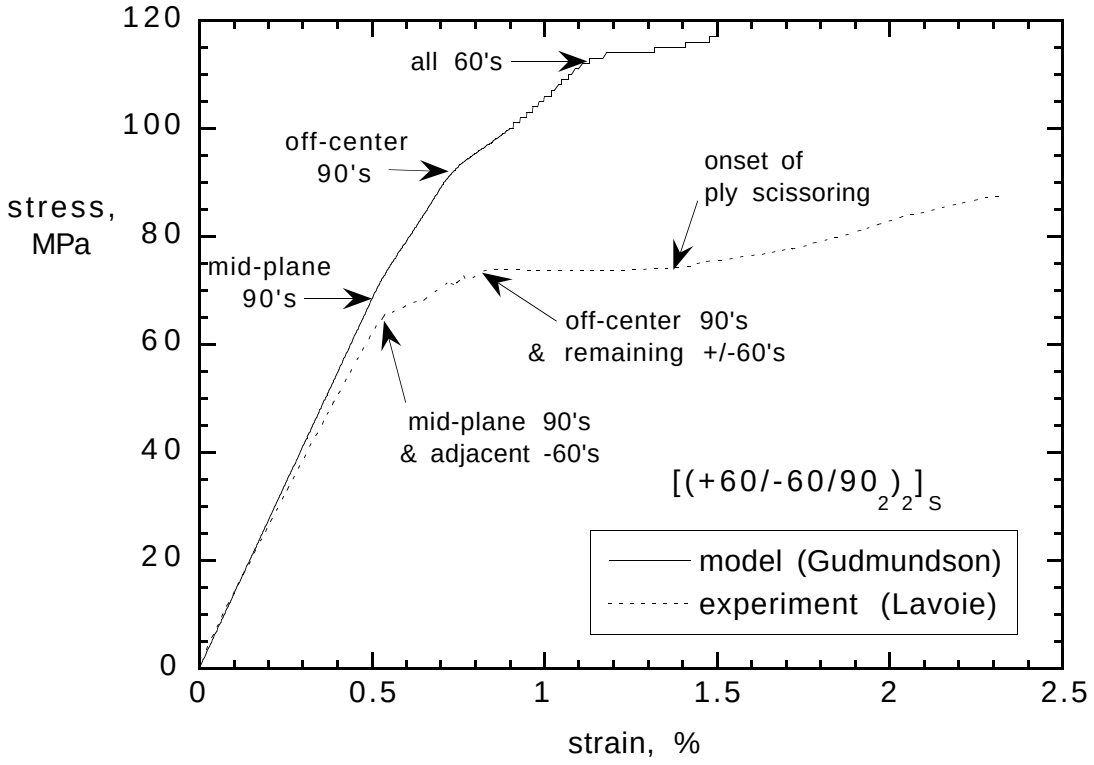

Figure 20. Modeled (solid line) and actual (dashed line) stress-strain response of the sublaminate-level scaled $[(+60/-60/90_2)_2]_s$ layup. Arrows indicate the onset of matrix microcracking in the various plies, or ply groups.

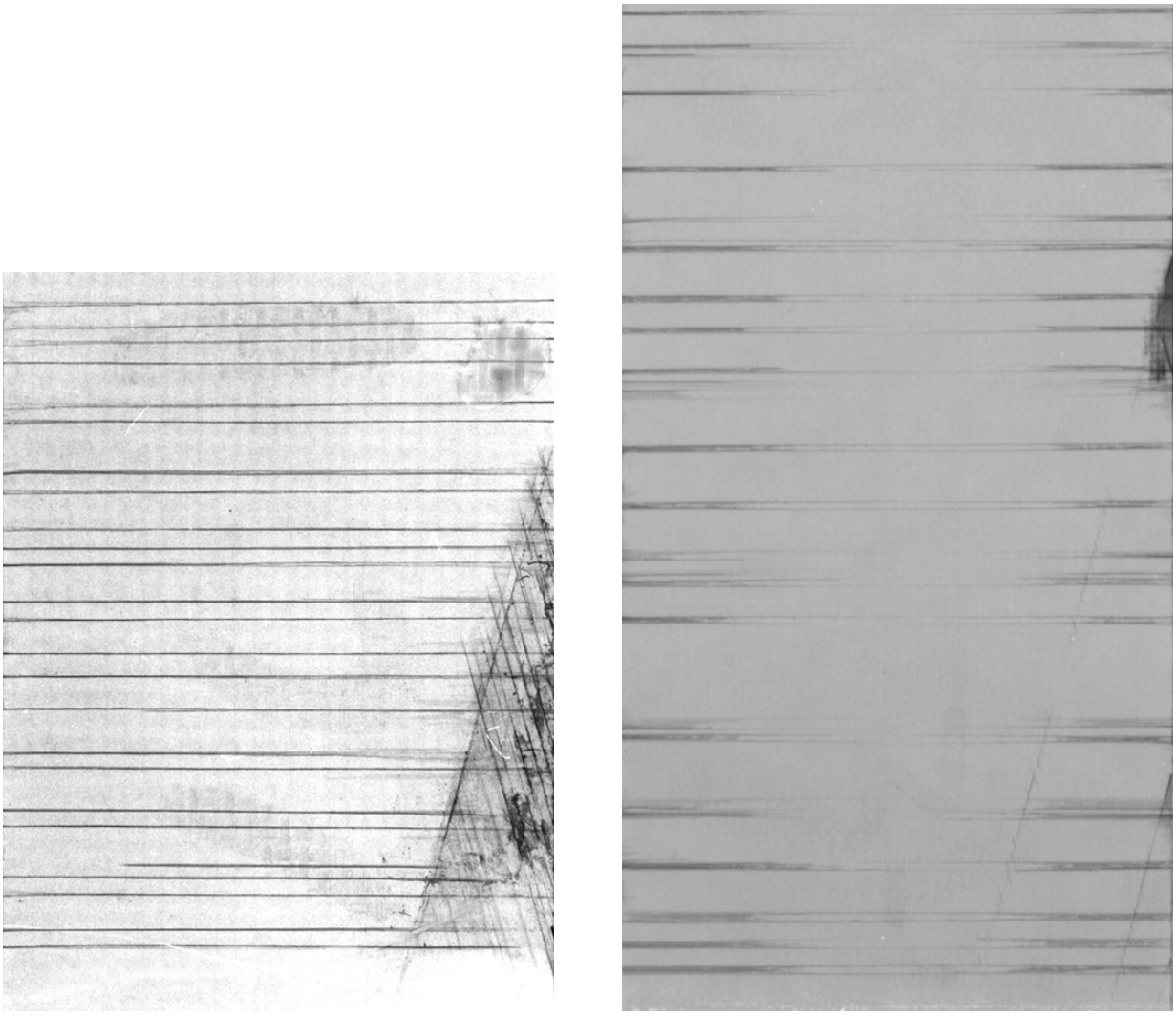

(a) (b)

Figure 21. An x-ray of a captured +15° delamination in an (a) n=1 size $[+15/-15/90_2]_s$ layup, loaded to 398 MPa. (b) n=3 size $[+15_3/-15_3/90_6]_s$ layup, loaded to 192 MPa.

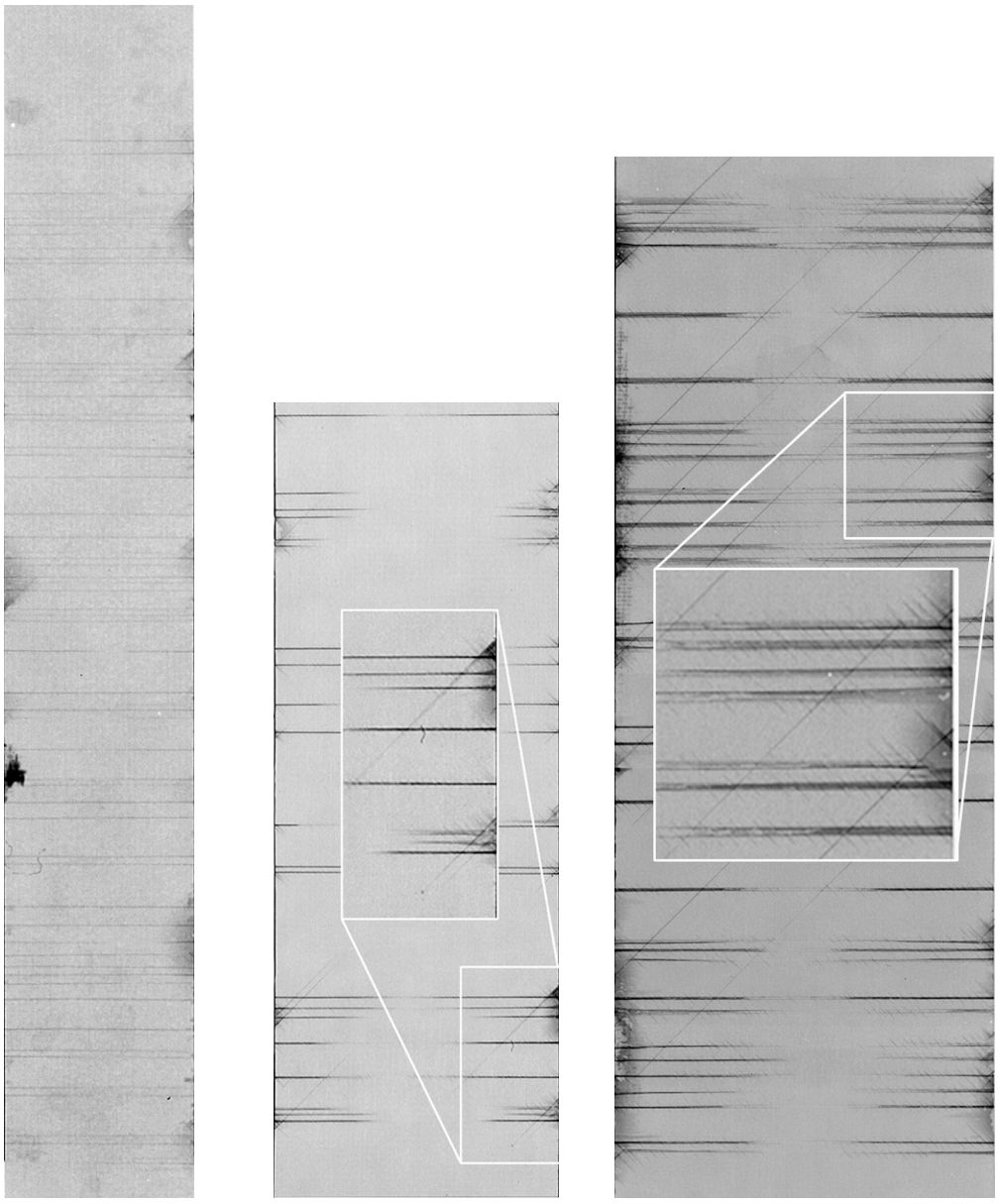

(a) (b) (c)

Figure 22. Three sizes of $[+45_n/-45_n/90_{2n}]_s$ shown at stresses very near their respective failure stress. Several +45° delaminations appear before ultimate failure in (a) n=1 size at 147 MPa, and 105% of average failure stress in (b) n=2 size at 103 MPa, or 123% of average failure stress, and in (c) n=3 size at 69 MPa, or 87% of average failure stress.

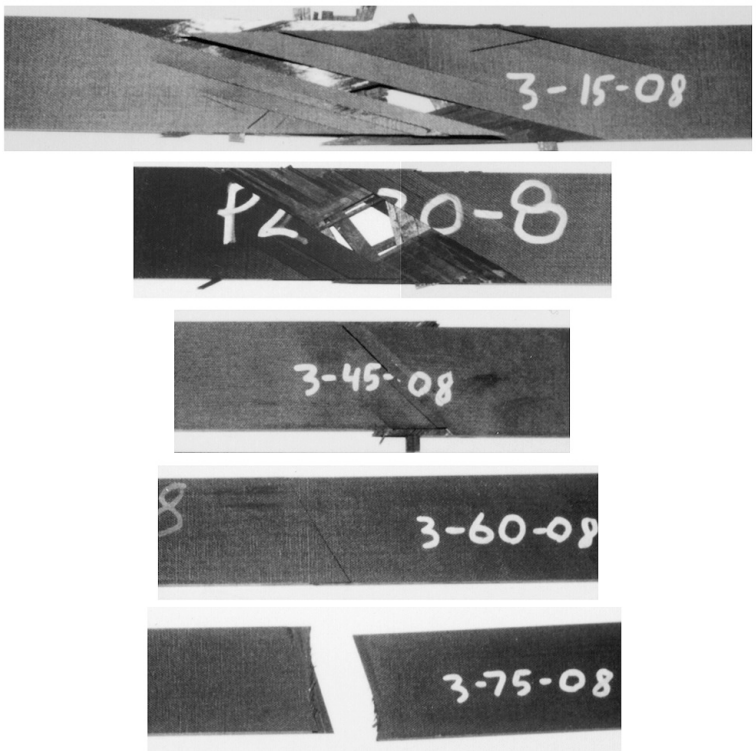

Figure 23. Photographs of failed $[+\theta_3/-\theta_3/90_6]_s$ laminates.

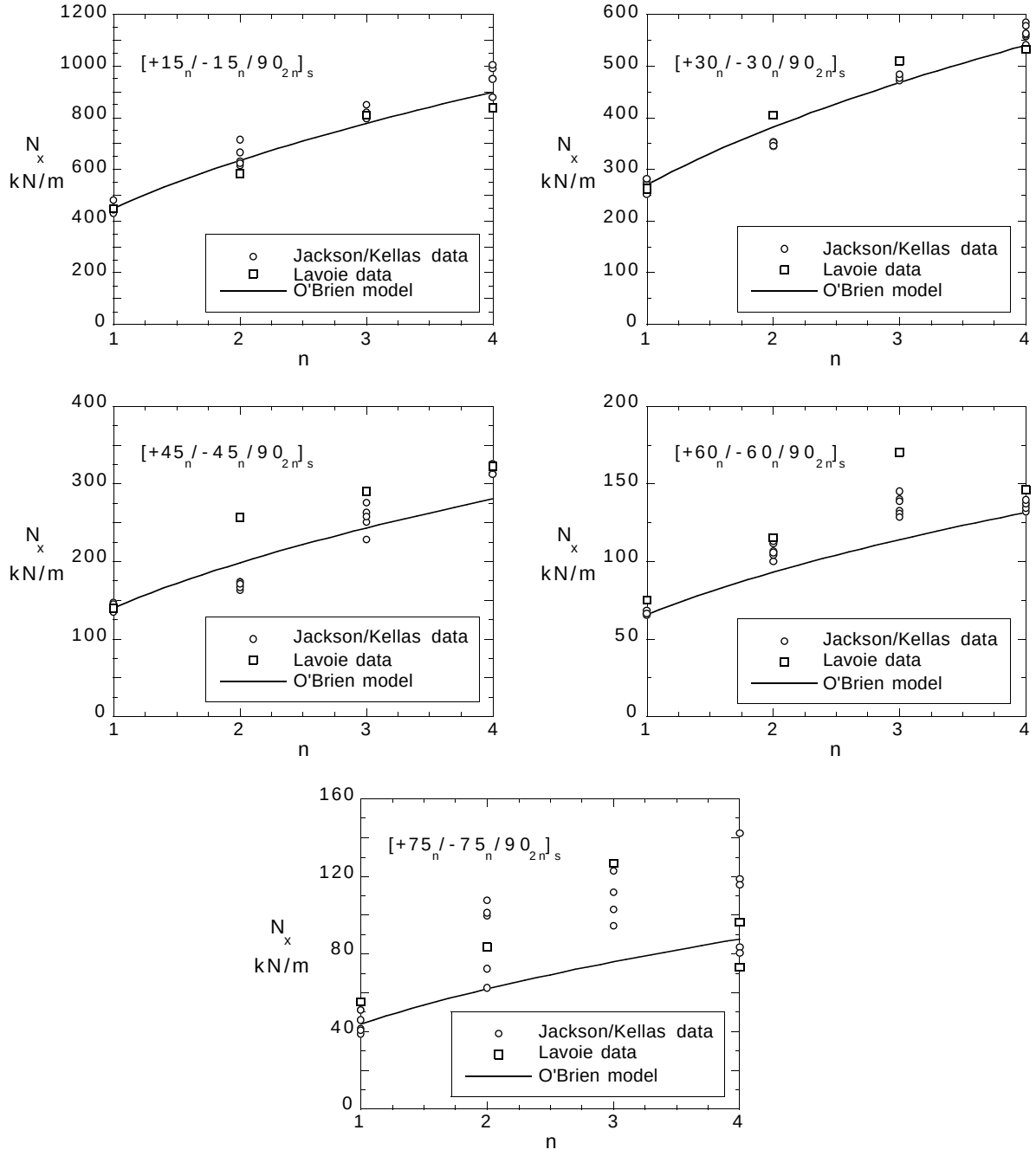

Figure 24. The strength scaling (displayed as a force-resultant) of $[+\theta_n/-\theta_n/90_{2n}]_s$ AS-4/3502 carbon/epoxy laminates is effectively predicted using a strain-energy release rate model for delamination. Experimental data from Jackson and Kellas (1993) (circles), one year later by Lavoie (diamond), and O'Briens (1993) model (line).

Part II

Strength Scaling of Composite Laminates Amidst Invariant 0° Ply Strength

Abstract

The effective tensile strength of the 0° plies within different cross-ply, and quasi-isotropic laminates of varying size and stacking sequence is investigated. For those layups having failure confined to the gauge section, no size effect was observed in the strength of 0° plies. In laminates exhibiting a size-strength relationship, failures were observed to occur in the gauge section for the smallest laminates, and at the grip for the larger laminates. There existed, apparently, a size-dependent laminate-grip interaction, manifested as an increasing stress concentration in the 0° plies at the grip as the laminate size increased.

A large number of 3-point bend tests of unidirectional beams were conducted to obtain valid parameters (Weibull modulus and strength) for a Weibull model, which would be used to predict the ultimate strength of 0° plies within different cross-ply and quasi-isotropic laminates. No significant difference between the maximum stress in bending or tensile strength of valid tests was found. Weibull statistics-based strength theory predicted unidirectional strength loss of over 30% for the range of volumes tested. Strength scaling of laminates containing 0° plies was shown to exist without concomitant scaling of unidirectional strength. The observations made lead to discussion on the measurement of unidirectional strength, and conclude with suggestions for developing guidelines for design of laminates for that purpose.

Keywords: strength scaling, size effect, Weibull statistics, tension testing, bend testing, mechanical testing, composite materials, fiber reinforced materials, carbon epoxy.

1. Introduction

The issue of size-related strength scaling in structural composite materials has become a growing concern in recent years. Unlike metallic materials, use of advanced composites is comparatively recent, but growing. Their design and stress analysis are much more complex than for metals. But few universities have expertise with composites, and industry is very much in a learning phase with regard to cost efficient manufacturing. Until the strength scaling issue is clarified, designers will be forced to specify excessively large safety factors, and will need to conduct more of the costly, full scale structural tests than might otherwise be necessary. Some

recent articles have reported large strength scaling in composite laminates with 0° plies, see Kellas and Morton (1992), Jackson, Kellas, and Morton (1992), and Jackson and Kellas (1993). The purpose of this investigation was to determine whether the strength of composite laminates containing 0° plies is a function of specimen size, and if so, what conditions and/or influences cause the strength-size effect.

Literature on the subject of size effects and strength scaling is sparse relative to other specializations. A compilation of some current investigations on strength size effects provides a broad picture of the diverse topics that fit under the general topic area of size effects, Jackson (1994). The focus of the present work is narrowed to size effects related to tensile strength. A sense of the ongoing debate can be found when Edge (1994) rejects most of the cases cited by Zweben (1994) as evidence of possible size effects.

Statistics-based models have been used to account for size effects in strength for samples of very different size. Batdorf (1989) discusses strength as governed by probability theory and statistics. He cites relevant works, should the reader be interested in pursuing those topics further. Weibull's statistics-based strength theory (hereafter referred to as Weibull theory) has been used successfully with brittle materials such as glass, Weibull (1939). In such brittle, monolithic materials, there is a distribution of defects with distributed size, which cause the strength to vary in a way that fits a Weibull distribution. The Weibull theory was extended to unidirectional composite materials because the stress-strain response often resembles that of brittle materials, and the strength exhibited significant scatter. However, the diameter of individual fibers is constant, which limits the maximum size of the defects. Regardless of the size of the composite structure, the defect size is limited by the fiber diameter, hence this extension of Weibull theory is questionable. Another issue regarding use of the Weibull theory is whether the scatter in strength of the unidirectional material in a series of bend tests (characterized by an exponent called the Weibull modulus) can be used to predict the tensile strength variation with size. Perhaps the question should be: is Weibull theory applicable at all to fibrous composites?

Bullock (1974) used Weibull theory to correlate unidirectional tensile strength with strength in 3-point flexure, and found agreement to be excellent. Whitney and Knight (1980) found that strength variability differed between tensile coupon data and flexure data, which was not in accordance with Weibull theory. They raised questions about specimen preparation and the test methods as possible contributors to data scatter. They found from 0% to 3% difference in strength for two sizes of flexure specimens. With regard to the tensile strength scaling observed by Whitney and Knight (1980), Wisnom suggested that the variability of strength in tension tests may arise from sensitivity to gripping and tabbing methods. Wisnom tested unidirectional laminates of different lengths in 3-point bending, Wisnom (1991a), and different thicknesses in 4-point bending, Wisnom (1991b). In both cases, variability in bending was less than expected, based on the strength scaling observed. He also observed that the number and frequency of failures

initiating on the compression side at the loading nose increased as the thickness increased. From observation of the brush-like appearance of failed specimens, Wisnom (1992) postulated that longitudinal splitting occurs which reduces the laminate into bundles of fibers, and developed a model which predicted a gentler size-strength scaling effect. Jackson, Kellas, and Morton (1992) studied unidirectional beams (and other laminates) under eccentric compression, a loading which produced very large bending and end displacements. They observed a large size effect on the strength and strain at failure.

Another use of Weibull theory scrutinized in the current work is the method for determining the Weibull modulus. The Weibull modulus is a parameter in the Weibull distribution which provides a measure of the scatter in a set of data. Weibull strength theory relates the strength of two sizes of test specimens using the Weibull modulus, and works well for monolithic brittle materials. In several works, the Weibull modulus was computed from the strength data of two sizes of test specimens, the motivation being that the number of test specimens is usually restricted. This approach is shown not to work.

Strength size effects have been reported for multi-directional laminates. O'Brien (1982) studied the delamination-prone quasi-isotropic laminate $[+45_n/-45_n/0_n/90_n]_s$. He was able to predict the strength of a 16-ply (n=2) laminate, from the strength of an 8-ply (n=1) laminate. This result was achieved using knowledge of how laminate stiffness changed with increasing strain, and the observation that both size of laminates had the same failure strain. Kellas and Morton (1992), and Jackson and Kellas (1993), examined the same stacking sequence, and tested thicknesses corresponding to n=1 through n=4. Both found a large strength size effect, and a large reduction in strain to failure for the larger laminates. They also tested $[90_n/0_n/90_n/0_n]_s$ ply-level scaled cross-ply laminates, and found little strength scaling. Johnson (1994) found that sublaminate-scaled cross-ply $[90/0/90/0]_{ns}$, and quasi-isotropic $[+45/-45/0/90]_{ns}$ laminates did not exhibit strength scaling. An exception was noted for the 8-ply (n=1) quasi-isotropic laminate which developed a stiffness-reducing delamination. The present work describes a research project that addresses the strength-size effect in composite laminates containing 0° plies loaded in tension until ultimate failure.

The current work relied heavily upon experimental data taken from the literature, in combination with the new experimental work to improve understanding of the origins of strength scaling of polymer matrix composite laminates containing 0° plies. The experimental results provide a case against the existence of a volume size effect in the tensile strength of unidirectional carbon/epoxy composite material. The tensile strength scaling observed by other researchers, and duplicated here in part, was real, and originated in the nature of the test method and the laminate stacking sequence. Failure analysis pointed to a size-dependent laminate-grip interaction peculiar to particular laminate stacking sequences. Said differently, the layups which exhibited a large strength scaling effect tended to fail in the gauge section for the smallest (thinnest) size, and at the grip for the larger (thicker) sizes. For the various laminates in which the tensile strength did not

depend on size, specimens fractured within the gauge section. Three-point bend testing of unidirectional beams was conducted and the strength was remarkably close to that of the valid tension tests. There was, however, need to reject a large portion of those data because of bearing failures, which cast doubt upon the reliability of that method for obtaining unidirectional strength.

2. Materials And Specimens

The composite material used for this study was 0.125 mm thick unidirectional carbon/epoxy prepreg: Hercules Magnamite AS-4/3502. Laminates were cured at 177°C. A variety of laminates were fabricated, including four unidirectional laminates of $[0]_{8n}$, four ply-level scaled cross-ply laminates of $[0_{2n}/90_{2n}]_s$, and four ply-level scaled $[+45_n/-45_n/0_n/90_n]_s$ quasi-isotropic laminates, where n= 1,2,3, or 4. The specimen dimensions are given in Table 1. In this study, two methods of building up a laminate thickness are encountered. Blocking together of plies with the same orientation is called ply-level scaling. Alternatively, repeated layering of a base stacking sequence is called sublaminate-level scaling. The advantage of sublaminate-level scaling is that plies of similar orientation are dispersed. Unless stated otherwise, the specimens were scaled geometrically, that is, length and width were also scaled according to the scale factor, n. Tension test results for the same AS-4/3502 carbon/epoxy with stacking sequences of $[90_n/0_n/90_n/0_n]_s$ and $[+45_n/-45_n/0_n/90_n]_s$ (n=1,2,3, or 4) from Kellas and Morton (1992), and of $[90/0/90/0]_{ns}$ and $[+45/-45/0/90]_{ns}$ (n=1,2,3, or 4) from Johnson (1994), were analyzed and compared with the present results. Specimens ends were covered with a 100 grit cloth. This procedure was intended to protect the fibers from damage by the grip face, and was allowed according to the applicable ASTM standard D3039/D3039M-95a.

Three types of end tabs were applied to a second set of quasi-isotropic laminates of stacking sequence $[+45_n/-45_n/0_n/90_n]_s$ where n=1, and 2. The in-plane dimensions were fixed to 290 mm x 25 mm. This battery of tensile tests were intended to reveal whether it was the nature of the end tab, or a peculiarity of the stacking sequence, which was responsible for the severe strength-scaling observed by Kellas and Morton (1992), and Jackson and Kellas (1993). Table 2 shows which tabs were used on each specimen. The 100 grit cloth tab was compared with a 1 mm thick aluminum tab, and a glass/epoxy tab. Both were bonded to the specimen using an epoxy adhesive. The composite end tabs were given a 10:1 taper using a wet grinding wheel.

Both hydraulic and hand-tightened wedge-action grips were used to introduce the tensile load into the specimen. The hydraulic pressure delivered to the grips was chosen using a formula provided by MTS Corporation for their grips, and was based upon the maximum expected tensile load and the model of grip used. The objective was to provide enough grip clamping force to prevent slippage, but no more. The hand-tightened grips were also clamped just firmly enough to avoid slippage.

Ninety-three unidirectional specimens were fabricated from the $[0]_{32}$ laminate and tested in 3-point bending to determine the statistical strength distribution of the AS-4/3502 composite material. Specimens were nominally 4.48 mm thick, 145 mm long and 11.75 mm wide. Specimens were machined from flat panels using a high speed diamond saw with a 50/50 mix of water and ethylene glycol coolant. This machining operation resulted in constant width specimens having very smooth cuts. The gauge length for the 3-point bend test was 101.6 mm. The 3-point bend fixture was manufactured by Instron for use in a universal test machine running in tension mode, a sketch appears in Figure 1. The center loading nose (a cylindrical pin making line contact) moved at a rate of 5 mm per minute. A piece of 100 grit cloth placed between the pin and specimen did not eliminate compression-side bearing failure, indeed, just over half failed in the tension side. All bearing failures were rejected.

3. Analysis

3.1. PREDICTION OF 0° LAMINAE STRENGTH USING WEIBULL THEORY

Use of Weibull theory to predict volume-dependent strength requires the stress distribution throughout a reference volume of material, and a statistically significant sample of strengths for that volume. Then, if the stress distribution of a larger (or smaller) volume of material is known, the strength can be predicted. The probability that a material can survive a stress distribution $\sigma(x,y,z)$ throughout its volume, V, is given by Weibull (1939) as

$$P_s = \exp\left\{-\int_V \left(\frac{\sigma(x,y,z)-\sigma_u}{\sigma_0}\right)^m dxdydz\right\} \tag{1}$$

where σ_u is the threshold stress below which the material will never fail, and was set to zero here (some researchers use it as an adjustable parameter). The Weibull modulus, m, represents the slope of the distribution on a semi-log plot. It is also called a flaw-density exponent because it is a measure of the scatter in the strength data. The failure stress of maximum frequency is σ_0 and it occurs, for the Weibull distribution, at a probability of survival $P_s = e^{-1}$, or $\ln(-\ln(1-P_f))=0$.

For the tensile test, the stress distribution in the 0° plies was assumed to be constant, and is denoted as σ_t. This assumption is conservative because stress risers due to edge effects, grip region stress concentration, and cracked neighboring plies, were ignored. The volume, V_t, for the tensile specimens was the volume of the 0° plies inside the gauge section. Equation 1 then takes the form

$$P_s \, exp\left\{-V_t\left(\frac{\sigma_t}{\sigma_0}\right)^m\right\}. \tag{2}$$

For the non-uniform stress distribution in the 3-point bend test, Equation 1 becomes

$$P_s = exp\left\{-\frac{V_f}{2(m+1)^2}\left(\frac{\sigma_f}{\sigma_0}\right)^m\right\}, \tag{3}$$

where σ_f is the peak tensile stress at the midspan of the beam. The volume chosen for the flexure test, V_f, was the usual (thickness*width*length)/2. The factor, $[2(m+1)^2]^{-1}$, has the effect of transforming the volume in flexure with a gradient on stress, into an equivalent volume in tension under uniform stress. Given the same probabilities of failure in flexure and in tension, Equations 2 and 3 are set equal to each other and solved for the tensile failure stress, σ_t, in terms of the flexure stress, σ_f, the Weibull modulus, m, and the ratio of volumes in flexure and tension as follows:

$$\sigma_t = \sigma_f\left(\frac{1}{2(m+1)^2}\frac{V_f}{V_t}\right)^{\frac{1}{m}}. \tag{4}$$

The strength data is fit to a Weibull distribution using the following probability of survival function:

$$P_s=1-P_f=\exp\left[-\left(\frac{\sigma}{\sigma_0}\right)^m\right], \tag{5}$$

or

$$\ln[-\ln(P_s)]=m(\ln\sigma-\ln\sigma_0), \tag{6}$$

where strength data are represented by σ. The strength data must be ordered, beginning with the lowest failure stress, and each data point assigned a probability of survival, P_s. Equation 7 was used to rank the strength data. The sample size is N, and the sample number, n, starts from 1.

$$P_s=1-\frac{n-0.3}{N+0.4}, \tag{7}$$

3.2. CALCULATION OF STRESS IN THE 0° PLIES

The ultimate stress in the 0° plies at ultimate tensile failure, $\sigma_{ult.}^{0^o}$, was computed by the stiffness ratio method. The ultimate tensile stress of the laminate, $\sigma_{ult.}^{lam.}$, the tensile modulus of the

unidirectional plies, E^{0^o}, and the secant modulus of the laminate at failure, E_{sec}^{lam}, were needed. The equation was

$$\sigma_{ult.}^{o^o} = \sigma_{ult.}^{lam.}\left(\frac{E^{0^o}}{E_{sec.}^{lam.}}\right) \tag{8}$$

The secant modulus accounts for the stiffness loss due to damage such as matrix cracking and delamination. Because there is no plasticity, it was common to observe that strain returned to zero when the specimen was unloaded, see Hahn and Tsai (1974). In actual practice, the laminate strain at failure was simply multiplied by the modulus of the 0° plies:

$$\sigma_{ult}^{0^o} = E^{0^o}\varepsilon_{lam}. \tag{9}$$

The assumption was made that the strain in the 0° plies was the same as the laminate strain, and that this could be measured using strain gages or clip-on type extensometers. The presence of local effects, such as delamination or cracking in surface plies, can render the strain readings spurious if care is not taken when selecting the type of strain measuring instrument.

3.3. CALCULATION OF MAXIMUM STRESS FOR THE THREE-POINT BEND TEST

Failure of the beam initiates on the surface of the tension side, where shear stresses drop to zero. The maximum stress in bending is at the surface of the beam and can be calculated from beam theory, see Beer and Johnston (1981). The assumption from strength of materials, that plane sections will remain plane, will break down if the material exhibits nonlinearity in the elastic moduli. Composites are known to have bimodular behavior, that is, the lamina stiffness, E_{11}, increases slightly at high tensile loads, and decreases slightly for high compression loads. Sensmeier (1988) reported up to 13% difference in strain at the top and bottom of a 30-ply AS-4/3502 unidirectional beam. A nonlinear beam analysis is needed to calculate the maximum stress in bending, but this was not be done. Instead, the strength of materials expression was used.

$$\sigma_{max} = \frac{Mc}{I}, \tag{10}$$

where *M* is the bending moment, *c* is the distance from the neutral axis to the surface, and I is the moment of inertia. For a beam having a rectangular cross section the moment of inertia is $I=1/12bh^3$, where h is the depth, and b the width. In 3-point bending L is the distance between the outer pair of pin supports, and *P* the load on the center pin. The equation for the maximum stress in bending, σ_{max}, (referred to as σ_f in Equations 3 and 4) becomes

$$\sigma_{max} = \frac{3PL}{2bh^2}. \quad (11)$$

4. Results

In Section 4.1, the 3-point bend test results are described and an independent measure of the tensile strength of the unidirectional material established. In Section 4.2, tensile test results are described, indicating where appropriate, the source of the data. Results for each stacking sequence are described sequentially. The effect of specimen size on strength is determined, and reasons for any differences given. Then the flexure strength is compared with the tensile strength of the 0° plies. Also, size-dependent strength predictions made using the Weibull theory are compared with the experimental data. In Section 4.3 the effect of width, and the effect of end tab, are investigated to better understand the source of the strong strength scaling effect in the ply-level scaled $[+45_n/-45_n/0_n/90_n]_s$ laminate, and determine whether the strength scale effect is a material property related with volume, a geometry effect related to width, a thickness effect, or a test method problem.

4.1. THREE-POINT BEND TESTS

Of the 93 tests conducted, 51 specimens fractured in tension. A typical failed 3-point bend specimen is shown in Figure 2. Considerable delamination was in evidence, there was also splitting. The fracture surface was rough and fibrous, and fracture propagated through half the thickness, catastrophically. The remaining 42 specimens suffered bearing failure, which initiated on the compression side just under the pin. The bearing failure manifested itself as a brittle fracture which propagated through just over half the thickness, followed by tensile failure of the remaining cross-section. These failures were also catastrophic. The fracture surface of the brittle fractured portion was smooth and scalloped, without delaminations. The location on the panel from which each specimen was machined had been recorded. The 42 specimens exhibiting bearing failures were concentrated nearer to the center of the panel from which they were cut, where the thickness (and resin content) were greatest. Specimens with bearing failure were not used to compute either the Weibull modulus or the characteristic strength. There is some concern that the failures were almost equally likely to occur in tension or in bearing due to the contact stress from the pin.

Nonlinearities in the stress-strain response in tension and compression will render the stress calculation used in Equation 11 in error. The load-deflection response was nearly linear, but a slight oscillation was observed. A typical 3-point bend load vs. midspan displacement plot appears in Figure 3. The probability of survival versus strength is plotted in Figure 4, along with the fitted Weibull probability of survival function, Equation 6. The 51 valid 3-point bend tests yielded a Weibull modulus, m=29.3, and a characteristic strength, σ_0= 1974 MPa. The

manufacturer reported an average tensile strength of 1846 MPa. The work of Sensmeier (1988), on measuring true strains on the tension and compression sides of a beam in bending might be used in a nonlinear beam analysis to compute a more accurate characteristic strength value than offered here.

4.2. TENSILE TEST RESULTS WITH COMPARISON TO WEIBULL PREDICTION

In all cases the specimens were tested using a grit cloth instead of end tabs, the exception being the investigation into effect of end tab on strength. The failed test specimens of Jackson and Kellas (1993) were examined because of the large number of specimens available. The test specimens from the studies of Kellas and Morton (1992), and Johnson (1994) were not generally available for inspection, so their papers were relied upon for information about the specimen fracture morphology. Some definitions of the various locations for failure are described here. The grip region equals 0.075*L, where L is the total specimen length. Gauge section failure was defined as fracture having occurred greater than one specimen width from the grip. An "at grip" failure occurs exactly 0.075*L from the specimen end. A failure occurring under the grip occurs a distance less than 0.075*L from the specimen end. After related groups of tensile tests are described, for each size and layup, 0° ply strength versus volume of 0° plies is plotted. The bending strength and the Weibull prediction of the decline in strength with increasing volume is included on the same plot. Several tables report both laminate strength and the computed 0° ply strength. Also, all plots which have a Weibull prediction curve are comparing the 0° ply stresses and not the laminate stress. It may be helpful visually, to refer to Figures 6, 7, and 11 when reading through sections 4.2.1, 4.2.2, and 4.2.3, respectively.

4.2.1. Tensile Tests of $[0]_{8n}$ and $[0_{2n}/90_{2n}]_s$

Unidirectional $[0]_{8n}$ The unidirectional tensile test data of Jackson and Kellas (1993) appear in Table 3. The average tensile strength of the unidirectional $[0]_{8n}$ specimens was 1539 MPa for the smallest (n=1) specimen, and 1322 MPa for the largest (n=4) specimen; a drop of about 14%. Failure location for each specimen is documented in Table 4. Fractures always ran across the width, and were invariably either under the grip, or at the end of the grip. The exceptions were two of twenty-four specimens which failed within one specimen width of the grip. Thickness gradients across the width of the gripped region as small as 1% were indicated by a residue of grit and adhesive stuck tenaciously to the specimen in the thickest zones. The increased pressure might be expected to increase the amount and/or likelihood of damage to the fibers by the particles bonded to the grit cloth. It was not difficult to find evidence that this had happened. The only marks were impressions from the grit in the resin layer at the surface of the specimen. On some specimens, these pinpoint marks were elongated into scratches located just under the grip, where the grip terminates. However, it remains uncertain that this fiber damage in the grip region was also responsible for failure initiation.

Cross-Ply $[0_{2n}/90_{2n}]_s$ The cross-ply tensile test data of Jackson and Kellas (1993) appear in Table 5. Except for three gauge section failures of the n=1 specimens, all failures were at the grip, as documented in Table 6. The average stress in the 0° plies, at laminate failure, of the n=1 specimens was 1713 MPa, and dropped by about 17% to 1410 MPa in the n=4 specimen size. The plot shown in Figure 5 shows typical stress versus strain traces for the different sizes of cross-ply laminates. Delamination occurs for this layup, and may account for the nonlinearities.

From the mean strength in flexure, σ_f=1974 MPa, and a Weibull modulus, m=29.3, the Weibull strength prediction versus volume was plotted along with the tensile test data for unidirectional $[0]_{8n}$ and cross-ply $[0_{2n}/90_{2n}]_s$ specimens, in Figure 6. The Weibull strength prediction was somewhat higher than the data, but the rate of strength decline with volume was similar. Recall, however, that the tensile testing resulted, almost without exception, in grip region failures.

4.2.2. Tensile Tests of $[90_n/0_n/90_n/0_n]_s$, $[90/0/90/0]_{ns}$, and $[+45/-45/0/90]_{ns}$

Cross-Ply $[90_n/0_n/90_n/0_n]_s$ The ply-level scaled cross-ply tensile test data of Kellas and Morton (1992) appear in Table 7. Average failure stress, and strain at failure are given. There is a 2% drop in strength from the n=1 to n=3 size, and another 4% from n=3 to n=4. The surface 90° plies protect the 0° plies against potential fiber damage by the grips. It is important to note that such protection was absent for the unidirectional and $[0_{2n}/90_{2n}]_s$ cross-ply laminates. This protection eliminated potential for damage due to grit particles, and in effect acted as co-cured end tabs. Judging from the figures given by Kellas and Morton (1992), the fractures appear to have been confined to the gauge section in the n=1, 2, and 3 size specimens. The n=4 specimen appears to have a brush-like failure.

The experimentally recorded strain data exhibited variability that did not correspond with the laminate strength data, specifically, the strain data were too low. This problem was recognized by Kellas and Morton (1992). The axial stiffness of cross-plied carbon-epoxy laminates is not very sensitive to matrix cracking. Also, since no delamination was observed in the x-rays taken of the specimens, it is unlikely that the strain actually varied with size to the same extent as reported in Table 7. It matters that the strain data be reasonably accurate, because the stress in the 0° plies at failure was computed by multiplying the laminate strain at failure by the modulus, E_{11}, of the 0° plies. Specifically, the laminate strengths differed by 6% between the n=1 and n=4 sizes, but a 32% difference in strain was reported, which is translated directly into a 32% difference in the 0° ply stress at failure. This scrutiny was to justify adjusting the strain data. It was assumed that the value of 1.38% for the n=1 size was correct, and that the laminate stiffness for the other three sizes (n=2,3, and 4) was the same. Based upon those assumptions, the failure strain of the n=2,3, and 4 sizes could be adjusted. Both sets of strain data, reported and adjusted, are given in Table 7.

Cross-Ply $[90/0/90/0]_{ns}$ Gauge section failures were observed for all specimens of this stacking sequence tested by Johnson (1994). Data appears in Table 8. No volume related strength scaling trend was discernible. There was little scatter in strength for any particular size laminate, but among the different sizes, the variability in strength created a broad band.

Quasi-Isotropic $[+45/-45/0/90]_{ns}$ Specimens with varying lengths, widths, and thicknesses were tested by Johnson (1994). Tensile test results appear in Table 9. From the photographs of Johnson (1994), and after discussion with him, it was confirmed that specimens of all sizes failed in the gauge section. Notice from Table 9, that the strength of the 8-ply (n=1) layup was lower than the strength of n=2,3, or 4 layups. The lower strength of the n=1 layup was explained by lower stiffness, due to extensive delamination, as described earlier by O'Brien (1982). He found that for laminate failure that was controlled by the failure strain of the 0° plies, the more compliant (delaminated) laminate failed at a lower stress. Similarly, Johnson (1994) found that as long as delamination was avoided, strength scaling was avoided, for this stacking sequence. Unfortunately, the strain data varied significantly, though the strength data did not. It was elected not to intervene and adjust Johnson's reported strain data, and as a consequence, the computed values of 0° ply strength varied significantly. From Table 9, the computed 0° strength data decreases with increasing volume for the first four volumes, then rises again for the next two. That variability doesn't follow any explainable trend, so these 0° ply strength numbers should be regarded as coarse estimates.

In Figure 7, the Weibull prediction is plotted with the 0° ply strength data for the three different types of laminates just described. A slight decreasing trend in strength with increasing volume can be discerned. However, by considering the scatter in the data, and the fact that the 0° ply strengths are coarse estimates, there is arguably no strength scaling in the 0° tensile strength. These data reside within a ±150 MPa band, and a group average 0° tensile strength of 1812 MPa. The manufacturer reported a tensile strength of 1846 MPa, and the 3-point bend strength was 1974 MPa, higher by 2% and 9%, respectively. The Weibull theory predicted a strength of about 1350 MPa for the largest volume of 0° material (about 98,000 mm^3); a decrease of 32%.

4.2.3. Tensile Tests of $[+45_n/-45_n/0_n/90_n]_s$

Kellas and Morton (1992), and Jackson and Kellas (1993) tested layups having n=1,2,3 and 4, and their data is repeated in Tables 10 and 11, respectively. The specimens from Jackson's study were available for post-test failure analysis, and the location of failure for each specimen is given in Table 12. For each size, midplane delamination over 90% of the width was the dominant damage form before ultimate failure, see Figure 8. All failures occurred in the gauge section for the 8-ply (n=1) specimens. The fracture end of the 8-ply specimen appeared compact, and tightly

constrained; but the largest size had a shattered appearance that was mainly due to splitting of the 0° plies and then debonding from the 45° plies, see a comparison in Figure 9.

The peak stress developed in the 0° plies of the 8-ply n=1 size laminates was roughly 1973 MPa (average of corresponding values from Table 10 and 11), while the characteristic strength in 3-point bending, σ_0, was 1974 MPa.

There was a tendency for failures to occur near the grip and at the grip for the 16-ply (n=2) specimens, and peak stress in the 0° plies at laminate failure dropped to about 1755 MPa. With few exceptions, the 24-ply (n=3) and 32-ply (n=4) specimens failed less than the width of the specimen from the grip, with many failures at the grip, see Figure 10. The 0° ply peak stresses were averaged to 1440 MPa and 1300 MPa, for the n=3, and n=4 sizes, respectively. From the n=1 to the n=4 size, both strength and failure strain dropped by 40%.

The failure stress of the 0° plies, at laminate failure, were plotted, along with the 3-point bend strength, in Figure 11. The solid line, originating from the triangular symbol, is the Weibull prediction made based on the bend test data. The rate at which the strength was predicted to decline with increasing volume was controlled by the Weibull modulus, m. From the bend tests, m was found to be 29.3. However, the strength data in Figure 11 indicate a much sharper decline in strength with increasing volume. The line running through these data is a curve fit, as discussed next.

The Weibull modulus for the 0° tensile strength was also computed from the data for two sizes of specimens, instead of using a statistically significant data set as was done for the 3-point bend tests. From Equation 2 the expression to use would be: $(V_1/V_2) = (\sigma_2/\sigma_1)^m$. For illustration, the volumes and corresponding strengths for the n=1 and n=4 sizes in Table 11 are used. For n=1, $V_{n=1}$=383 mm^3, and $\sigma_{n=1}$=1992 MPa; and for n=4, $V_{n=4}$=24500 mm^3, and $\sigma_{n=4}$=1185 MPa. The Weibull modulus computed is 8, implying much higher scatter than was observed in either the tensile or 3-point bend tests. The backing out of the Weibull modulus from strength tests of different size specimens is clearly invalid.

4.3. WIDTH AND END TAB EFFECTS ON STRENGTH OF $[+45_n/-45_n/0_n/90_n]_s$ LAMINATES

4.3.1. Effect of Specimen Width on Strength

The tensile strength data of the $[+45_n/-45_n/0_n/90_n]_s$ quasi-isotropic layup for various widths, and thicknesses (values for n) are given in Table 13, and plotted in Figure 12. The purpose of these tests was to establish clearly that thickness was the dimension responsible for the strength scaling, and to eliminate volume as a strength scaling parameter. Initially, tests of this layup were

conducted for n=1, 2, 3, and 4, by Kellas and Morton (1992), and repeated by Jackson and Kellas (1993). Their specimens were geometrically scaled, see Table 1 for dimensions. Surplus 50 mm wide n=4 size specimens, from Jackson and Kellas' study, were machined into 12.5 and 25 mm widths. A new, n=1 size laminate was fabricated and specimens cut to 25 x 290 mm. Tensile tests were then conducted on specimens having uniform in-plane dimensions of 25 x 290 mm, with n=1, 2, and 4. There were four repeated tests for each condition. Strength was found to vary with n in much the same way for these fixed-width specimens as they did for the laminates scaled in three dimensions, see Table 13. For the case of fixed n (n=4) and widths varying as 12.5, 25, and 50 mm, no significant effect of width on strength was noted. Failure of the n=2 and n=4 specimens were grip region dominated, despite the protection afforded to the 0° plies by the ±45° plies.

4.3.2. Effect of End Tab on Strength

The strength of the $[+45_n/-45_n/0_n/90_n]_s$ quasi-isotropic layup has been shown to drop considerably for thicknesses having n >1. The failure analysis pointed to a transition from gauge section failures for n=1 specimens, toward grip failures for n>1. It was thought that experimenting with different end tabs might reduce the grip region stress concentration that apparently caused failure to predominate in the grip region. In this way, the strength scaling might be eliminated. Aluminum and glass/epoxy composite end tabs were used, in addition to the grit cloth tabs. Table 2 gives details about the material and dimensions of the end tabs. The two laminates tested were 8-ply (n=1) and 16-ply (n=2). Only two tests for each type of specimen and end tab were conducted. Strength data appear in Table 14.

Note that the aluminum tab protruded by about 10 mm from under the grip, and debonded from the specimen at high load. Also, it was impossible to apply grip pressure to the tapered portion of the composite tab. In each case the tapered portion of the composite tab delaminated from the specimen up to the point where grip pressure was applied. Failure for the specimens with grit cloth or aluminum tabs occurred less than one specimen width from the grip. The strength was not notably different between specimens having aluminum tabs or the grit cloth tab. However, the strength of the specimens having the composite tab was substantially lower. The location of failure was not simply near to the grip but was at the grip, where the clamping action ended. The strength of n=1 and n=2 composite-tabbed specimens was 17% and 35%, respectively, below those having aluminum or grit cloth tabs.

5. Discussion

5.1. GRIP FAILURES IN THE $[0]_{8n}$ AND $[0_{2n}/90_{2n}]_s$ SPECIMENS

The majority of failure locations were at the grip for the unidirectional and cross-ply $[0_{2n}/90_{2n}]_s$ layups. These layups had 0° surface plies, and were gripped with a grit cloth between the specimen and grip face. O'Brien and Salpekar (1993) used a finite element model to estimate the stress concentration in the grip region. The boundary condition they used to simulate the grip was fixed displacement of the butt end of the specimen (which is not the same as fixing the displacement of the gripped face, and applying a compressive gripping force). They found a stress concentration about 17% above the far-field stress. Given their results, it would be surprising if these layups did not fail very close to the grip. However, failure *at* the grip, almost without exception, suggests that damage to surface fibers by the particles in the grit cloth should not be ruled out. It is recommended that grit cloth not be used in place of end tabs when 0° plies are present at the surface. Regardless of how widely this recommendation is already known, a reading of the latest ASTM standard (D3039/D3039M-95a) could be interpreted as permitting the use of grit paper/cloth in place of end tabs when testing undirectional composite.

5.2. STRESS CONCENTRATION DUE TO 90° MATRIX CRACKS

Cracks in the 90° plies act to raise the stress in adjacent 0° plies, and have been shown by Jamison, Schulte, Reifnsider, and Stinchcomb (1984), to cause fiber fracture early in the fatigue life. They also found that the number of broken fibers did not increase because of the development of local delamination at the 0°/90° interface in the vicinity of the crack. At loads close to failure in the quasi-static tension test, the same local delaminations appeared. This may explain why there was no detectable effect on 0° ply strength from stress concentration induced by matrix cracks in adjacent 90° plies. The assertion was based upon comparison of the laminate strengths of the ply-level scaled $[90_n/0_n/90_n/0_n]_s$ layup (Table 7) with the sublaminate scaled $[90/0/90/0]_{ns}$ layup (Table 8). The former has increasing 90° ply block thickness, while in the latter there is no change with size. It was sometimes difficult to make comparisons between data sets, even when the stacking sequence, material and test method was the same. The strength of the 8-ply (n=1) laminate of Kellas and Morton (1992) was about 70 MPa below that of the same laminate tested by Johnson (1994). If one data set was adjusted by 70 MPa, then the percent difference in strength between similar size laminates was not significantly different. A sample calculation for the n=3 size gave: [(865.8 + 70) - 908]/908 = 3%. Thus, for n=1,2,3, and 4 the percent difference was 0%, -1%, +3%, and -7%. The last being -7% was a significant difference, and was in the correct direction to argue that thicker blocks of cracked plies next to the 0° plies could be having a measurable effect. However, the figures of representative failed specimens from Kellas and Morton (1992) suggest a tendency for grip region failures for the n=4 size (no explicit data was given on failure location).

5.3. ADJUSTMENTS MADE TO STRAIN DATA

Kellas and Morton (1992) noted considerable difficulty in recording correct strain near failure. This was apparent for the cross-ply $[90_n/0_n/90_n/0_n]_s$ and quasi-isotropic layup $[+45_n/-45_n/0_n/90_n]_s$ of Kellas and Morton (1992), and the quasi-isotropic layup $[+45/-45/0/90]_{ns}$ of Johnson (1994). The strain variability was not reflected in the strength data, nor in the damage developed by each layup, up to and including failure. Consequently, use of the reported strain data results in excessive variation in computed stress in the 0° plies. The strain data were adjusted in Table 7 and 10. The problem of strain measurement was most severe for the $[+45_n/-45_n/0_n/90_n]_s$ quasi-isotropic layup because delamination disturbed the clip-on extensometers that were used. Jackson and Kellas (1993) had used strain gages, placed at the midline of the specimen, where delamination never reached, so the recorded strain was more accurate.

5.4. STIFFNESS CHANGE, FAILURE STRAIN AND LAMINATE STRENGTH

O'Brien (1982) argued that because the failure strain for the two sizes of $[+45_n/-45_n/0_n/90_n]_s$ quasi-isotropic laminates that he tested was the same, then the difference in strength between the 8-ply (n=1) and 16-ply (n=2) laminates was due entirely to differences in the extent of delamination. Delamination significantly affected the laminate stiffness, and hence the load carried by each at the common failure strain of 1%. At the ultimate strain of the T300/5208 material, the 16-ply (n=2) layup had delaminated more than the 8-ply (n=1) layup. For AS-4/3502, the failure strain is around 1.45%. At this higher strain, the extent of delamination of the 8-ply (n=1) layup had reached that of the thicker (n=2,3, and 4) layups, and the secant modulus becomes the same for each, see Figure 13. This plot of representative quasi-isotropic stress-strain traces shows that while the thicker specimens lose stiffness at lower applied strain than the thinner specimens, and they also failed at a lower strain. The 8-ply (n=1) specimen, while stiffer than the thicker specimens for much of the test, eventually sustains the same damage (namely extensive delamination) and before failure, has the same secant modulus. The similar delamination of each size just before failure is apparent from Figure 8. The origin for the strength scaling was in the grip.

5.5. ERROR IN EXTENDING WEIBULL THEORY TO UNIDIRECTIONAL COMPOSITES

The only data set which followed the Weibull strength versus volume curve were the tensile tests of the unidirectional $[0]_{8n}$ and the cross-ply $[0_{2n}/90_{2n}]_s$ layups, the majority of which were invalid tests due to grip failures. For the $[90/0/90/0]_s$ cross-ply laminate all failures were in the gauge section, where the stress distribution was most uniform, and away from the grips where it certainly is not. Use of Weibull theory to predict strength of the 0° plies in this case should be acceptable. Recall Equation 4 for predicting tensile strength, σ_f, from strength in 3-point flexure,

σ_f, and insert the various terms: average flexure strength, σ_f = 1911 MPa, Weibull modulus, m = 29.3, volume in flexure, V_f = 168.4 mm^3, volume in tension, V_t = 630 mm^3. The predicted tensile strength of 1321 MPa is 31% below the flexure strength. The actual tensile strength was 1901 MPa, which is 1% less than the flexure strength. Carbon fiber production and handling, during the period in which Bullock (1974) studied size effects on strength, was much more variable than today, which may explain why such low Weibull modulus numbers were reported. Chatterjee, Adams, and Oplinger's (1993) report on tensile test methods makes at least one point clear, obtaining gauge section failures in unidirectional composite is very difficult.

The results of this study establish that Weibull theory is not valid for use with unidirectional composites at the macroscopic level, at which many thousands of fibers are working together, at least not with carbon/epoxy of the level of uniformity and quality available today. No remarks are made here about its applicability at the microscopic level, at which single fibers or small bundles of fibers are considered.

5.6. EXPLANATION FOR GRIP FAILURES IN UNIDIRECTIONAL COMPOSITES

There are a number of theoretically sound analyses which support the argument that unidirectional, organic matrix composites should fail *at* the grip, and split, exhibiting a brush-like failure morphology. First, grip region stress analyses show that there is a stress concentration at the grip of approximately 1.15, O'Brien (1993). The Weibull modulus of m= 29.3 makes it very unlikely that failure can initiate anywhere else. Second, unidirectional laminae of carbon/epoxy will split, rather than continue fracturing across the fibers, as observed by Stinchcomb, Reifnsider, Yeung, and Masters (1981). When the same unidirectional plies were sandwiched between constraining plies oriented at either 90° or ±45°, there was much less splitting, and shorter splits. The understanding of the mechanics of constraint has progressed considerably since then, see references of Part I, and it can be argued that increasing the thickness of the unidirectional ply block affords less constraint against splitting. In particular, the $[+45_n/-45_n/0_n/90_n]_s$ layup was shown to have a very different failure morphology as n was increased from 1 to 4. For n=1 the constraint was sufficient to confine failure to a localized zone, while the n=4 size coupon was severely split, see Figure 9.

5.7. FUTURE WORK: IMPROVED UNIDIRECTIONAL STRENGTH TEST METHODS

As is well known, obtaining true unidirectional strength for stiff carbon fiber composite material is very difficult, as reported in the many works compiled by Chatterjee, Adams, and Oplinger (1993). Unidirectional strength testing could be made more accurate, repeatable, and straightforward. The variety of laminates and corresponding tensile strength data examined within this report show varying propensity toward failure in the gauge section, or in the grip region. This fact can be used to advantage: stacking sequences exist which consistently induce gauge section

failures. A systematic program of study to design an optimized laminate for obtaining correct unidirectional strength of high performance carbon/polymer composite should be initiated.

The optimized laminate would be designed so that tensile load could be introduced using standard grips, without intolerable stress concentration. Obviously the optimum design would protect the 0° plies from damage by the clamping pressure and serrations in the grips. The requirements for end tabs would be eliminated, along with the extra steps in preparation. The laminate itself would be its own continuous co-cured end tab without any possibility of debonding, or stress concentration, because there is no chamfer. To enhance accuracy of strain measurement, the stacking sequence should suppress delamination. A parallel analytical study to develop stacking sequence design tools based on only measurable lamina elastic properties should also be carried forward.

6. Conclusions

1) The tensile strength of the 0° fiber-dominated laminates, $[0]_{8n}$ and $[0_{2n}/90_{2n}]_s$, which had unidirectional plies on the surface, and which were gripped using a grit cloth, tended to fail at the grip. The test results were therefore unacceptable. Use of grit cloth instead of end tabs in those cases should be discouraged. Strength scaling in those laminates should be regarded as originating with the test procedure.

2) The tensile strength of $[+45_n/-45_n/0_n/90_n]_s$ quasi-isotropic laminates was shown to decrease with increasing thickness, or n, and did not depend upon specimen width or volume. Failure was located at the grip for the layups having n>1, therefore, test results for those laminates were unacceptable. Strength scaling for this laminate stacking sequence originated with the grips. The strength scale effect should be regarded as a problem for this stacking sequence, even when gripped according to standard testing procedures.

3) When tensile tests of composite laminates containing unidirectional plies fractured consistently in the gauge section, then the 0° ply stress at the instant of laminate failure was the same as the strength of the unidirectional beam tested in 3-point bending.

4) The strength of unidirectional AS-4/3502 carbon/epoxy composite did not have a strength versus volume dependency of a magnitude sufficient to be distinguishable from the data scatter. A strength scaling effect in connection to length was not ruled out, only in connection to volume.

5) The Weibull theory predicted a strength-volume dependency in unidirectional carbon/epoxy that did not exist in tensile tests of composite laminates having gauge section failures. Weibull

theory, successfully used to predict strength scaling in brittle materials like glass, should not be used to predict strength scaling of unidirectional fibrous composites.

7. References

Batdorf, S.B. (1989). Note on Composite Size Effects. Journal of Composites Technology and Research, JCTRER **11**(1), pp. 35-37.

Beer, F.P., and Johnston, Jr., E.R. (1981). Mechanics of Materials. McGraw-Hill Book Company, ISBN # 0-07-004284-5.

Bullock, R.E. (1974). Strength Ratios of Composite Materials in Flexure and in Tension. Journal of Composite Materials **8** (April), pp. 200-206.

Chaterjee, S., Adams, D., and Oplinger, D.W. (1993). Test Methods for Composites A Status Report Volume I: Tension Test Methods. June. Department of Transportation, and Federal Aviation Administration report, DOT/FAA/CT-93/17, I.

Edge, E.C. (1994). Is There a Size Effect in Composites? Comments on Designer's Corner by Carl Zweben. Composites, **25**(10), pp. 957-958.

Hahn, H.T., and Tsai, S.W. (1974). On the Behavior of Composite Laminates After Initial Failures. Journal of Composite Materials, **8**, July, pp. 288-305.

Jackson, K.E., Kellas, S., and Morton, J. (1992). Scale Effects in the Response and Failure of Fiber Reinforced Composite Laminates Loaded in Tension and Flexure. Journal of Composite Materials 26(18), pp. 2674-2705.

Jackson, K.E., and Kellas, S. (1993). Effect of Specimen Size on the Tensile Strength of Geometrically Scaled $[+\theta_n/-\theta_n/90_{2n}]_s$ Composite Laminates. Army Symposium on Solid Mechanics, August 17-19, Plymouth, MA.

Jamison, R.D., Schulte, K., Reifsnider, K.L., and Stinchcomb, W.W. (1984). Characterization and Analysis of Damage Mechanisms in Tension-Tension Fatigue of Graphite/Epoxy Laminates. Effects of Defects in Composite Materials, ASTM STP 836, American Society for Testing and Materials, Philadelphia, Pa, pp. 21-55.

Johnson, D.P. (1994). The Effects of Specimen Size on the Mechanical Response of Laminated Coupons Loaded in Tension and Flexure. Ph.D. Dissertation, Virginia Polytechnic Institute and State University, Blacksburg, Virginia. (see also: Kellas, S., Johnson, D.P., Morton, J., and Jackson, K.E. (1993). Scaling Effects in Sublaminate-Scaled Composite Laminates. 34th AIAA/ASME/ASCE/AHS/ASC Structures, Structural Dynamics and Materials Conference, AIAA/ASME Adaptive Structures Forum, April 19-22, 1993, La Jolla, CA, Part 6, pp. 3715-3725)

Kellas, S., and Morton, J. (1992). Strength Scaling in Fiber Composites. AIAA Journal, Vol. 30, No. 4, April, pp. 1074-1080. (or see: NASA Contractor Report 4335, November, 1990).

O'Brien, T.K. (1982). The Effect of Delamination on the Tensile Strength of Unnotched, Quasi-Isotropic, Graphite/Epoxy Laminates. Proceedings of the 1982 Joint Conference on Experimental Mechanics, Oahu-Maui, Hawaii, May 23-28, pp. 236-243.

O'Brien, T.K., and Salpekar, S.A. (1993). Scale Effects on the Transverse Tensile Strength of Graphite/Epoxy Composites. Composite Materials: Testing and Design (Eleventh Volume), ASTM STP 1206, E.T. Camponeschi, Jr., Ed., American Society for Testing and Materials, Philadelphia, PA, pp. 23-52.

Sensmeier, M.D., Griffin, O.H., Johnson, E.R. (1988). Static and Dynamic Large Deflection Flexural Response of Graphite-Epoxy Beams. NASA CR 4118, March.

Standard Test Method for Tensile Properties of Polymer Matrix Composite Materials. Test Method D3039/D3039M-95a. Volume 15.03 Space Simulation; Aerospace and Aircraft; High Modulus Fibers and Composites. 1996 Annual Book of ASTM Standards. American Society for Testing and Materials, Philadelphia, PA, pp. 111.

Stinchcomb, W.W., Reifnsider, K.L., Yeung, P., and Master, J. (1981). Effect of Ply Constraint on Fatigue Damage Development in Composite Material Laminates. Fatigue of Fibrous Composite Materials, ASTM STP 723, American Society for Testing and Materials, Philadelphia, PA, pp. 64-84.

Weibull, W. (1939). A Statistical Theory of the Strength of Materials. Ing. Vetenskaps Akad. Handl (Royal Swedish Institute Engineering Research Proceedings, NR 151.

Whitney, J.M. and Knight, M. (1980). The Relationship Between Tensile Strength and Flexure Strength in Fiber-Reinforced Composites. Experimental Mechanics, **XXXVII** part 1, pp. 211-216.

Wisnom, M.R. (1991a). Relationship Between Strength Variability and Size Effect in Unidirectional Carbon Fibre/Epoxy. Composites **22**(1), pp. 47-52.

Wisnom, M.R. (1991b). The Effect of Specimen Size on the Flexural Strength of Unidirectional Carbon Fibre-Epoxy. Composite Structures, **18**, pp. 47-63.

Wisnom, M.R. (1992). The Relationship between Tensile and Flexural Strength of Unidirectional Composites. Journal of Composite Materials, **26**(8), pp. 1173-1180.

Workshop on Scaling Effects in Composite Materials and Structures, compiled by K.E. Jackson, NASA Conference Publication 3271, July 1994.

Zweben, C. (1994). Is There a Size Effect in Composites? Composites, **25**(6), pp. 451-454.

Table 1. Specimen dimensions.

scale	n	plies	length mm (inch)	width mm (inch)	nominal thickness mm (inch)
1/4	1	8	146 (5.75)	12.70 (0.500)	1.092 (0.043)
1/2	2	16	292 (11.50)	25.40 (1.000)	2.159 (0.085)
3/4	3	24	438 (17.25)	38.10 (1.500)	3.302 (0.130)
Full	4	32	584 (23.00)	50.80 (2.000)	4.394 (0.173)

Table 2. Detail about end tabs used on the 290 mm x 25 mm quasi-isotropic $[+45_n/-45_n/0_n/90_n]_s$ specimens. Two tests per condition.

end tab details				specimen scale	
material	length (mm)	layup (if composite)	thickness (mm)	n=1	n=2
aluminum	47	isotropic	1.0	yes	yes
grit cloth	50	100 grit	0.5	yes	yes
glass/epoxy	59	$[0/90/+45/-45]_s$	1.2	yes	no
glass/epoxy	79	$[0_2/90_2/+45_2/-45_2]_s$	2.0	no	yes

Table 3. Unidirectional $[0]_{8n}$ strength, and failure strain. Data from Jackson and Kellas.

n	in-plane dimension mm	0° volume mm^3	laminate strength, MPa (1 st. dev.)	failure strain %
1	12.7 x 108	1532	1539 (n.a.)	1.14
2	25.5 x 219	12258	1358.8 (152.5)	1.03
3	38.2 x 324	41371	1393.8 (126.4)	1.01
4	50.9 x 431	98064	1322.3 (109.0)	0.95

Table 4. Unidirectional $[0]_{8n}$, strength, failure strain, and location of failure.

n	dimensions mm	load kN	strength MPa	location of failure and comments
1	108 x 12.7 x 1.1	22.29	--	slipped, no failure
"	"	--	--	slipped and split, no failure
"	"	--	--	slipped and split, no failure
"	"	19.51	1381	failed at the grip
"	"	--	--	slipped and split, no failure
"	"	23.98	1697	failed at the grip
2	219 x 25.5 x 2.2	88.62	1582	failed inside the grip
"	"	78.81	1407	failed at the grip
"	"	74.08	1323	"
"	"	73.81	1318	slipped and split 4.5 mm from edge
"	"	--	--	slipped and split, no failure
"	"	65.20	1164	failed inside the grip
3	324 x 38.2 x 3.4	203.0	1555	failed 25 mm from grip
"	"	161.2	1235	failed at the grip
"	"	192.6	1475	"
"	"	190.2	1457	"
"	"	180.3	1381	"
"	"	164.5	1260	"
4	431 x 50.9 x 4.5	327.8	1448	failed at the grip
"	"	--	--	failed at the grip, very splintered
"	"	286.4	1265	failed 40 mm from grip
"	"	--	--	partly failed inside the grip
"	"	283.8	1254	slipped and failed at the grip
"	"	--	--	partly failed inside the grip

Table 5. Cross-ply $[0_{2n}/90_{2n}]_s$ strength, failure strain, and 0° stress. Data from Jackson and Kellas.

n	in-plane dimension mm	0° volume mm^3	laminate strength, MPa (1 st. dev.)	failure strain %	0° stress, MPa (1 st. dev.)
1	12.7 x 108	766	843.2 (109.0)	1.24	1712.7 (191.4)
2	25.5 x 219	6129	814.5 (59.7)	1.11	1527.6 (93.6)
3	38.2 x 324	20690	796.6 (41.4)	1.08	1492.8 (79.7)
4	50.9 x 431	49000	764.7 (22.6)	1.02	1409.5 (31.5)

Table 6. Cross-Ply $[0_{2n}/90_{2n}]_s$, strength, failure strain, and location of failure.

n	dimensions mm	load kN	strength MPa	strain %	location of failure and comments
1	108 x 12.7 x 1.1	13.07	924.6	1.30	failed 10 mm from grip
"	"	11.47	811.6	1.16	failed 14 mm from grip
"	"	11.38	805.0	1.18	failed at the grip
"	"	10.69	756.7	1.14	"
"	"	12.21	864.0	1.24	"
"	"	11.15	707.7	1.15	"
"	"	14.60	1033.0	1.53	failed in the gauge section
2	219 x 25.5 x 2.2	41.53	738.1	1.12	failed at the grip
"	"	47.05	836.2	1.14	"
"	"	45.82	814.4	1.12	"
"	"	50.16	891.4	1.21	"
"	"	46.41	824.7	1.13	"
"	"	41.24	732.9	1.02	"
"	"	48.60	863.8	1.02	"
3	324 x 38.2 x 3.4	102.3	824.6	1.15	failed at the grip
"	"	99.4	801.4	1.07	"
"	"	96.7	780.0	1.06	"
"	"	98.4	793.5	1.07	"
"	"	105.5	850.9	1.15	"
"	"	90.4	729.2	1.00	"
4	431 x 50.9 x 4.5	168.4	763.5	1.04	failed at the grip
"	"	167.7	760.4	1.03	"
"	"	162.4	736.3	1.00	"
"	"	176.4	799.7	1.05	"
"	"	168.0	761.6	1.01	"
"	"	164.0	743.3	0.99	"
"	"	173.9	788.3	--	"

Table 7. Cross-ply $[90_n/0_n/90_n/0_n]_s$ strength, failure strain, and 0° stress. Data from Kellas and Morton.

n	in-plane dimension mm	0° volume mm^3	laminate strength MPa	failure strain % (reported)	failure strain % (adjusted)	0° failure stress MPa
1	12.7 x 89	630	884.2	1.38	1.38	1901.6
2	25.4 x 178	5050	872.5	1.17	1.36	1874.1
3	38.1 x 267	17150	865.8	1.25	1.35	1860.3
4	50.8 x 356	40400	830.2	0.93	1.29	1777.6

Table 8. Cross-ply $[90/0/90/0]_{ns}$ strength, failure strain, and 0° stress. Data from Johnson.

n	in-plane dimension mm	0° volume mm^3	laminate strength, MPa (1 st. dev.)	failure strain %	0° failure stress MPa (1 st. dev.)
1	12.5 x 125	537	956 (56.6)	1.29	1777.6 (105.2)
2	12.5 x 125	1074	1091 (21.5)	1.38	1901.6 (37.5)
3	12.5 x 125	1611	968 (15.1)	1.38	1901.6 (29.7)
1	25.0 x 250	2147	946 (1.1)	1.32	1819.0 (2.1)
2	25.0 x 250	4293	951 (55.5)	1.31	1805.2 (105.4)
3	37.5 x 375	14490	908 (57.4)	1.25	1722.5 (108.9)
4	50.0 x 500	34340	971 (81.9)	1.28	1763.8 (148.8)

Table 9. Quasi-isotropic $[+45/-45/0/90]_{ns}$ strength, failure strain, and 0° stress. Data from Johnson.

n	in-plane dimension mm x mm	0° volume mm^3	laminate strength, MPa (1 st. dev.)	failure strain %	0° stress MPa (1 st. dev.)
1	12.5 x 125	537	548 (25.2)	1.40	1929.2 (77.9)
2	12.5 x 125	1074	662 (39.0)	1.27	1750.1 (103.1)
3	12.5 x 125	1611	612 (62.7)	1.24	1708.7 (175.1)
1	25.0 x 250	2147	526 (14.7)	1.18	1625.9 (45.4)
2	25.0 x 250	4293	660 (21.7)	1.32	1819.0 (61.6)
3	37.5 x 375	14490	652 (39.1)	1.40	1929.2 (113.2)
4	50.0 x 500	34340	677 (45.9)	1.28	1763.8 (121.5)

Table 10. Quasi-isotropic $[+45_n/-45_n/0_n/90_n]_s$ strength, failure strain, and 0° stress. Data from Kellas and Morton.

n	0° volume (mm^3)	laminate strength, MPa	failure strain % (reported)	failure strain % (adjusted*)	0° failure stress,MPa
1	315	556.9	1.2	1.42	1953
2	2525	498.8	1.18	1.28	1760
3	8575	427.2	1.42	1.09	1499
4	20200	402.2	1.47	1.03	1416

* Failure strain was adjusted using failure stress and strain of $[+45/-45/0/90]_S$ laminate from Jackson and Kellas, as a reference point.

Table 11. Quasi-isotropic $[+45_n/-45_n/0_n/90_n]_s$ strength, failure strain, and 0° stress. Data from Jackson and Kellas.

n	0° volume (mm^3)	laminate strength, MPa (1 st. dev.)	failure strain %	0° failure stress,MPa (1 st. dev.)
1	383	634.6 (26.0)	1.45	1992.2 (110.8)
2	3065	566.5 (14.9)	1.27	1750.1 (43.6)
3	10345	464.7 (28.5)	1.00	1381.9 (135.2)
4	24500	377.7 (18.8)	0.86	1185.1 (63.6)

Table 12. Quasi-isotropic $[+45_n/-45_n/0_n/90_n]_s$, strength, failure strain, and location of failure.

n	dimensions mm	load kN	strength MPa	strain %	location of failure and comments
1	108 x 12.7 x 1.1	8.28	607.9	1.46	failed in the gauge section
"	"	8.58	629.9	1.39	"
"	"	8.24	605.0	1.34	"
"	"	8.71	639.7	1.46	"
"	"	9.20	675.0	1.43	"
"	"	8.50	624.0	1.44	failed 16 mm from the grip
"	"	9.0	660.7	1.60	failed in the gauge section
2	219 x 25.5 x 2.2	31.54	567.4	1.28	failed 22 mm from the grip
"	"	31.95	574.8	1.29	failed 19 mm from the grip
"	"	31.02	558.0	1.27	failed 38 mm from the grip
"	"	31.61	568.7	1.28	failed at the grip
"	"	31.89	573.6	1.29	failed at the grip
"	"	29.92	538.2	1.28	failed 41 mm from the grip
"	"	32.5	584.6	1.12	failed 6 mm from the grip
3	324 x 38.2 x 3.4	53.93	436.5	0.99	failed 28 mm from the grip
"	"	57.84	468.2	1.02	failed 6 mm from the grip
"	"	52.28	423.1	0.94	no data
"	"	60.30	488.1	1.06	failed 6 mm from the grip
"	"	62.62	506.9	1.14	failed 28 mm from the grip
"	"	57.70	467.0	1.04	failed at the grip
"	"	57.20	463.0	0.83	failed at the grip
4	431 x 50.9 x 4.5	77.86	344.1	0.78	failed at the grip
"	"	87.36	386.1	0.89	failed at the grip
"	"	82.61	365.1	0.83	failed 12 mm from the grip
"	"	84.01	371.3	0.84	failed at the grip
"	"	87.22	385.5	0.87	failed in the gauge section
"	"	88.90	392.9	0.90	failed at the grip
"	"	90.20	398.6	--	failed in the gauge section

Table 13. Experimental results for ultimate strength of scaled $[+45_n/-45_n/0_n/90_n]_s$ laminates. Thickness and width are varied separately and compared to the 3-D scaled strengths.
Length was 292 mm, unless otherwise noted.

scale, n	layup	strength (MPa)		
		various widths (mm)		
		12.5	25	50
1	$[+45/-45/0/90]_s$	avg. = 623[1,2]	611.3 597.7 619.1 623.8 avg.= 613	--
2	$[+45_2/-45_2/0_2/90_2]_s$	--	avg. = 588[1]	--
4	$[+45_4/-45_4/0_4/90_4]_s$	414.6 420.1 401.5 361.0 avg. = 399.3	385.2 448.0 398.0 avg. = 410.4	avg. = 375[1,3]

1 Individual data are in Table 12
2 specimen length was 146 mm
3 specimen length was 584 mm

Table 14. Effect of end tab on strength of quasi-isotropic $[+45_n/-45_n/0_n/90_n]_s$ specimens, of uniform specimen dimension of 290 mm x 25 mm.

tab type	strength (MPa)	
	n=1	n=2
grit cloth	611 598	617 615
aluminum	601 582	589 542
composite	502 496	458 368

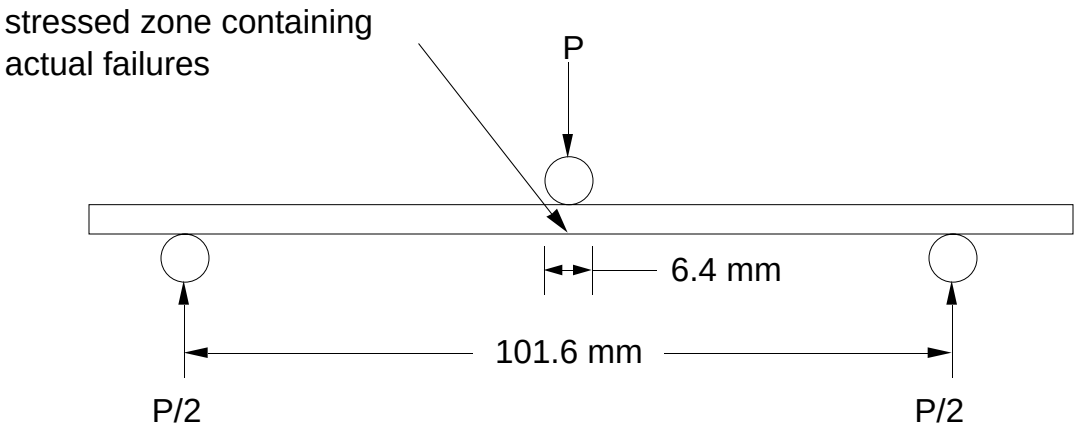

Figure 1. Schematic of 3-point bend test.

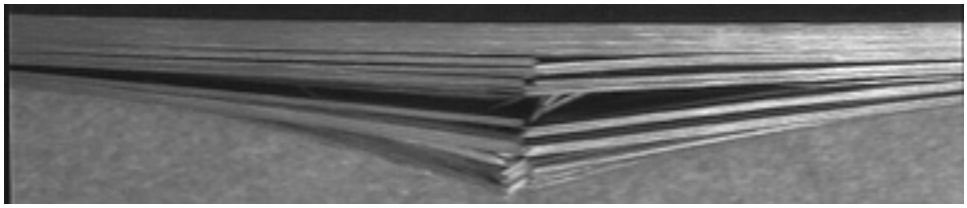

Figure 2. Typical fracture profile of a 3-point bend specimen. About 55% of failures were on the tension side, as shown. The remainder suffered bearing failure on the compression side, and were excluded.

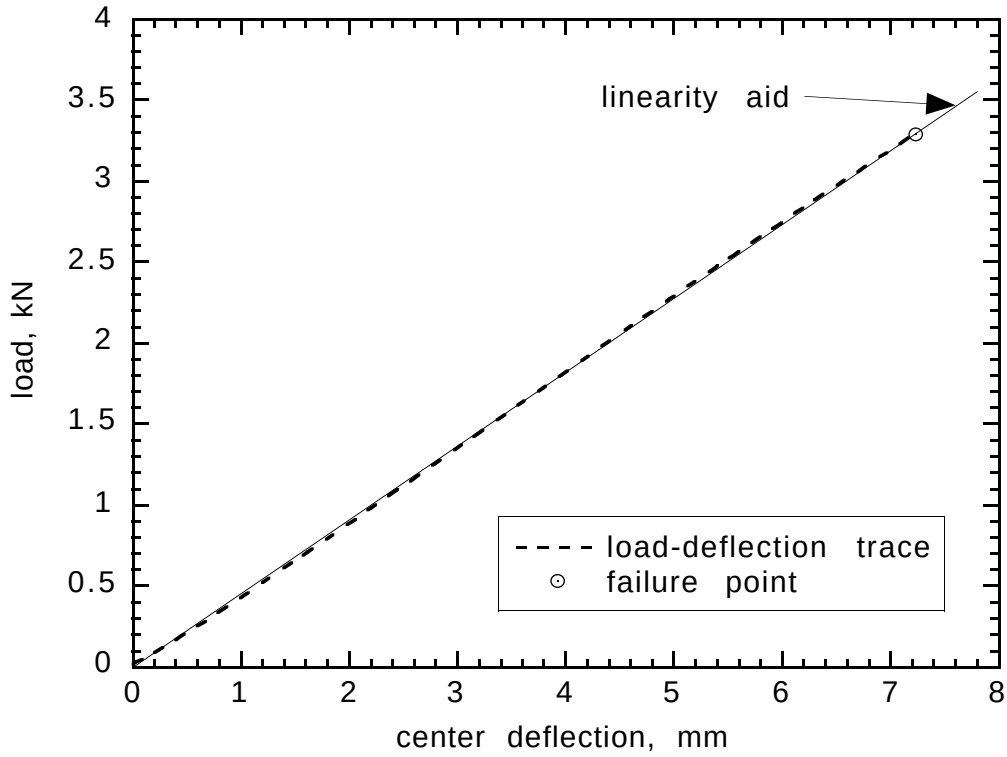

Figure 3. Typical load vs. displacement trace for a 3-point bend test of $[0]_{32}$ unidirectional AS-4/3502 graphite/epoxy.

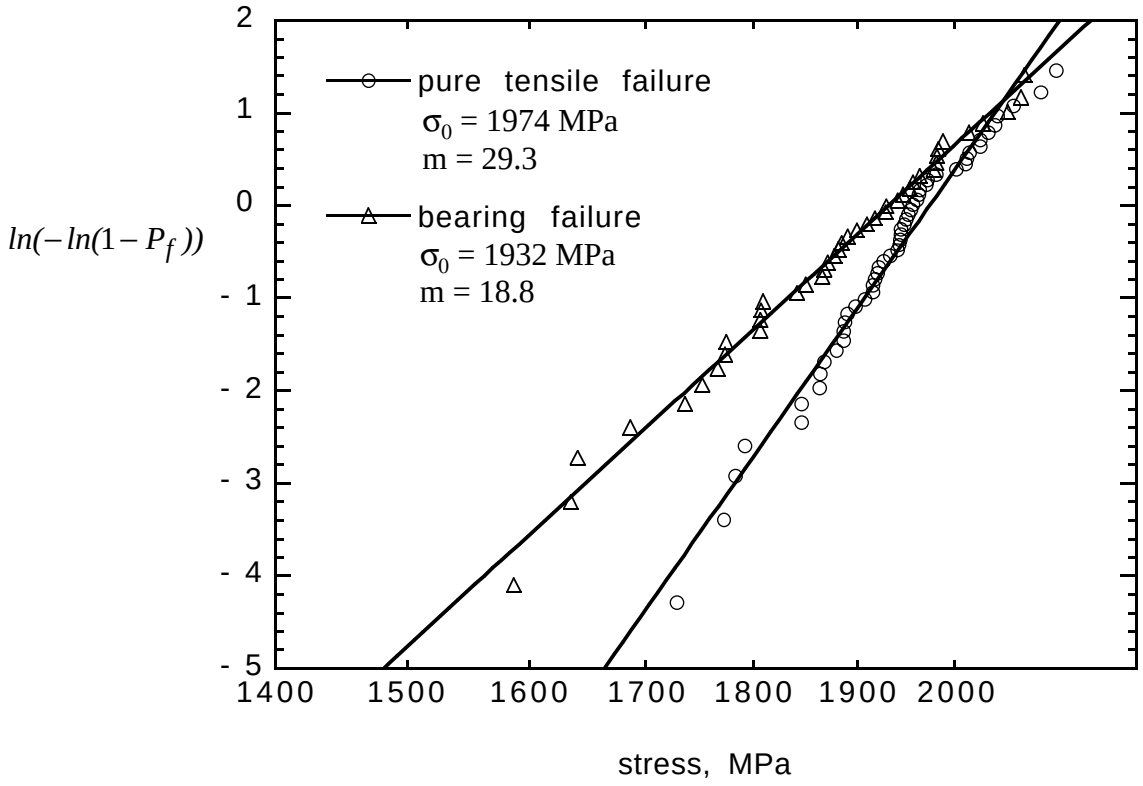

Figure 4. Survivability as a function of stress for unidirectional $[0]_{32}$ AS-4/3502 graphite/epoxy tested in 3-point bending.

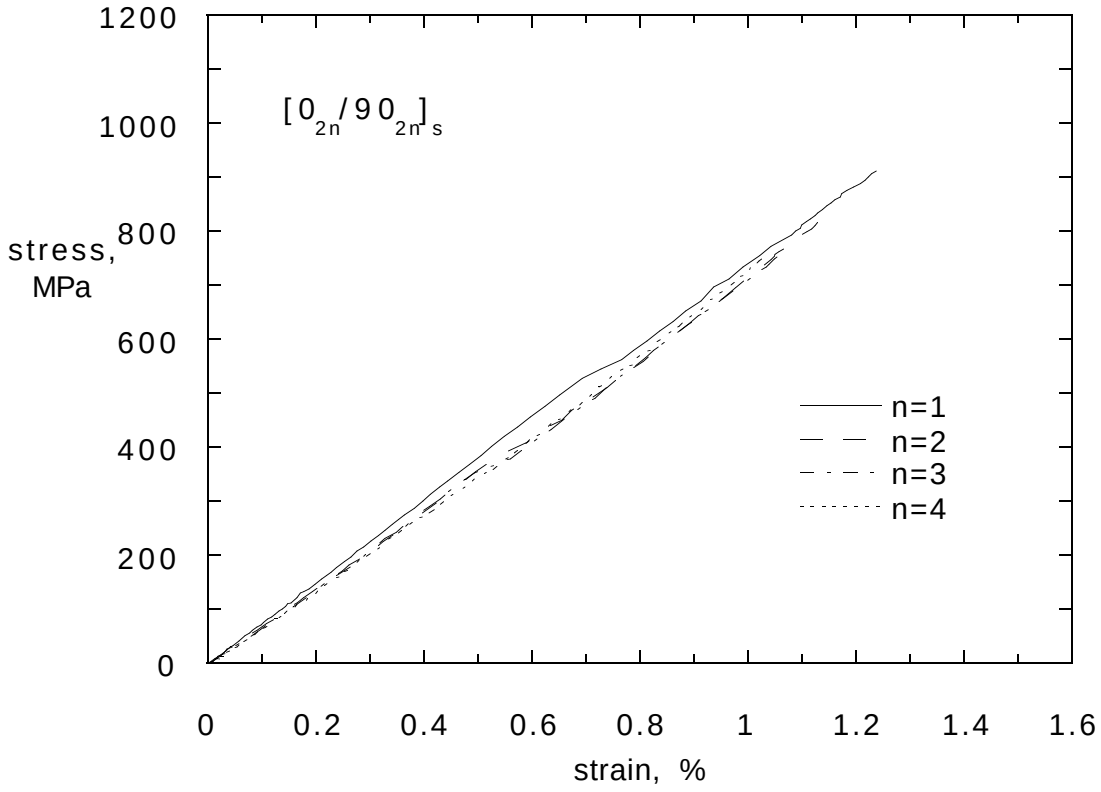

Figure 5. Stress vs. strain plots of $[0_{2n}/90_{2n}]_s$. Only one n=1 8-ply specimen had a gauge section failure. Limited delamination and much matrix cracking are characteristic of each. Failure strain, not only stress, is reduced as n increases, and is due to increasing grip region stress concentration. Data is from Jackson and Kellas (1993).

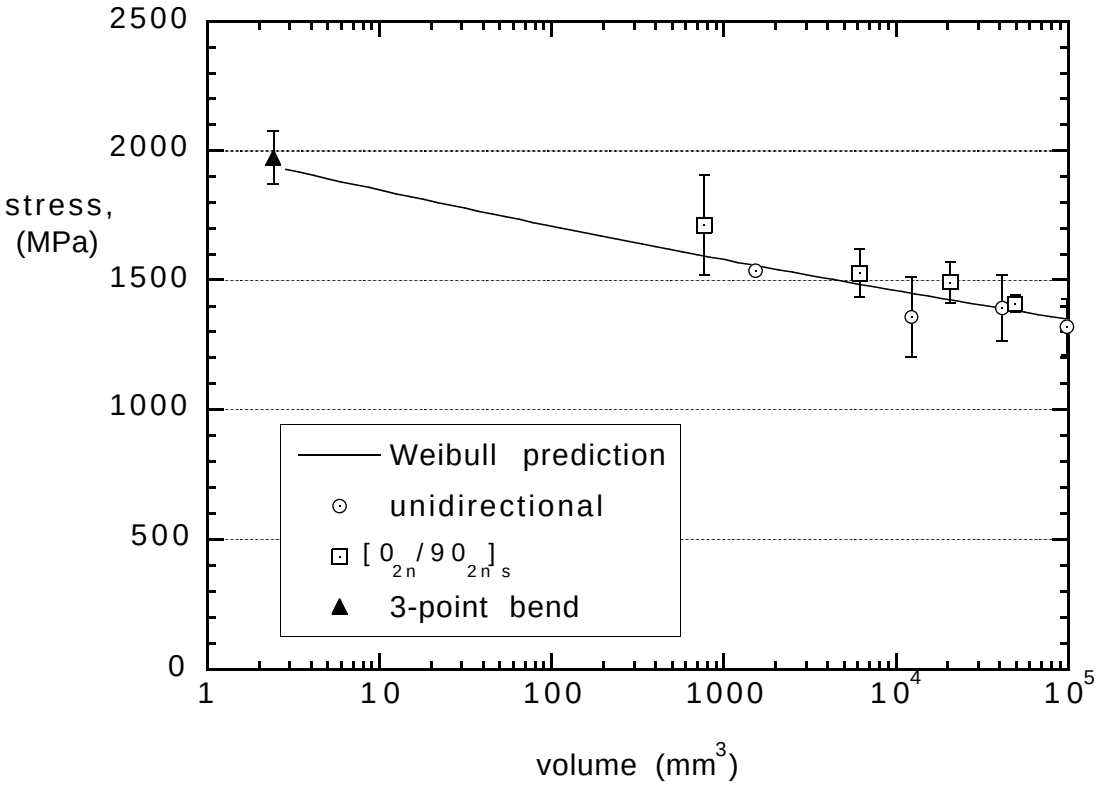

Figure 6. Plot of stress at failure of <u>unidirectional</u> plies for: unidirectional $[0]_{32}$ beams in 3-point bend (triangle), and in tension for unidirectional $[0]_{8n}$ coupons (circles), cross-ply $[0_{2n}/90_{2n}]_s$ coupons (squares), with Weibull prediction (solid line). Prediction is based on flexure strength. Note: tensile tests failed at the grip, except for three tests of the smallest volume cross-ply.

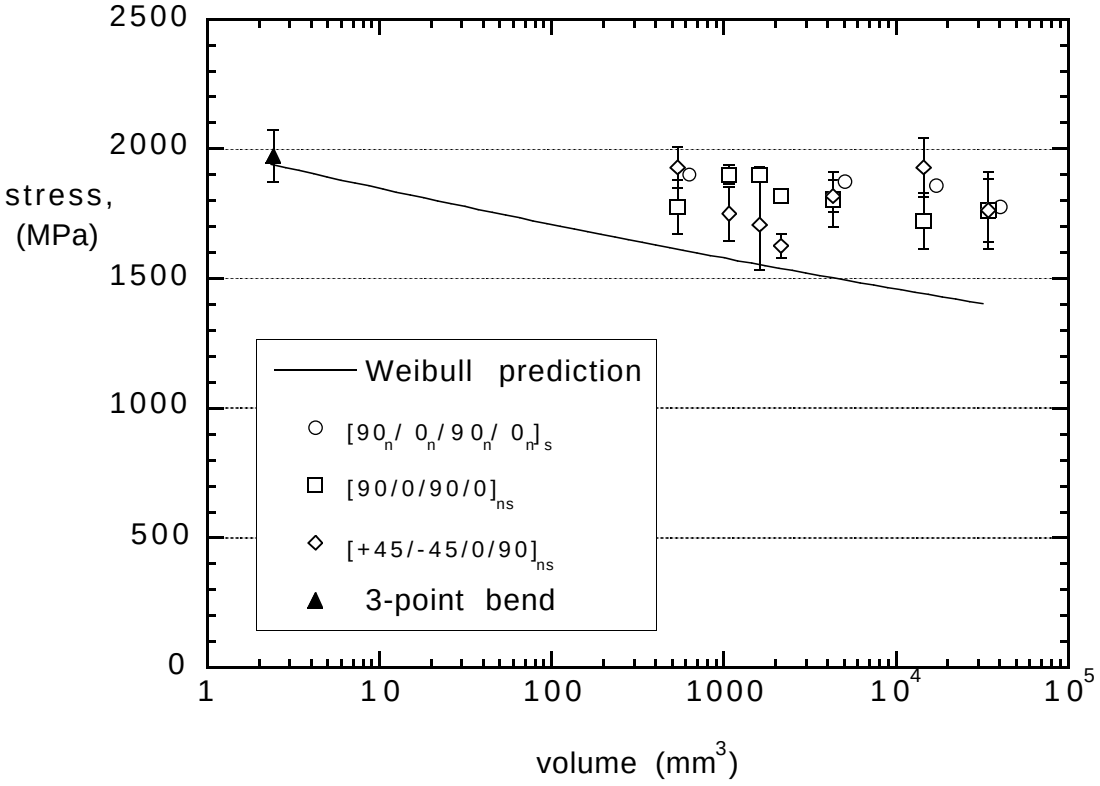

Figure 7. Plot of stress at failure of <u>unidirectional</u> plies for: unidirectional $[0]_{32}$ beams in 3-point bend (triangle), tension for cross-ply $[90_n/0_n/90_n/0_n]_s$ (circles), cross-ply $[90/0/90/0]_{ns}$ (squares), quasi-isotropic $[+45/-45/0/90]_{ns}$ (diamond) coupons, and Weibull prediction (line). Note: gauge section failures were predominant.

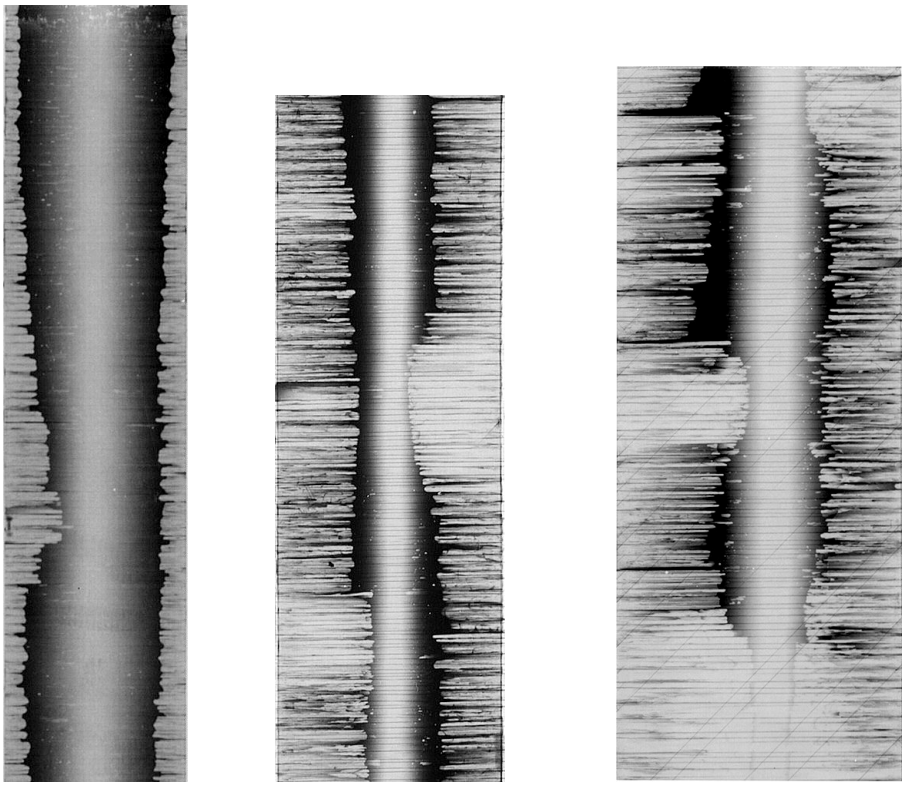

(a) 8-ply (b) 16-ply (c) 24-ply

Figure 8. X-ray of delamination in ply-level scaled $[+45_n/-45_n0_n/90_n]_s$ layups loaded until failure was imminent: (a) n=1, 8-ply; (b) n=2, 16-ply; (c) n=3, 24-ply. Delamination in each has progressed over about 90% of the width. The dye penetrant appears black where it is thickest; at the middle, where the delamination meets the crack tip, the dye penetrant has thinned to a light gray, making it difficult to see the full extent of delamination.

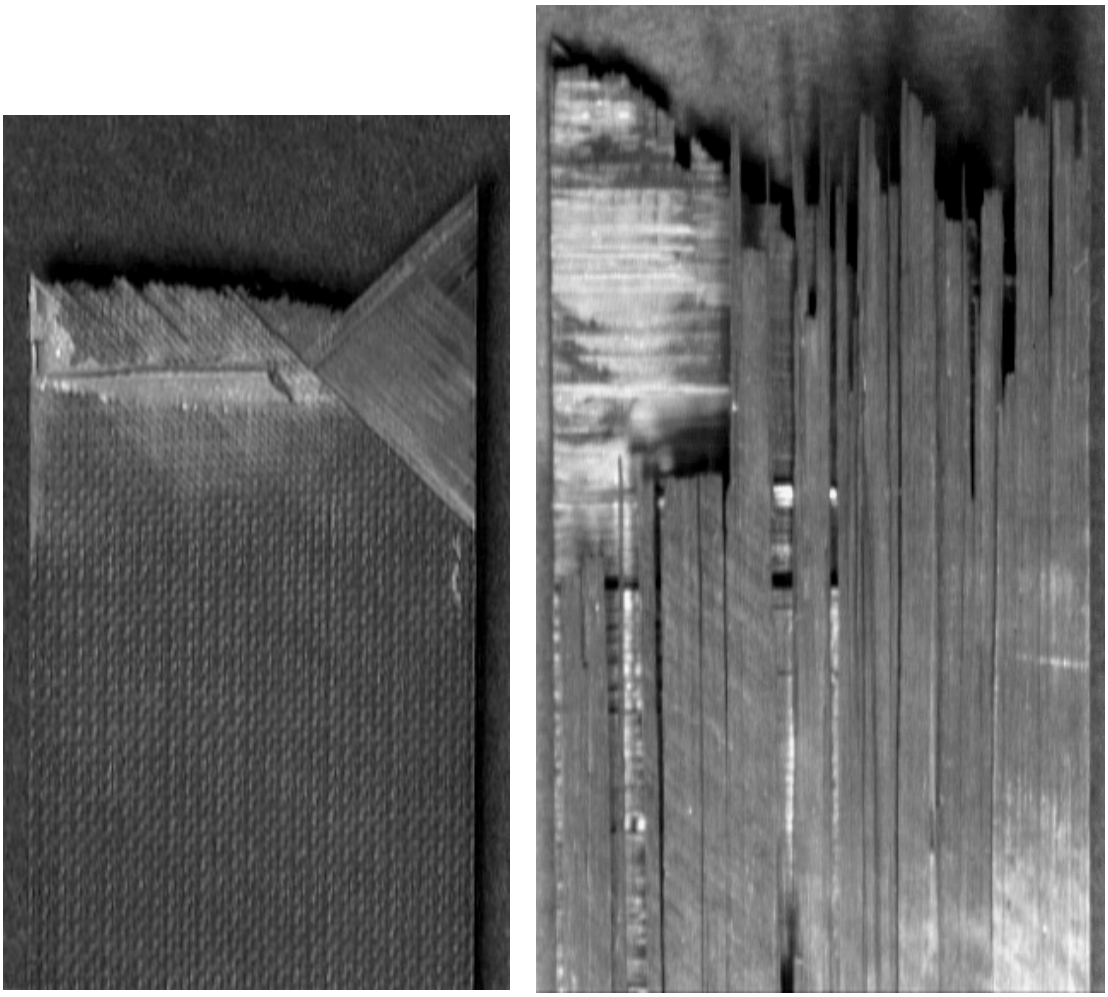

(a) 8-ply (b) 32-ply

Figure 9. Effect of constraint by off-axis plies on 0° plies on the typical fracture profiles for two quasi-isotropic layups. In (a) more constraint results in intact fracture of the 8-ply $[+45/-45/0/90]_s$ laminate. In (b) there is less constraint in the 32-ply $[+45_4/-45_4/0_4/90_4]_s$ laminate. The 0° plies split and delaminate from angle plies (interior shown).

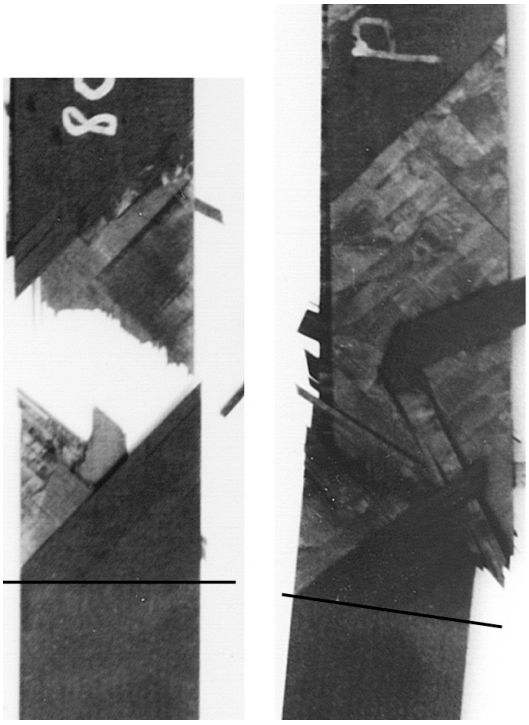

Figure 10. Grip failures for the $[+45_3/-45_3/0_3/90_3]_s$ laminate. The black lines mark where the grip ends.

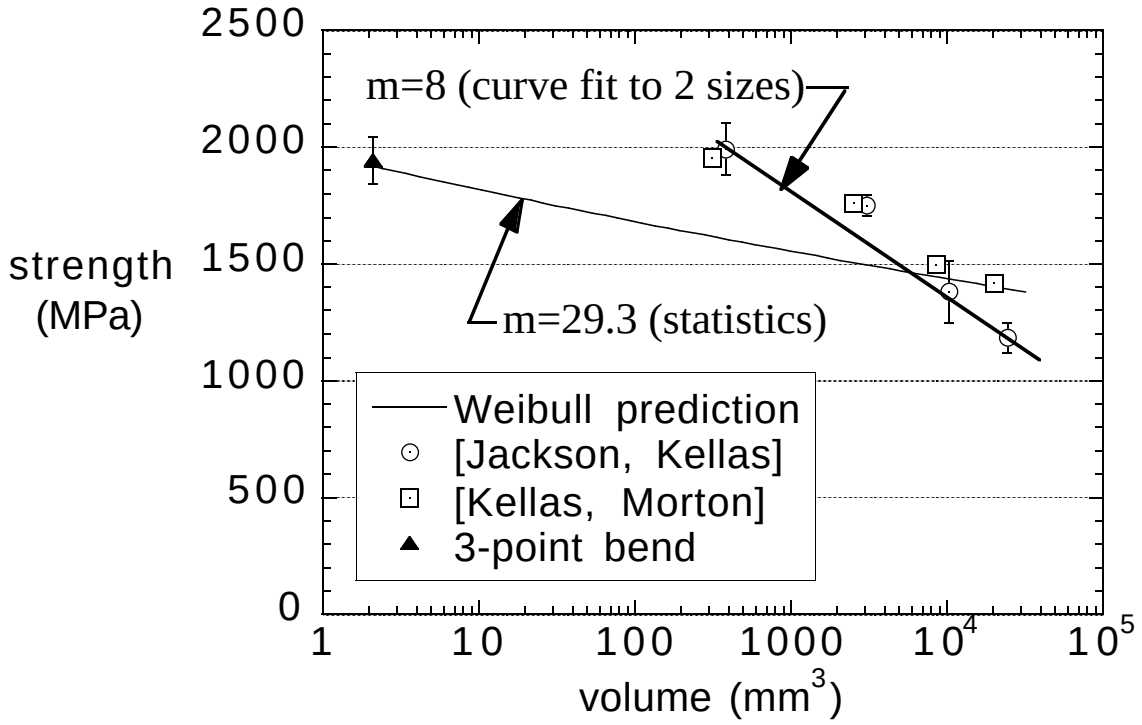

Figure 11. Plot of stress at failure of <u>unidirectional</u> plies for: unidirectional $[0]_{32}$ beams in 3-point bend (triangle), in tension for quasi-isotropic $[+45_n/-45_n/0_n/90_n]_s$ coupons (circles and squares), and Weibull prediction (line marked "m=29.3"). The line marked "m=8" is a curve fit and illustrates that incorrect Weibull modulus, m, is computed.

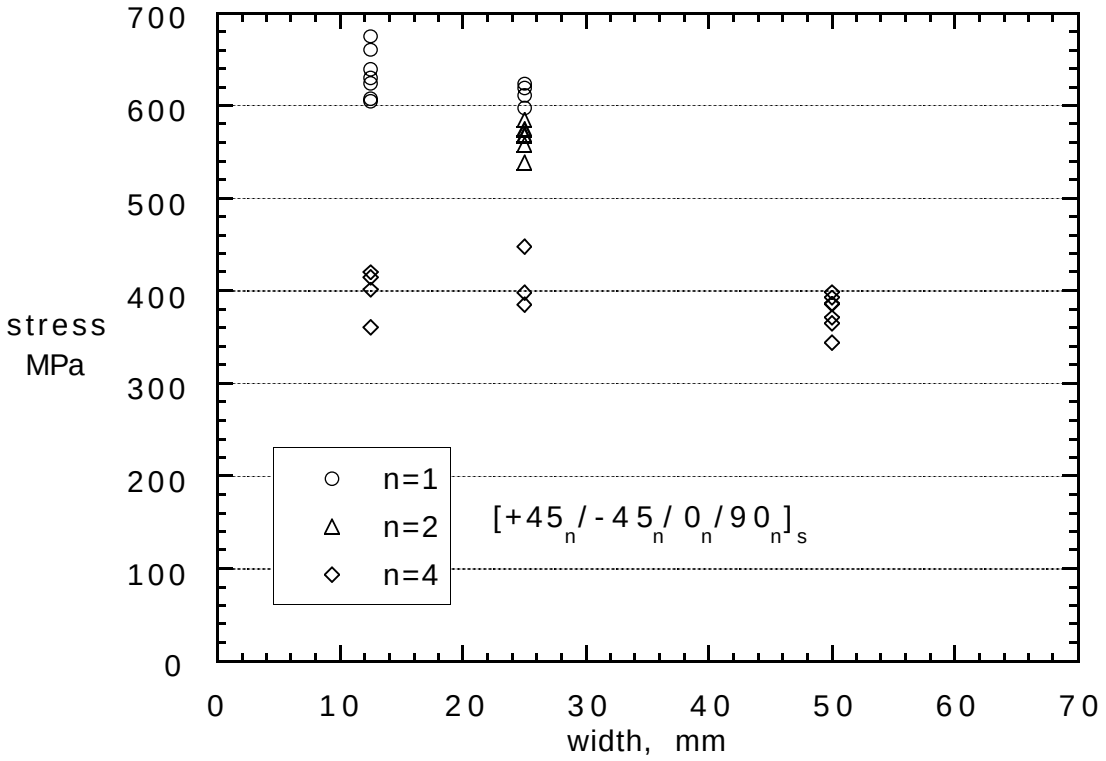

Figure 12. Strength of the $[+45_n/-45_n/0_n/90_n]_s$ laminate for different thickness and width. Changing width of the n=4 size had no particular affect on strength. Varying n while the width was fixed had a strong affect on strength.

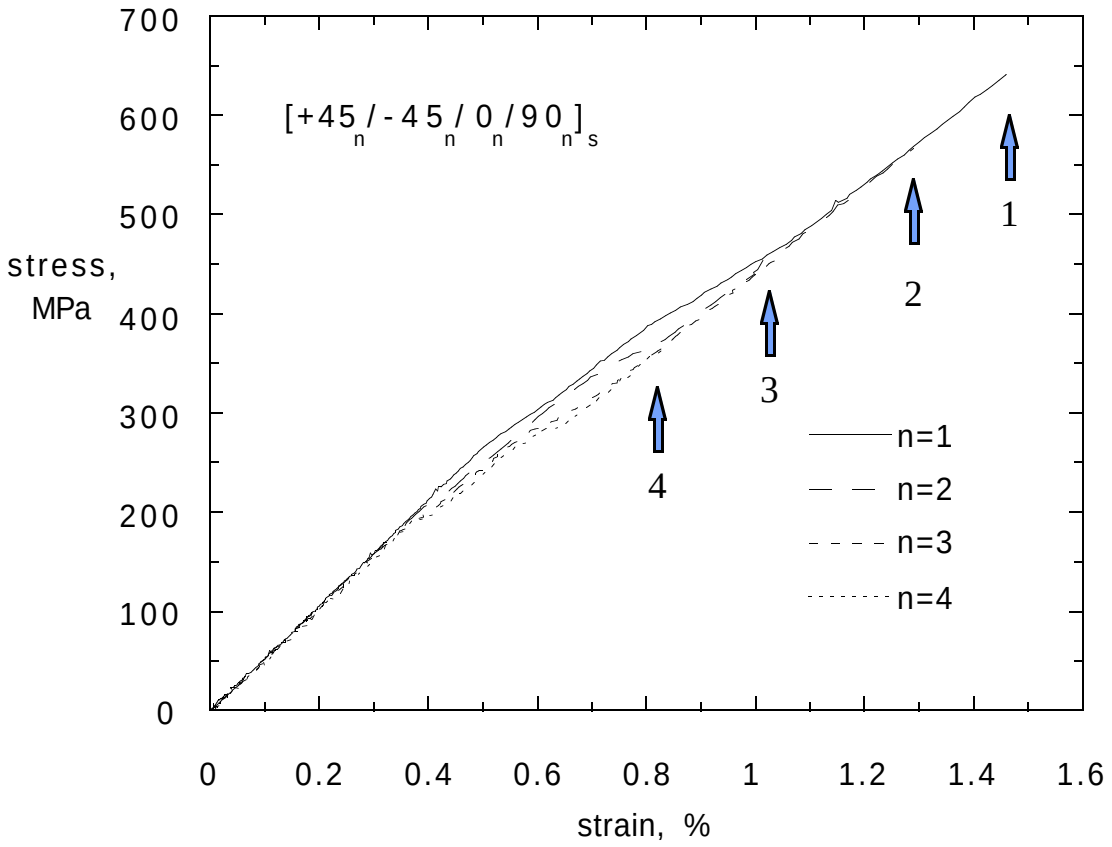

Figure 13. Representative stress vs. strain plots of $[+45_n/-45_n/0_n/90_n]_s$. Numbers indicate where each size typically failed. Severe delamination and matrix cracking are characteristic of all. Note that stiffness of each has declined to the same level before failure.

Part III

Prediction of Stress-Rupture Life of Glass/Epoxy Laminates in an Acidic Environment from Lamina Behavior

Abstract

A means to predict remaining strength and life of composite components in harsh environments and under complex time-varying loadings can help to optimize designs and cut costs. This paper reports an effort to predict the life of quasi-isotropic E-glass/913 epoxy composite laminates under constant load and in an acid environment. An experimental program involving stress-rupture tests of unidirectional coupons immersed in a weak hydrochloric acid solution was conducted to determine their stress-life response. Creep tests were conducted on unidirectional coupons parallel and transverse to the fibers, and on ±45° layups to characterize the lamina stress- and time-dependent compliances. These data were used in a composite stress-rupture life model, based on the critical element modeling philosophy of Reifsnider, to predict the life of two thickness-scaled quasi-isotropic laminates. Predictions compare favorably with experimental data.

Keywords: creep, stress-rupture, creep-rupture, stress relaxation, composite material, glass/epoxy, stress-corrosion cracking, durability, life.

1. Introduction

All-composite civil structures are appearing more frequently in load-bearing applications because of their low cost, light weight, and environmental resistance. Low cost glass-fiber/plastic composites are used in the process industry when the environment is highly aggressive and metal corrosion a serious problem. Some other applications are for storage tanks, piping, and in off-shore applications. These structures have tended to be overdesigned because material costs and reliability demands were low. As stresses rise and applications become more reliability sensitive (bridges for example), the need to design cost efficiently becomes even more important. For this reason, and because civil structures are asked to serve dependably for long periods of time, it is becoming increasingly urgent that engineers have tools to design composite structures for life, and not only for strength.

Creep of polymer composites, especially at elevated temperatures has been studied at length, and numerous models have appeared [1-4]. In comparison to fatigue, there is little work

on the time-dependent strength of composites under static loading. In part, this is because high performance applications of polymer matrix composites usually specify carbon fiber, which does not stress-rupture. Glass fibers are known to suffer stress-rupture behavior under static loading conditions when exposed to moisture, and other aggressive agents, especially acids. Some published results on stress-corrosion and stress-rupture of glass/polymer composites appear in references [5-19]. Very little exists in the literature on prediction of the stress-rupture life of composites in aggressive environments [20-22]. There is a need for characterization and modeling of the stress-rupture life of glass-fiber composite materials. A mechanistic modeling approach, called the critical element model, see Reifsnider and Stinchcomb [23], was developed for modeling fatigue life of composite materials. The framework of the modeling approach was used is this study to model the time dependent processes of creep and stress-rupture to predict life of composite laminates from the behavior of the laminae.

The experimental phase of this project was limited to six months duration. A composite material which could be environmentally conditioned so that it would exhibit stress-rupture type failures within the time constraint was needed. E-glass/913 epoxy was chosen because the E-glass fiber is known to be highly susceptible to stress-corrosion cracking when exposed to acids. Far superior fibers, such as R-glass, have been developed to resist stress-corrosion cracking due to acid attack. However, the stress-rupture life model could be tested as readily using either, and time constraints were severe.

In this Part, the experiments conducted to gather stress-rupture life data for unidirectional E-glass/913 epoxy lamina, and creep response parallel and transverse to the fibers, and in shear, is described. The stress-rupture life model used to predict the life of two ply-level scaled quasi-isotropic laminates under constant load is described. The purpose of examining ply-level scaled layups was to explore the possibility that under long term loading conditions, a size effect in the strength and stiffness might become more apparent via the nature of the damage developed. The results of the experiments on both the creep and stress-rupture tests are reported, and the failure modes are described. The predictions for creep and stress-rupture life are compared to the experimental data, and some possible refinements are noted. Comment is made on future work needed to expand the utility of the model to more general cases.

2. Experiments

2.1. MATERIALS AND SPECIMEN PREPARATION

The material used in this study was E-glass/913, a glass/epoxy composite supplied as unidirectional prepreg. Plates were made with in-plane dimensions of 300 x 300 mm and the following stacking sequences: $[0]_2$, $[0]_8$, $[90]_8$, $[+45/-45/+45/-45]_s$, and two ply-level scaled quasi-isotropic laminates $[0/90/+45/-45]_s$, and $[0_2/90_2/+45_2/-45_2]_s$. Laminates were cured as per the

manufacturers standard cure cycle at 120°C. All specimens, except for the 90's, were dry cut using a medium diamond wheel cut-off saw. The 90's were wet cut with a fine blade. The cut finish was not of a very high quality for the dry cut specimens. However, both edges of all specimens were wet ground on 240 grit silicon carbide paper until no visible defects remained. Grinding continued with 400 grit and finished with 600 grit paper to minimize the influence of any remaining microscopic defects. Specimens were found to be matrix microcrack free.

The creep/stress-rupture test frame with specimen installed is shown if Figure 1. Creep testing of composites having pinned end tabs requires special care in the surface preparation. The bond area of all specimens was grit blasted, then wiped with acetone. The aluminum end tabs were degreased and etched for improved bonding with the adhesive. The degreaser was a Minco 3410 aqueous alkaline degreasing bath, which was a non-silicate, non-caustic cleaner for aluminum. The chemical analysis was: Borax ($Na_2B_4O_7$) 38.0%, anhydrous Na_3PO_4 12.2%, extractable alcohol 9.6%, and deionized water 42.8%. This cleaner-concentrate was mixed with water at a ratio of 40 grams cleaner concentrate per one liter of water. The bath was circulated and its temperature kept at 60°C. The etch was a chromic/sulfuric acid pickle. The analysis for a 50 liter bath is: 3030 g chromic acid, 8600 ml sulfuric acid, 75 g aluminum, and 12 g of cupric-copper sulfate. The aluminum end tabs were suspended in the degreasing bath for 20 minutes, transferred into the first fresh water bath for 90 seconds, and then into the second fresh water bath for 20 minutes. The end tabs were transferred to the pickling bath and soaked for 30 minutes, then rinsed in fresh water baths for 90 seconds in one, and 20 minutes in the second.

Several types of aluminum end tabs were used. Quasi-static tensile test specimens had 50 x 25 x 1 mm thick aluminum end tabs. For the creep tests of $[90]_8$ and $[+45/-45/+45/-45]_s$ specimens, end tabs with 30° chamfer were used, see Figure 2(a,b). The stress-rupture test specimens had tabs with either a 4° or 30° chamfer. The 30° chamfer was intended for the more highly stresses specimens. All tabs with pin holes were closely machined so that the pin would have a very close fit. Stress-rupture specimens also required the clamp, as shown in Figure 2(a), to prevent debonding at higher loads.

All tabs were bonded to the specimens using a Redux 403 two-part epoxy paste adhesive. The rectangular tabs for the quasi-static tensile tests were aligned by eye, and pressure was applied using binder clips. The creep and stress-rupture tests needed precisely aligned tabs so that load would be evenly distributed between each tab, see Figure 2(b). The pin holes in the end tabs were aligned with a specially designed fixture. The specimen was aligned parallel and centered with the pin holes using guides in the same fixture. A uniform pressure was applied along the entire bond area of the tab, including the chamfered portion, by using a spring loaded bar having matching chamfers. The adhesive bond was allowed to cure overnight at room temperature, then specimens were placed in an oven at 60°C for at least one hour.

2.2. QUASI-STATIC TENSILE TESTING

Quasi-static tensile tests were conducted using a Zwick 100 kN capacity screw driven universal test machine. The grips were of the wedge action type. Strain was recorded using a clip-on extensometer having a 20 mm gauge length, and able to average out-of-plane bending. Load and strain were recorded on an x-y chart recorder. The crosshead speed was 2 mm/min. Specimens were loaded until the strain reached about 1%, then the extensometer was removed, and loading continued until failure. The stress at the onset of matrix cracking was also recorded.

2.3. CREEP AND STRESS-RUPTURE TESTING

2.3.1. *Strain Measurement*

Strain was recorded for both creep and stress-rupture tests using a pair of extensometers having capacitive type transducers. Readings were averaged, unless one became clearly incorrect. A photograph of a specimen ready for a creep test was given in Figure 1. The reliability of the transducers was verified by measuring the elastic modulus and comparing the readings to those obtained from the clip gage used in the quasi-static tensile tests. Readings were in agreement.

2.3.2. *Environmental Conditioning*

The temperature and humidity of the environment in which the stress-rupture tests were performed was precisely controlled. All specimens were kept in the open air of the lab until ready for testing. No specimen was tested until after having been stabilized for at least four months. Therefore, it was assured that the moisture content of all the specimens was uniform and at equilibrium when the tests were initiated. In the case of the 90° and ±45° angle-ply specimens the moisture content remained stable for the duration of the test.

The laminates were immersed in tap water at 60°C for one week, then were dried in an oven at 60°C for an additional week. This treatment is known to reduce the fracture toughness of the matrix. All specimens were subjected to this treatment, except the 2-ply unidirectional ones.

A stress-corrosion cracking environment was simulated by submerging opposing faces of the specimen (exclusive of edges) in a dilute (0.01 molar) hydrochloric acid solution. A photograph of the specimen with environment chambers attached is shown in Figure 3. Thin glass slides, 37 x 25 mm, were bonded on three edges to the gage section of the specimen using a clear silicon rubber sealant. Spacers were used to create a 2 mm wide gap between the specimen and the glass. The edges of the specimen were sealed to prevent the environment from penetrating by interfacial diffusion or by following a void or crack. Diffusion could only occur through the matrix into the front and back faces of the specimen. The region of the specimen below the chambers was wrapped in an absorbent tissue to soak up acid in case fracture of the specimen also

breached the chamber. Just before the tensile load was applied to the specimen, the chambers were filled with the acid by inserting a pipette through a small opening in the bag. To protect personnel and equipment from acid that might splash during rupture of the specimen, the entire gauge section was jacketed in clear plastic, and openings were sealed with a tacky adhesive cord normally used as a vacuum bag sealant, as shown in Figure 2(a).

2.3.3. Creep Tests

Loads were selected for the creep tests of the 90° and ±45° angle-ply specimens to induce strains similar to that which was experienced by the quasi-isotropic laminate. The 90° specimens were loaded at stresses ranging from 15 to 35 MPa. The ±45° specimens were loaded at stresses ranging from 30 to 100 MPa (this was axial stress on the coupon, not shear stress). Creep data was also obtained for the unidirectional specimens, with loads chosen based on expected life.

2.3.4. Stress-Rupture Tests

Stress-rupture tests were carried out on the 2-ply unidirectional, and the 8-ply and 16-ply quasi-isotropic specimens. Strain and time to failure were recorded. Failure was defined as complete separation of the specimen. The loads were selected, by trial and error, so that failures occurred in the range between 10 and 1700 hours.

3. Stress-Rupture Life Modeling

The stress-rupture life of the two quasi-isotropic laminates is modeled using the microkinetic approach developed by Reifsnider [23-25]. These are good recent references to introduce the reader to this modeling philosophy, and a variety of different cases are examined there. The most accurate and reliable predictions of the residual strength (damage tolerance) and life (durability) of a composite require careful laboratory observations of actual damage modes exhibited by the specific material of interest. How the various material properties change over time, including the stiffnesses and strengths, and the time and sequence of their appearance need be known. These properties can be quantified with time- and stress-dependent functions that represent strengths and compliances. The compliances can be fed to a classical laminated plate analysis module to get time-dependent stress in the critical element. In the case examined here, the critical element is represented by 0° plies because their failure induces total failure of the laminate. The experimental work needed to describe the change in the stress state in the 0° plies of the laminate are described in the section on experiments. The change in the various compliances with time and stress was characterized from viscoelastic creep tests.

The "life integral" is described next, but only in relation to how it is used here. The stress-rupture life model incorporates experimentally-obtained applied stress versus life response, and viscoelastic creep-compliance responses of the laminae.

3.1. ESTIMATION OF REMAINING STRENGTH AND LIFE

From the microkinetic theory, there is an equation that relates changes in the state of stress in the critical element, and changes in the material state of the critical element, as a function of the global loading history, to remaining strength and life of the material. The critical element of a composite laminate is identified as that part of a representative volume that defines failure, meaning that its failure signals global component failure. For a composite coupon, the critical element is identified as being those plies whose failure (in this case) signals complete failure of the laminate. For structural laminates, the critical element is usually taken to be the primary load bearing plies; here they would be the 0° plies oriented with the tensile loading. The strength and stiffnesses of the critical element define its material state, and may be affected by time, temperature, cyclic mechanical and/or thermal loading, and environmental degradation. This study was concerned with how the durability (life) of the critical element (the 0° plies) was affected by time-varying tensile stress when exposed to hydrochloric acid, an aggressive agent known to seriously degrade the strength of E-glass fibers. The strength and life of the critical element is influenced by subcritical elements.

Subcritical elements constitute the portion of the representative volume, which may undergo change, but the changes do not signal global component failure. The changes most often considered are those which cause stress redistributions in the critical element. Some examples are matrix microcracking, aging, stress relaxation, and delaminations, each of which degrades component stiffness, and increase (usually, but not always) the stress on the critical element. The experimental portion of this study was designed so that only stress redistribution (due to stress relaxation in the various plies) would affect the stress in the critical element. The laminate was designed to not delaminate, and matrix cracking (especially in the 90° plies) was avoided by conducting the tests at loads below the first-ply failure stress.

The total cycles to failure, N (time, in this case), is modeled after the stress-rupture life of the 0° plies and is taken to be

$$N = 10\wedge\left\{\left[\frac{\frac{\sigma_{11}}{X_t} - A}{B}\right]^{1/p}\right\} \tag{1}$$

where X_t is the instantaneous tensile strength of the 0° plies, σ_{11} is the fiber-aligned stress in the 0° plies, and A, B, and p are experimentally determined coeffcients. The remaining strength, F_r, starts at 1, and is given as

$$F_r = 1 - \int_0^{n/N} (1 - F_a) j \left(\frac{n}{N}\right)^{j-1} d\left(\frac{n}{N}\right) \tag{2}$$

and depends upon the elapsed time, *n*, and the projected time to failure, *N*. The expression for F_a is

$$F_a = \frac{S_a}{S_u} = A + B(\log N)^p \tag{3}$$

and is defined as the applied stress in the critical element, S_a (σ_{11} before), divided by the ultimate strength of the critical element, S_u (X_t before). The coefficients A, B, and p are experimentally determined from a series of stress-rupture tests of unidirectional coupons at different stresses.

The coefficient, *j*, affects the shape of the remaining strength curve. Depending upon its value, the strength can appear to drop off gradually over time, or drop suddenly at the end (called sudden death). When *j* is low, strength is modeled as dropping gradually during most of the life, accelerating near the end. When *j* is high the strength is modeled as undiminished for much of the life, and dropping very rapidly at the end. Direct remaining strength data were not taken for this work, so a correct value for *j* is not known, but was thought to be high, therefore a value of 7 was chosen. In this study, there was no significant effect of the value of *j* on the remaining life predictions because the applied stress changed little during the test. The ultimate strength of the critical element, S_u, can be dependent on time and temperature. In this model, the strength of the glass fibers is degraded over time under the action of the acid environment. The applied stress on the critical element, S_a, is also time dependent because the compliance of the subcritical elements vary with time and stress.

3.2. MODELING LOSS OF STRENGTH IN THE UNIDIRECTIONAL PLIES

The stress-rupture process of E-glass/913 epoxy composite is well described by Hogg [9], and Hogg and Hull [10]. The acid diffuses through the polymer matrix until it reaches the fibers. Then a chemical reaction occurs which weakens the fibers so that, when under tension, a very clean crack propagates. Once a crack has started through the fibers, the matrix may also crack. If so, acid is rapidly transported to the surfaces of the unbroken fibers. Diffusion of acid through the matrix then becomes a second order transport process, as acid is directly introduced to the surface of intact fibers. Cracks can then grow more quickly and so the remaining strength falls more

quickly. Cracking also accelerates because the decreasing cross section raises the mean stress on the intact fibers. The crack growth process in individual fibers, or in the lamina was not modeled. Instead, the life of the critical element as a function of time and stress was determined by fitting a curve to a series of stress-rupture tests conducted at various tensile loads. Equation 1 was rearranged as Equation 3 for this purpose, and the coefficients, A, B, and p are selected for a best fit.

3.3. CREEP MODEL OF COMPLIANCE CHANGE

The change of the transverse and shear moduli as a function of stress and time are incorporated into the life predictions because these changing compliances change the stress in the critical element. Laboratory creep data was taken parallel to the fiber direction using the $[0]_2$ specimens, transverse to the fiber direction using the $[90]_8$ specimens, and in shear by use of the $[+45/-45/+45/-45]_s$ tensile specimens. The compliances, S_{ij}, were obtained from the strain data, ε_{ij}, using the relations:

$$S_{11}(t)= \varepsilon_{11}(t)/\sigma_{11},\ S_{22}(t)=\varepsilon_{22}(t)/\sigma_{22},\ \text{and}\ S_{66}(t)=\gamma_{12}(t)/\tau_{12},\ \text{where}$$

$$\gamma_{12}(t)= \varepsilon_{xx}(t)(1+\nu_{\pm 45})\ \text{and}\ \tau_{12}=\sigma_{xx}/2. \tag{4}$$

The symbols σ_{11}, σ_{22}, τ_{12}, are lamina-coordinate principal stresses. The time-dependent shear strain is $\gamma_{12}(t)$, and the formula for it is from Rosen [27]. Poisson's ratio of the ±45's is symbolized by $\nu_{\pm 45}$, and was assumed to remain constant. The fiber direction time-dependent compliance, $S_{11}(t)$, was represented using the linearized Findley [4] fitting function:

$$S_{11}(t)=S_{11}(0)+At^n, \tag{5}$$

where the coefficient $S_{11}(0)$ is the initial elastic compliance, while A and n are coefficients used to fit the experimental data.

The transverse time-dependent compliance, $S_{22}(t)$, was also represented using the linearized Findley fitting function:

$$S_{22}(t)=S_{22}(0)+At^n, \tag{6}$$

where the coefficient $S_{22}(0)$ is the initial elastic compliance, and A and n are a second set of coefficients used to fit the experimental data.

The shear compliance, $S_{66}(\tau_{12},t)$, was represented using Lou and Schapery's [3] quadratic fitting function:

$$S_{66}(\tau_{12},t) = S_{66}(\tau_{12},0)\left[1+g\tau_{12}^2\right]+m\left[1+f\tau_{12}^2\right]t^n \tag{7}$$

where the coefficient $S_{66}(0)$ is the initial elastic shear compliance at a computed shear stress τ_{12}, and *g, m, f,* and *n* are coefficients used to fit the experimental data accounting for both stress and time. The FORTRAN computer code written for this problem is given in the Appendix. The classical laminated plate theory portion used in the stress analysis is omitted there.

3.4. OTHER MECHANISMS INFLUENCING LIFE

There are a host of other material changes and damage forms which can significantly influence life. Two that act on life in this study are mentioned now, others are relegated to the future work section. Matrix cracking in off-axis plies cause stress concentration in neighboring plies. This stress concentration and the overall stiffness change could be represented using a simple shear lag model [26]. Cracks also could provide a path for transport of the acid bath. In this study, matrix cracking did not appear at any time during the life, at least not until 0° stress corrosion cracks appeared. The justifications for ignoring their effects are discussed in Section 5.3.4.

4. Results

4.1. QUASI-STATIC STRENGTH TESTS AND DAMAGE CHARACTERIZATION

4.1.1. Unidirectional $[0]_8$ Specimens

The moduli and strengths are given in Table 1. The post-failure morphology has a broom-like appearance, Figure 4(a). Closer inspection suggests that cracks can grow across the fibers for some characteristic distance before a split begins and stops the crack from breaking more fibers. The first fibers to fracture were at the edge, and very near the grip. A progression of fiber bundle fractures and splitting progressed across the width of the specimen. The fiber bundles were approximately 1.5 to 2.5 mm wide, and from one to eight plies thick. For the moment, I presume that the length of the crack that ran across the fibers is dictated by the magnitude of the shear and peel stresses that can be supported before a split forms and runs along the length. After the first fibers fracture and a bundle splits, all subsequent fiber fracturing occurred at either grip. This sequence repeated itself until each half of the failed specimen looked broom-like and about the length of the gauge section.

4.1.2. Quasi-Isotropic Specimens

8-ply Quasi-Isotropic $[0/90/+45/-45]_s$ specimens Matrix microcracking in the 90° plies occured before the ultimate tensile load was reached. A failed tensile test specimen is shown in

Figure 4(b). Both specimens tested, Q8-6 and Q8-8, exhibited a very straight fracture across the surface 0° ply on one side which extended for 2.6 and 2.9 mm, respectively. Failure initiation was well away from the grip. Then, short splits begin to appear in the 0° ply which was accompanied by growing randomness in the location for continuation of fracturing of the fibers. The length of the splits was at first very small, about 0.5 mm or less, but became longer as the fracture progressed across the specimen width. The width of the splits was less than a millimeter. As the 0° ply fractured, the +45° ply developed damage in the form of microcracks, reducing the constraint with the 0/90 sublaminate, which then delaminated. There were no fiber failures in 45° plies. The length of the fracture zone was 30 and 36 mm, and was defined by the region of shear out of the 45° plies.

16-ply Quasi-Isotropic $[0_2/90_2/+45_2/-45_2]_s$ specimens Failure of Q16-5 was at the grip, and Q16-3 failed one specimen width away from the grip, and is shown in Figure 4(c). Both became saturated with 90° cracks, but there were also -45° cracks and perhaps some +45° cracks. Failure of the surface 0° plies started on one side of the specimen at the edge and progressed across the width. During this period load sheds to the underlying 45's which quickly strain, crack, and shed most of the load onto the 0° plies on the opposite face. Some fracturing of the 0° fibers occurred near the original crack, but very quickly long splits blunted them, and the remainder of the 0° plies failed in the manner of the unidirectional specimens. About half way across the width, the splitting became completely unrestrained and ran along the length of the specimen. This splitting behavior was observed in the unidirectional specimens.

4.2. VISCOELASTIC CREEP TESTS

4.2.1. Lamina Creep Characterization

Creep tests of $[0]_2$, $[90]_8$, $[+45/-45/+45/-45]_s$ specimens were conducted at room temperature (21°C) to characterize the time-dependent and stress-dependent compliances. The initial elastic compliances, $S_{22}(0)$, and $S_{66}(0)$, were measured using the extensometers and appear in Table 2, but these data were not tight.

The strain-time plots for the unidirectional tests are shown in Figures 5, 6, and 7. These creep plots share the same features as observed in metal creep. There are clearly defined primary, secondary, and tertiary creep phases. At the scale shown in these figures, the primary creep is difficult to see, but is there, and will be examined more closely. The secondary creep phase dominated the life of the unidirectional specimens. Tertiary creep represented the final phase in the life, and was due to the nucleation and growth of stress-corrosion cracks. Observations about the stress-corrosion cracks are made in Section 4.3. A significant simplifying assumption made was that the unidirectional specimens could be represented as having failed catastrophically. The presence of a tertiary creep phase made this assumption invalid in a strict sense. However, from

inspection of Figures 5, and 6, it was judged that the fraction of the life which was composed of tertiary creep was small and could be neglected. Unidirectional creep data were converted to compliance data and are shown in Figure 8. All the data was plotted together. A single Findley curve representing $S_{11}(t)$ was fit to the data. The fitting coefficients used in Equation 5 were:

$$S_{11}(0)=2.07\text{x}10^{-11},\ A=2.97\text{x}10^{-13},\ \text{and}\ n=0.200$$

Only one curve was needed because there did not appear to be any dependence of compliance on stress, only on time. The curve fitting function chosen did not include tertiary creep because it was argued that failure could be regarded as catastropic. In Figure 9, the time scale of Figure 8 is expanded to include only the first 10^6 seconds. The purpose was to show that, aside from tertiary creep, the chosen fitting function represented fairly well the primary and secondary creep phases.

Creep testing of the 90° and the ±45° specimens was conducted in a controlled temperature, controlled humidity environment. All the creep data for the 90's was converted to compliance, $S_{22}(t)$, data and was plotted together in Figure 10. There was no observed stress dependence, at least for the range of stresses considered, nor was there a tertiary creep phase either. Hence, compliance could be represented by a single Findley fitting function. The form of the function was given in Equation 6, and the values for the coefficients used to fit the data are:

$$S_{22}(0)=5.62\text{x}10^{-11},\ A=3.629\text{x}10^{-13},\ \text{and}\ n=0.355$$

The shear compliance, $S_{66}(\tau_{12},t)$, was observed to be dependent on both the applied stress, τ_{12}, and time, t. The data and corresponding curve fits appear plotted together in Figure 11. Lou and Schapery's quadratic fitting function (Equation 7) was used. The coefficients used to fit the data are:

$$S_{66}(0)=1.1\text{x}10^{-10},\ g=2.8\text{x}10^{-16},\ m=12.36\text{x}10^{-15},\ f=1.0\text{x}10^{-13},\ \text{and}\ n=0.37$$

4.2.2. Quasi-Isotropic Creep Data and Predictions

Creep data were taken during all stress-rupture tests of the 8-ply quasi-isotropic specimens, shown in Figures 12, 13, and 14, and for 16-ply quasi-isotropic specimens, shown in Figures 15, 16, and 17. By use of the forgoing compliance-time responses of the lamina, it was possible to make predictions of the creep response of the quasi-isotropic layup. Creep tests are compared with the predicted creep response for three different loadings, and consequently, three different lives, see Figure 18. A short life test of a 16-ply quasi-isotropic specimen at 154 MPa is shown in Figure 18(a). The prediction tracks the data closely; only during the tertiary phase, where stress-corrosion cracking is ongoing, is deviation significant. In Figure 18(b), the intermediate life test is of an 8-ply quasi at 112 MPa. Again, agreement is quite good.

Not until long life creep tests were modeled did a clear error appear. A long life test of an 8-ply quasi at 80 MPa is shown in Figure 18(c). Underprediction of creep at long times suggests that moisture absorption may be causing both moisture expansion and an increase in compliance.

4.3. STRESS-RUPTURE TESTS AND DAMAGE DEVELOPMENTS

Stress-Rupture testing was performed on $[0]_2$, $[0/90/+45/-45]_s$, and $[0_2/90_2/+45_2/-45_2]_s$ specimens in the presence of dilute (0.01 molar) hydrochloric acid.

4.3.1. Stress-Rupture of Unidirectional $[0]_2$ Specimens

Eight stress-rupture tests of unidirectional $[0]_2$ specimens were performed. In each case the strain vs. time response was typical of that of an ordinary creep test, see Figures 5, 6, and 7. No indication of the chemical processes being undergone within the fibers was apparent because no interrupted strength tests were performed. Therefore, how the strength might vary before the appearance of stress-corrosion cracks was unknown. Stress-corrosion cracks were observed to grow to lengths dependent upon the tensile load on the specimen. The number of stress-corrosion crack nucleation sites was greatest for the highest applied tensile stress test. The length that a stress-corrosion crack grew before a split formed depended upon the applied tensile stress; lower stresses permitted longer cracks to grow. The splits effectively reduced the cross section of the specimen, and raised the total strain in the remaining material. For the higher stressed specimen (225 MPa), in Figure 19, most of the individual stress-corrosion cracks are less than 1 mm in length. Also, a large number of cracks form. This explains the tortuous fracture profile. For the case of the lower stressed specimen (185 MPa), in Figure 20, there were two long cracks: one 9 mm, and one 3 mm long. The remaining cross-section became highly stressed, and a large number of small cracks formed, accompanied by extensive splitting. The basic process then, was to form few long cracks which grew normal to the applied load, then to transition to a combination of large numbers of short cracks with splitting, as the effective stress increased. Cracks typically grew completely through the thickness of these two-ply specimens. Some high stress tests (tensile loads of approximately 70% of quasi-static strength) were conducted in high strength acid baths (1 molar HCl) on 8-ply specimens. In those cases, cracking was usually arrested by delamination of the surface-cracked ply, and by splitting.

All stress-rupture life data was plotted as normalized applied stress to ultimate strength (S_a/S_u) vs. time to failure in Figure 21. Then a curve was fit to the data using the function indicated in Equation 3, resulting in values for the coefficients of A=1, B=-0.294, and p=0.582. Short duration life data of less than 10,000 seconds was lacking. In order to help the curve fitting routine to correctly traverse the gap, data from a single $[0]_8$ stress-rupture test was inserted into the plot. There were two inconsistencies in doing so. The specimen was four times thicker, and the acid concentration was 10 times sronger. The two inconsistencies cancel each other to some extent, so

it was judged that the error was not severe, and would outweigh the problem of omission. Without the short-life data point, the curve fitting routine would give an extremely rapid drop in normalized applied stress for a small increase in life, which was not realistic.

Three of the long-life tests were interrupted before failure (as indicated by the arrows). As a consequence, the fit curve has a built in lower bound on the low-stress/long-life portion of the curve.

4.3.2. Stress-Rupture of Quasi-Isotropic Specimens

Strain - Time Plots The strain vs. time plots are a rough indicator of the onset of damage, because as the cracks nucleate and grow the strain in the gage section increases rapidly. Strain vs. time plots for each quasi-isotropic stress-rupture test was given beginning with Figure 12 and continuing through to Figure 17. Except for the short duration tests of the 8-ply quasi's in Figure 12, it can generally be observed that the strain vs. time response is mainly that of ordinary creep, with a brief tertiary phase indicating the nucleation and rapid propagation of cracks.

Stress-Corrosion Crack Nucleation and Initiation of 90° Cracks Generally, the higher the far field stress, the larger the number of stress corrosion cracks that nucleated. The preferred location of the fracture line was close to the meniscus, or just below it, although perhaps a quarter of failures were well below the meniscus. Matrix cracks parallel to the fibers in the 90° plies would have the effect of concentrating stress in the unidirectional plies (the critical element) and so it was needed to verify whether or not these cracks appeared at any time during the test. From the quasi-static tensile tests, it was known that matrix microcracking starts at 215 MPa for the 16-ply. For the 8-ply, matrix microcracking was not heard at any time until the failure stress of about 320 MPa. Therefore, 90° matrix cracks were not anticipated because stress-rupture tests for 8-ply quasi's were conducted at stresses not more than 1/3 of the cracking onset stress (1/2 for 16-ply quasi's). To determine whether cracks appeared at any time, the failed specimens were first examined for the appearance of matrix cracks outside the region exposed to the environment. None were found. For the region within the environment, the presence of 90° matrix cracks without an accompanying 0° stress-corrsion crack was searched for, but none were found. Finally, when 0° stress-corrosion cracks existed, there were also 90° matrix cracks underlying them.

The evidence supports formation of 90° cracks after the nucleation of a 0° stress-corrosion crack. An advanced stress-corrosion crack, with a 90° crack which extended for the entire width, appears in the photo of the fractured specimen in Figure 22. A schematic drawing is given in Figure 23. It was clear that once a 0° stress-corrosion crack had nucleated and propagated through the thickness of the ply, then, a crack in the adjacent 90° ply initiated. The 90° cracks grow well

ahead of the 0° cracks. This likely guides growth of the 0° crack due to both the local stress concentration, and ingress of environment to the interior of the laminate. From the 0° tests it was already known that the cracks prefer to propagate normal to the applied load, at least until the stress was high enough to start a split. The presence of the off-axis plies supressed splitting, which further encouraged the cracks to remain in a line.

Stress-Corrosion Cracking of the ±45° Plies Inspection of completely failed specimens reveals that stress corrosion cracking forms in the +45° plies adjacent to the 90° crack, and in some cases also penetrated the middle -45 ° plies, see Figures 24 and 25. This scenario was more prevalent for the lightly loaded specimens. The more highly stressed specimens were less likely to have stress corrosion in the 45's, see Figure 22. There was simply less time for stress corrosion cracking to either initiate or progress very far into the 45° plies before the 0° plies could no longer support load.

Appearance of the Fracture Profiles The final failures look slightly different between the 8-ply (Figure 24), and 16-ply (Figure 25) specimens. The very region which looked different is the portion of specimen with the remaining ligament of 0° plies. This part failed due to tensile overload, and looks much like the fracture morphology as was described in Section 4.1.2.

4.4. STRESS-RUPTURE LIFE PREDICTIONS

Predictions of stress-rupture life of the 8-ply quasi-isotropic specimens under a steady tensile load and immersed in 0.01 molar HCl acid is given in Figure 26, and for 16-ply quasi's in Figure 27. The predicted life locus (solid line) runs between the data points. For the 8-ply, prediction appears slightly high, while the prediction for the 16-ply is almost perfect. The dashed line is the predicted life locus if creep in the off-axis plies is ignored, and shows that overprediction of life results. The error amounts to roughly a factor of two increase in the life prediction.

5. Discussion

5.1. QUASI-STATIC TENSILE STRENGTH DATA

5.1.1. Unidirectional $[0]_8$ Tensile Tests

All failures of unidirectional $[0]_8$ specimens were close to the grip, indicating the predominance of grip region stress concentration. Correct strengths are obviously preferable, so a correction factor was sought. Work done by O'Brien *et al.* [28] gives finite element analyses of grip region stress concentration. They compute a stress concentration of nearly 1.2 for the graphite/epoxy material they modeled. The degree of orthotropy (E_{11}/E_{22}) was shown to affect the

stress concentration. Since the unidirectional glass/epoxy had an orthotropy ratio of 3.3 (11.6 for the unidirectional carbon/epoxy), it was accepted that the correction factor of 1.2 was not strictly correct. The strength actually used in the predictions was raised by a factor of 1.2 from 862 MPa to 1034 MPa. Having established that initiation of the fiber fracturing near or at the grip should be expected, the issue of the splitting is addressed. For organic matrix composites, the poor interfiber fracture toughness makes it likely that cracks running across fibers will reorient themselves toward the direction requiring the least energy to continue the fracture. Unidirectional composite, lacking constraint against splitting, will prefer to split, as was seen in Figure 4(a). The effect of ply constraint on resistance to splitting was addressed by Stinchcomb, Reifsnider, Yeng, and Masters [29].

5.1.2. Quasi-Isotropic Specimens

There was no splitting of the surface unidirectional plies outside of the damaged zone in the 8-ply quasi-isotropic specimens, but there was for the 16-ply specimens. The unrestrained splitting behavior seems to occur depending upon the thickness of the 0° plies. Stress redistribution around a stress-corrosion crack drives peeling and splitting of the bundle of fibers from the laminate, and this depends on thickness. It would appear that to control unrestrained splitting of surface zero degree plies, their thickness must not exceed some threshold that can probably be related to the stiffnesses and interfiber fracture toughness.

5.2. CREEP TEST DATA

A thorough calibration of the extensometers (to meet ISO 9001 standards) was performed late in the experimental program. Though the transducers passed, this did not assure smooth creep data. The extensometers were designed for shorter, stiffer specimens than used here. It was especially difficult to obtain smooth creep data from the 2-ply 0° and 8-ply 90° specimens, because of their flexibility.

The setup for each test was long, and often needed to be repeated until good elastic modulus measurements were obtained. Correct elastic modulus data was a good indicator that the extensometers were installed well, but was no guarantee that data would continue to be smooth. Good results often depended on talent, experience, or just luck. This suggested that although ISO 9001 standards were met when the extensometers were mounted on a calibration rig, it did not mean they will be met when mounted to a composite test specimen. Further work should be done to establish the allowable bending stiffness of composite creep specimens to ensure smooth creep data when using these extensometers.

5.2.1. Unidirectional $[0]_2$ Creep Tests

The measured creep response of the unidirectional specimens was actually a combination of creep and the influence of moisture expansion due to moisture uptake during the stress-rupture tests. Tests were not conducted to characterize moisture absorption effects independently from the creep response, therefor the relative contribution of each to the compliance change was not known. However, as both the unidirectional and quasi-isotropic tests were under the same temperature and moisture conditions, the compliance data of the unidirectional specimens should accurately represent the changing compliance of the same plies in the quasi-isotropic specimens.

5.2.2. Fitting Curves to the $[+45/-45/+45/-45]_s$ Creep Tests

The curve fit for the shear compliance, $S_{66}(\tau_{12},t)$ is not as good as for $S_{11}(t)$ or $S_{22}(t)$, as is clear when Figures 8 and 10 are compared to Figure 11. Choosing the coefficients was actually a lengthy trial and error process because the curve fitting software used could not simultaneously optimize the fit to all curves. Rather, a fit was found for one curve and then the coefficients were adjusted until all other curves were approximately represented. The coefficients were chosen so that the predicted responses fell within the bounds of the experimental data.

The initial elastic shear modulus from extensometer data was taken while loading the pan of the creep frame, and appears in Table 2. The data is highly scattered. Apparently the relative slowness of loading the pan allowed the large initial viscoelastic response to literally creep into the elastic measurements.

5.2.3. Moisture Absorption Effects on Creep Response and Life

Moisture absorption influenced the overall creep response of the quasi-isotropic specimens at long test times, as was shown in Figure 18(c). The computed stress on the critical element should be correct if the creep response can be correctly predicted, at least before any cracks formed. Since creep in the long time tests is actually greater than predicted, the computed stress in the critical element will be low, and the life over-predicted.

Only the viscoelastic creep at room temperature of dry specimens was measured to form representations for $S_{22}(t)$ and $S_{66}(\tau_{12},t)$. To account for the effects of moisture requires additional tests. One test is to characterize the rate of diffusion of the HCl acid bath into the laminate. Another test is to obtain the moisture expansion coefficients. Finally, additional creep tests to characterize the dependence of compliance on the moisture content are needed.

5.3. STRESS-RUPTURE LIFE

5.3.1. Experimental Variability

Experimental variability in the stress-rupture life data was observed (see Table 3, and Figures 26 and 27). Of three tests at the same stress level, two would often have virtually identical lives, and the third would be an outlier. No scratches were found on any specimens that might be blamed for early exposure of the fibers to the acid. Nor was there any correlation between life and specimen thickness. The rationale for a correlation between the two is that fiber volume fraction, V_f, and thickness are often strongly correlated. Stresses calculated from cross-sectional area will not necessarily be related to stress on the fibers unless V_f is known. Furthermore, a high V_f means less resin to protect the fibers from the acidic environment. This said, there were too few tests at any one stress to find a correlation between life and thickness.

5.3.2. Model Predictions

Applied stress versus stress-rupture life plots of experimental data for the 8-ply $[0/90/+45/-45]_s$ specimens and for the 16- ply $[0_2/90_2/+45_2/-45_2]_s$ specimens was given, along with a predicted life locus, in Figures 26 and 27, respectively. At first glance, the predictions look good for both 8-ply and 16-ply specimens. The apparent success of the predictions rests upon two observations. First, relative to the total life of the specimen, failure occured shortly after the first stress corrosion cracks appeared. Second, the positioning of the 0° plies on the outside of the laminate simplified the problem by eliminating the need to consider the rate of diffusion of the environment through protective plies.

All the creep was not accounted for, especially at long times, as was shown in Figure 18(c). The additional creep was likely due to moisture uptake. Life predictions would be expected to be high, which seems to be the case. Creep significantly affects life, but is less than an order of magnitude effect, at least at room temperature. At elevated temperature creep will play a much more significant role. Diffusion rate and corrosion rate would also be significantly affected by temperature [20]. Characterizing temperature effects on rates of creep, corrosion, and moisture diffusion will be important to predicting life of more complex loading cases and more challenging laminate stacking sequences.

5.3.3. Effect of "n" on Stress-Rupture Life of $[0]_n$ Unidirectional Specimens

The thickness of the quasi-isotropic specimens affects their life when exposed to the HCl acid. The thicker specimens last longer. To model the effect of thickness on life of the unidirectional laminates was beyond the scope of this study. In order to eliminate this variable, the original seventeen 8-ply unidirectional specimens were replaced with a new set of ten 2-ply

specimens. This was the reason for the sparsity of data available to define the stress vs. life response.

5.3.4. *Other Damages to the Sub-Critical Elements: Observed, Yet Unaccounted For*

Matrix Microcracking If the 90° plies in the quasi-isotropic laminate had cracked at any time during the stress-rupture test, then the stress concentration on the 0° plies would need to be included. From both quasi-static tensile tests and stress-rupture tests of the quasi-isotropic specimens it was known that the threshold stress at which cracks initiated in the 90° plies was well above the stresses used in the stress-rupture tests. Matrix microcracking was only observed to form in the 90° plies once cracking in the 0° plies had begun. However, as this occurred very late in the life of the specimen it was judged not to be a significant factor influencing the total life.

Stress-Corrosion Cracking It is expected that once a 90° crack forms (as was observed in response to formation of 0° cracks, as was shown in Figures 22 and 23), that the environment would be transported along the crack and into the laminate where interior plies would come under attack. These events did occur, as was clear from Figures 24 and 25. Substantial portions of the 45° plies were cracked. It was assumed that the additional life would be brief once 0° cracks appeared, and so stress-corrosion cracking of off-axis plies was ignored, as was the resulting increased stress on the critical element.

5.4 FUTURE WORK

Considerable further work is needed to model stress-rupture life of more general problems. The laminate studied here was deliberately chosen to avoid delamination and a host of other anticipated complications. What follows is a list of complicating effects, more general loadings, and environmental conditions which should be examined in the laboratory and incorporated into the model.

1) Characterize the effects of moisture on expansion and compliance, and hence on life.

2) High stress testing should be conducted on laminates made with acid resistant glass fibers, such as R-glass. Then, the effect of matrix microcracks neighboring to load bearing plies on long term life due to stress concentration and/or the crack serving as a path for rapid ingress of acid can be studied. This information can be used to model the way load bearing, but subcritical elements crack and shed load to the critical element.

3) Effect of temperature on the rate of diffusion of the environment to both surface and subsurface load bearing plies.

4) Incorporate effects of fatigue and transient overloads [16]. This will necessitate well characterization of the remaining strength will time and stress.

5) Investigate the potential to use short term elevated temperature tests to predict long term life.

6. Conclusions

Stress-rupture life of E-glass/913 quasi-isotropic composite laminates has been predicted from lamina stress-rupture life data, and creep response, using a mechanistic stress-rupture life model based on the critical element modeling philosophy. The effects of creep in the various plies has been shown to significantly affect the prediction of stress-rupture life. Increasing thickness by ply-level scaling was found to increase the life because there was more material to be degraded.

7. References

1. Sturgeon, J.B. (1978). Creep of Fibre Reinforced Thermosetting Resins. in Creep of Engineering Materials, A Journal of Strain Analysis Monograph, edited by C.D. Pomeroy, Mechanical Engineering Publications Limited, London, Chapter 10, pp. 175-195.

2. Scott, W.D., Lai, J.S., and Zureick, A.-H. (1995). Creep Behavior of Fiber-Reinforced Polymeric Composites: A Review of the Technical Literature. Journal of Reinforced Plastics and Composites, Vol. 14, June, pp. 588-617.

3. Lou, Y.C., and Schapery, R.A. (1971). Viscoelastic Characterization of a Nonlinear Fiber-Reinforced Plastic. Journal of Composite Materials, Vol. 5, pp. 208-234.

4. Findley, W.N., Lai, J.S., and Onaran, K. (1976). Creep and Relaxation of Nonlinear Viscoelastic Materials. New York: Dover Publications.

5. Heywood, R.B. (1961). The Fatigue and Stress-Rupture Properties of Some Glass Reinforced Polyester Laminates. Royal Aerospace Establishment Tech Note Chem 1376, February.

6. Steele, D. (1965). The Creep and Stress-Rupture of Reinforced Plastics. Trans. J. Plastics Inst., Vol. 33, pp. 161-167.

7. Lyons, K.B., and Phillips, M.G. (1981). Creep-Rupture and Damage Mechanisms in Glass-Reinforced Plastics. Composites, October, pp. 265-271.

8. Aveston, J, and Sillwood, J.M. (1982). Longterm Strength of Glass Fibre Reinforced Plastics in Dilute Sulphuric Acid. Journal of Materials Science, Vol. 17, pp. 3491-3498.

9. Hogg, P.J. (1983). Factors Affecting the Stress Corrosion of GRP in Acid Environments. Composites, Vol. 14, No. 3, pp. 254-261.

10. Hogg, P.J., and Hull, D. (1989). Progress in Rubber and Plastic Technology, Vol. 5, pp. 112-155.

11. Jones, F.R., Rock, J.W., and Bailey, J.E. (1983). The Environmental Stress Corrosion Cracking of Glass Fibre-Reinforced Laminates and Single E-glass Filaments. J. of Materials Science, Vol. 18, pp. 1059-1071.

12. Jones, C.J., Dickson, R.F., Adam, T., Reiter, H., and Harris, B. (1984). The Environmental Fatigue Behaviour of Reinforced Plastics. Proceedings of the Royal Society of London, A 396, pp. 315-338.

13. Jones, F.R., and Rock, J.W. (1984). A Method for Determining Crack Velocity Stress Intensity Curves for Stress Corrosion Cracking of GRP. Advances in Fracture Mechanics, Proceedings of the 6th International Conference on Fracture, New Delhi, India, December 4-10, pp. 3053-3060.

14. Sheard, P.A., and Jones, F.R. (1986). The Effect of Environment on Stress Corrosion of Single E-Glass Filaments and the Nucleation of Damage in Glass Fibre Reinforced Plastics. Proceedings of FRC '86, Inst. Mech. Engr. paper C38/86, pp. 63-68.

15. Jones, F.R. (1994). Chapter 6.5 Stress Corrosion Cracking of GRP. Handbook of Polymer-Fibre Composites, F.R. Jones, Ed., Polymer Science and Technology Series, Longman Scientific & Technical Publishers, Longman Group U.K. Ltd., Essex, England, pp. 379-388.

16. Rawles, J.D., Roscow, J.A., and Phillips, M.G. (1990). The Effect of Transient Overloads on the Long Term Performance of Glass Fibre Reinforced Polymer (GFRP) Pipes for Power Station Cooling Water Systems. The 1990 Pressure Vessels and Piping Conference, Nashville, Tennessee, June 17-21, American Society of Mechanical Engineers, PVP Vol. 196, pp. 17-21.

17. Crowther, M.F., Wyatt, R.C., and Phillips, M.G. (1989). Creep-Fatigue Interactions in Glass Fibre/Polyester Composites. Composites Science and Technology, Vol. 36, pp. 191-210.

18. Moore, R.H., and Dillard, D.A. (1990). Time-dependent Matrix Cracking in Cross-ply Laminates. Composites Science and Technology, Vol. 39, pp. 1-12.

19. Tavakoli, S.M., and Phillips, M.G. (1991). Compatibility and Durability in Glass/Phenolic Laminating Systems. ICCM8, The 8th International Conference on Composite Materials.

20. Phillips, M.G. (1983). Prediction of Long-term Stress-Rupture Life for Glass Fibre-Reinforced Polyester Composites in Air and in Aqueous Environments. Composites, Vol.14, No. 3, July, pp.270-275.

21. Dillard, D.A., and Brinson, H.F. (1983). A Numerical Procedure for Predicting Creep and Delayed Failures in Laminated Composites. Long-Term Behavior of Composites, ASTM STP 813, T.K. O'Brien, Ed., American Society for Testing and Materials, Philadelphia, PA, pp. 23-37.

22. Reifsnider, K.L., Stinchcomb, W., and Osiroff, R. Modeling of Creep Rupture Mechanisms in Composite Material Systems.

23. Reifsnider, K.L., and Stinchcomb, W. (1986). A Critical Element Model of the Residual Strength and Life of Fatigue-Loaded Composite Coupons. Composite Materials: Fatigue and Fracture, ASTM STP 907, H.T. Hahn (Ed.), American Society for Testing and Materials, Philadelphia, PA, pp. 298-303.

24. Reifsnider, K.L., (1991). Performance Simulation of Polymer-Based Composite Systems. In Durability of Polymer-Based Composite Systems for Structural Applications, A.H. Cardon and G. Verchery (Eds.), Elsevier Applied Science, New York, pp. 3-26.

25. Reifsnider, K.L., (1992). Use of Mechanistic Life Prediction Methods for the Design of Damage Tolerant Composite Material Systems. ASTM STP 1157, American Society for Testing and Materials, Philadelphia, PA, pp. 205-223.

26. Reifsnider, K.L. (1997). Some Fundamental Aspects of the Fatigue and Fracture Response of Composite Materials. Proceedings of the 14th Annual Meeting, Society of Engineering Science, G.C. Sih, Ed., Recent Advances in Engineering Science, pp. 373-384.

27. Rosen, B.W. (1972). A Simple Procedure for Experimental Determination of the Longitudinal Shear Modulus of Unidirectional Composites. Journal of Composite Materials, Vol. 6, pp. 552-554.

28. O'Brien, T.K., Salpekar, S.A. (1993). Scale Effects on the Transverse Tensile Strength of Graphite/Epoxy Composites. Composite Materials: Testing and Design (Eleventh Volume), ASTM STP 1206, E.T. Camponeschi, Jr., Ed., American Society for Testing and Materials, Philadelphia, pp. 23-52.

29. Stinchcomb, W.W., Reifsnider, K.L., Yeung, P., and Masters, J. (1981). Effect of Ply Constraint on Fatigue Damage Development in Composite Materials. Fatigue of Fibrous Composite Materials, ASTM STP 723, American Society for Testing and Materials, pp. 64-84.

Table 1. Elastic and Strength Properties of E-glass/913
from Quasi-Static Tensile Tests in Universal Test Machine

stacking sequence	spec. #	width (mm)	thickness (mm)	Young's modulus (GPa)	Failure Load (kN)	Tensile Strength (MPa)
$[0]_8$	UB-3	25.51	1.17	44.3	25.95	869.4
	UB-4	25.22	1.17	47.9	25.15	852.3
	UB-10	25.60	1.17	45.7	25.90	864.7
$[0/90/+45/-45]_S$	Q8-6	25.14	1.13	21.4	8.78	309.1
	Q8-8	25.26	1.12	21.6	9.18	324.5
$[0_2/90_2/+45_2/-45_2]_S$	Q16-3	25.15	2.32	22.9	18.18	311.6
	Q16-5	25.29	2.28	21.7	17.66	306.3

Table 2. Elastic Properties of E-glass/913 from Creep Test Data

stacking sequence	spec. #	width (mm)	thickness (mm)	Exx (GPa)	E22 (GPa)	G12 (GPa)
$[90]_8$	U90-6	24.04	1.00	14.1	14.1	–
	U90-7	23.92	0.99	15.2	15.2	–
	U90-8	23.95	1.01	13.6	13.6	–
	U90-10	23.90	1.00	13.4	13.4	–
$[+45/-45/+45/-45]_S$	S-1	25.24	1.19	23.5	–	8.95
	S-3	25.16	1.21	14.7	–	5.58
	S-4	25.34	1.18	15.9	–	6.04
	S-6	25.15	1.22	14.4	–	5.49
	S-7	25.28	1.16	19.3	–	7.32

Table 3. Stress-Rupture Life Results

stacking sequence	spec. #	Area (mm^2)	Applied Load (kN)	Applied Stress (MPa)	Young's Modulus (GPa)	Time to Failure (hours)
$[0]_8$	UA-4	27.08	16.39	605	na	0.13
$[0]_2$	U2-1	8.42	1.683	200	na	67.0
	U2-2	7.00	1.750	250	46.2	12.2
	U2-3	7.65	1.148	150	na	1701*
	U2-4	8.43	na	na	na	na
	U2-5	7.28	1.092	150	na	1700*
	U2-6	7.80	1.561	200	45.5	88.8
	U2-7	7.95	1.391	175	na	1600*
	U2-8	7.96	na	na	na	na
	U2-9	6.56	1.475	225	45.0	18.7
	U2-10	9.42	1.884	200	43.2	38.0
$[0/90/+45/-45]_S$	Q8-1	29.33	2.346	80	na	1053*
	Q8-2	28.15	3.604	128	23.0	47.3
	Q8-3	28.89	2.311	80	na	381.9
	Q8-4	29.14	3.264	112	24.9	120.0
	Q8-5	28.79	3.224	112	23.0	72.0
	Q8-7	28.32	3.171	112	22.3	130.3
	Q8-9	30.52	3.907	128	na	25.3
	Q8-10	28.35	3.629	128	na	22.6
$[0_2/90_2/+45_2/-45_2]_S$	Q16-1	53.96	6.690	124	23.77	100.1
	Q16-2	58.21	8.965	154	21.83	13.8
	Q16-4	56.36	6.087	108	23.43	335.8
	Q16-6	55.97	8.619	154	22.33	13.0
	Q16-7	56.47	7.002	124	23.59	59.8
	Q16-8	58.18	7.214	124	22.86	92.3
	Q16-9	58.53	6.322	108	23.49	119.5
	Q16-10	50.67	5.472	108	26.98#	123.0

* no failure, test was interrupted

na data not available

\# specimen was thin (panel edge)

Figure 1. Creep frame with 90° specimen and extensometers installed.

Figure 2(a). Unidirectional specimen showing clamps reinforcing the bonded end tabs. A clear plastic sheet is sealed with Tacky Tape brand of sealing strips to contain acid leaked from the acid cell upon failure of the specimen.

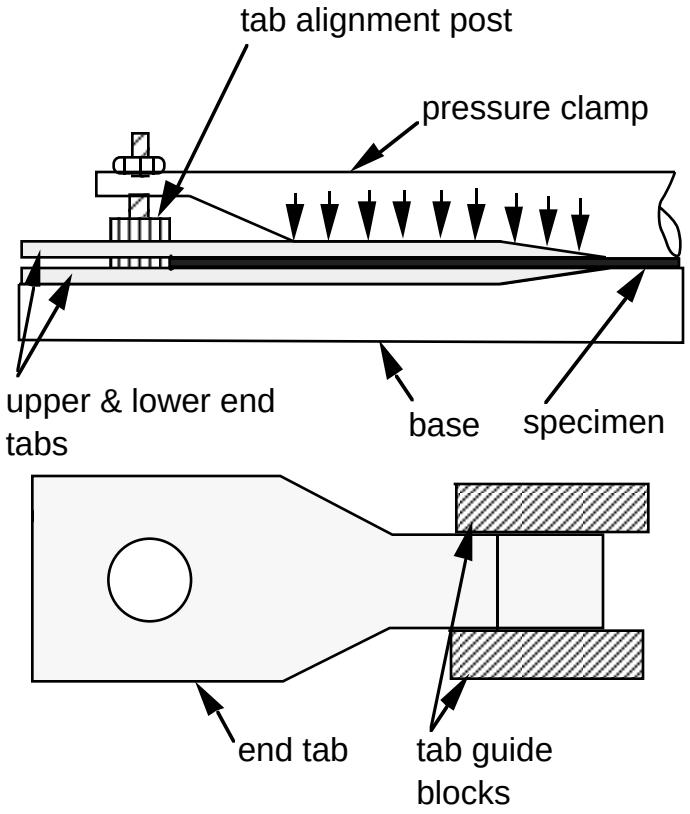

Figure 2(b). Diagram showing a portion of the fixture for aligning end tabs with the specimen. A uniform clamping pressure is applied along the bonded length of the tab (including the chamfered portion). The alignment post centers the holes in the tabs.

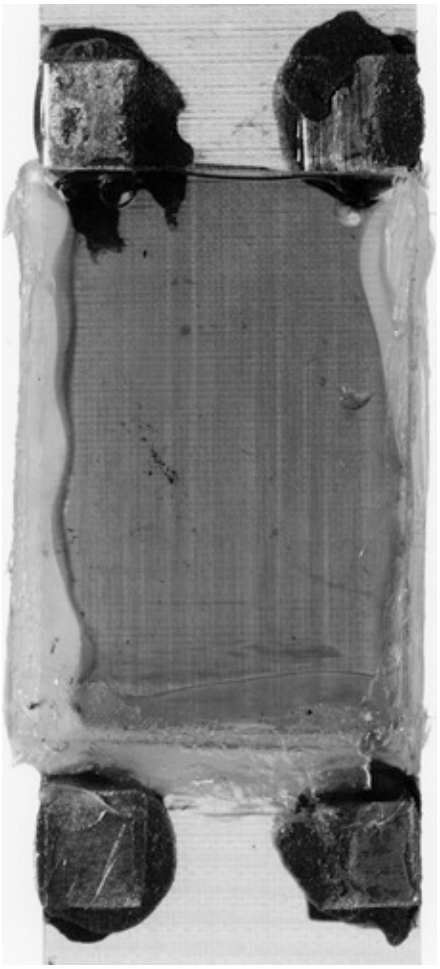

Figure 3. Close-up of the acid cell. The cells are glass slides 37 x 25 mm and are bonded in place, one on each side, with a clear silicon rubber sealant. The specimen edges are completely sealed. The squares of sheet aluminum are bonded using a paste epoxy adhesive and serve as pads for the extensometer screws to bite into.

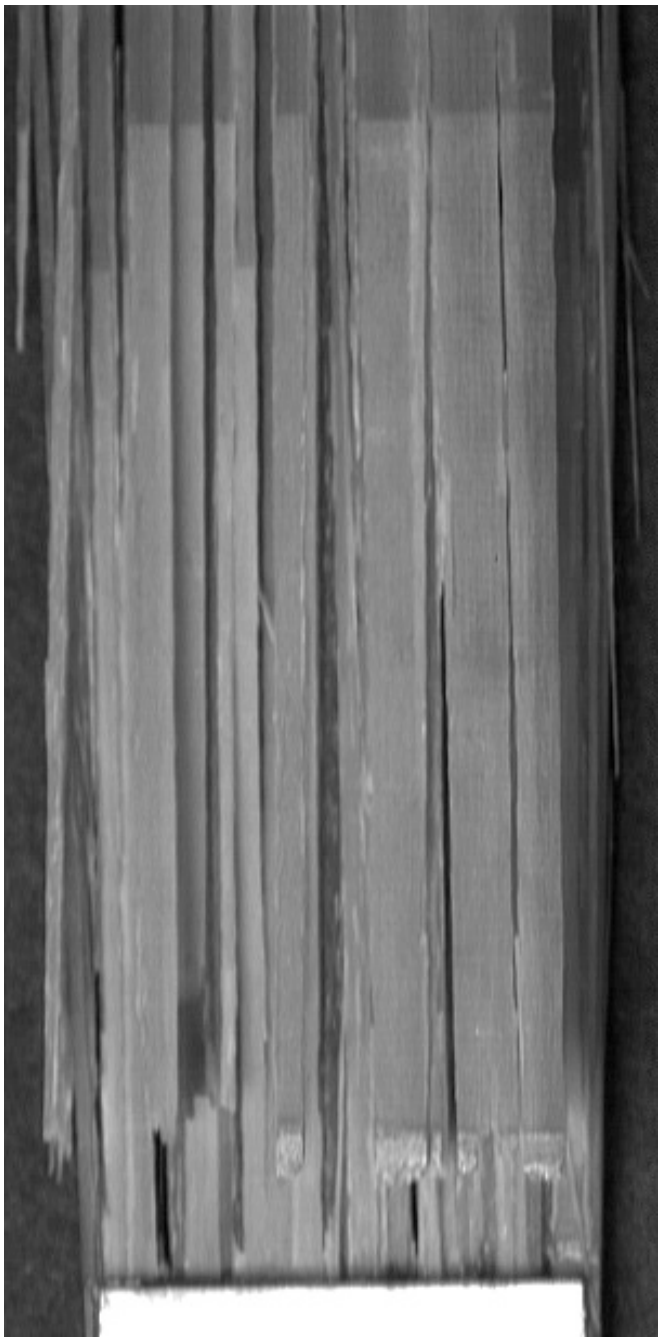

Figure 4(a). Fracture of $[0]_8$ quasi-static tensile specimen. Fracture initiated at the edge, at the grip edge, and proceeded by a repeated sequence of fiber fracture and splitting.

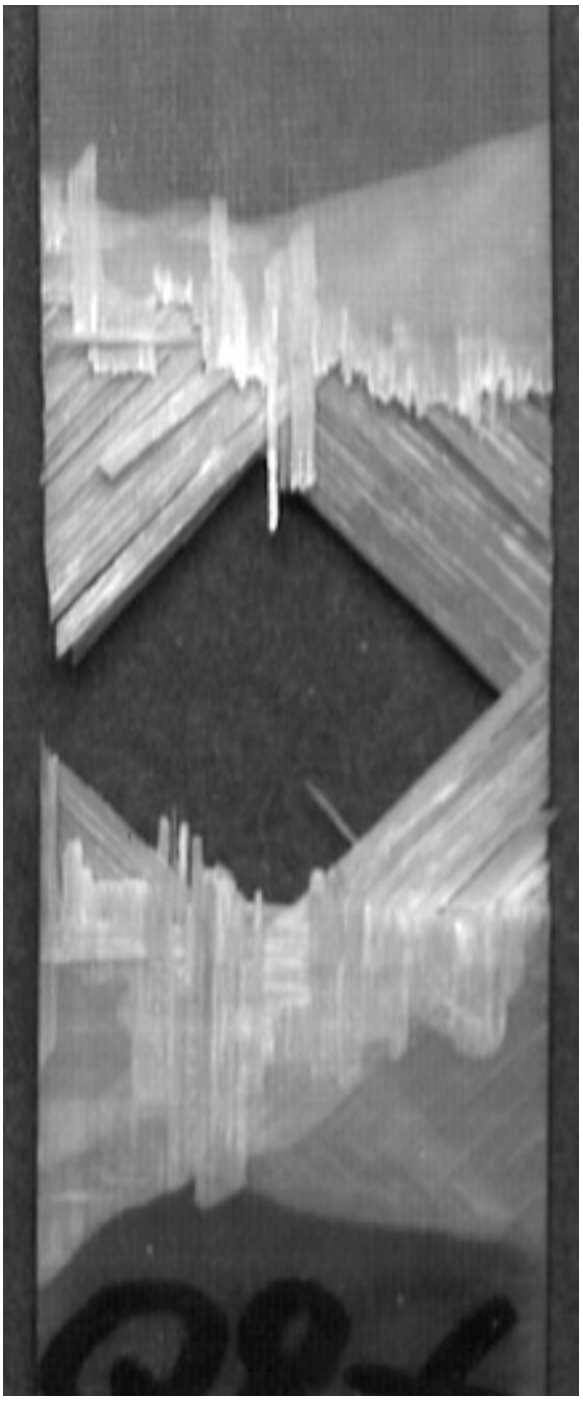

Figure 4(b). Representative fracture profile of a quasi-static tensile test of $[0/90/+45/-45]_s$ E-Glass/913-epoxy laminate. Higher constraint than in 4(a) prevents unrestrained splitting. The irregular profile is due to alternation of fiber bundle fracture and splitting. The 45 degree plies have not fractured, but instead split and shear out. Light areas are delamination.

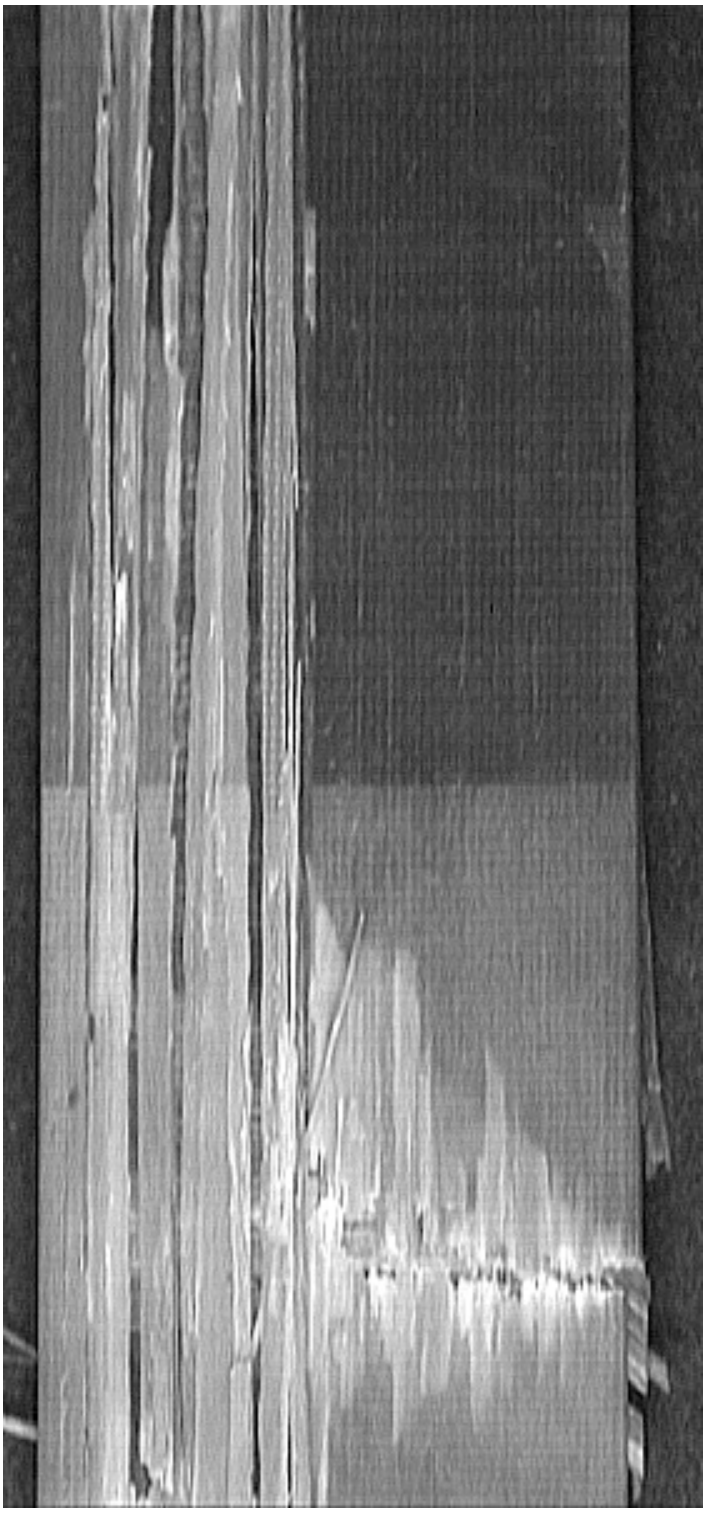

Figure 4(c). Representative fracture profile of a quasi-static tensile test of $[0_2/90_2/+45_2/-45_2]_s$ E-Glass/913-epoxy laminate. Lower constraint of 0° plies causes unrestrained splitting.

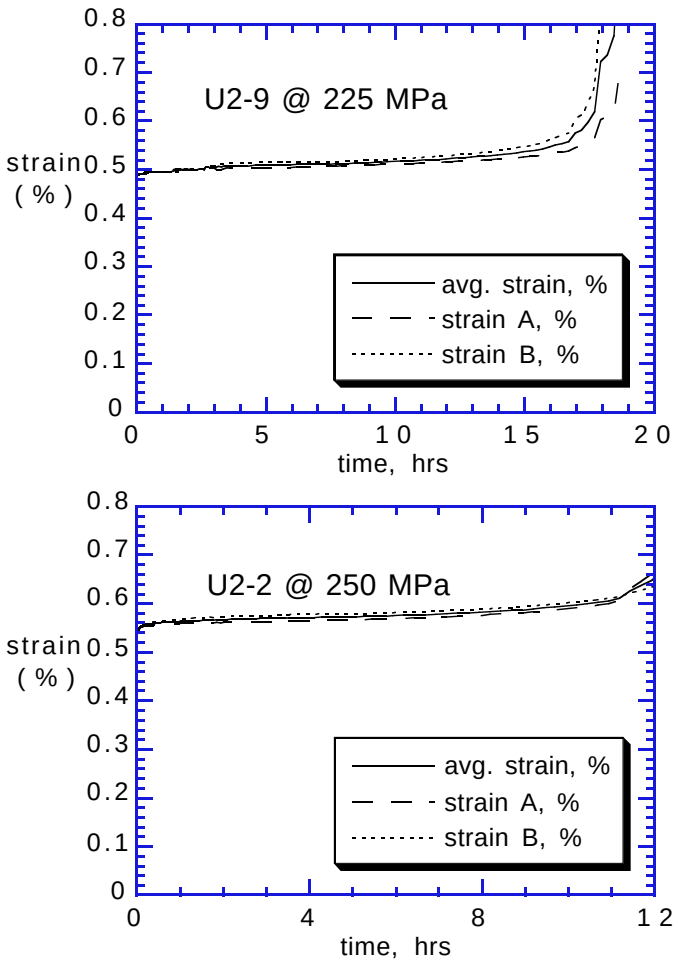

Figure 5. Creep results for constant stress tests of $[0]_2$ E-glass/913-epoxy in 0.01 molar HCl acid bath.

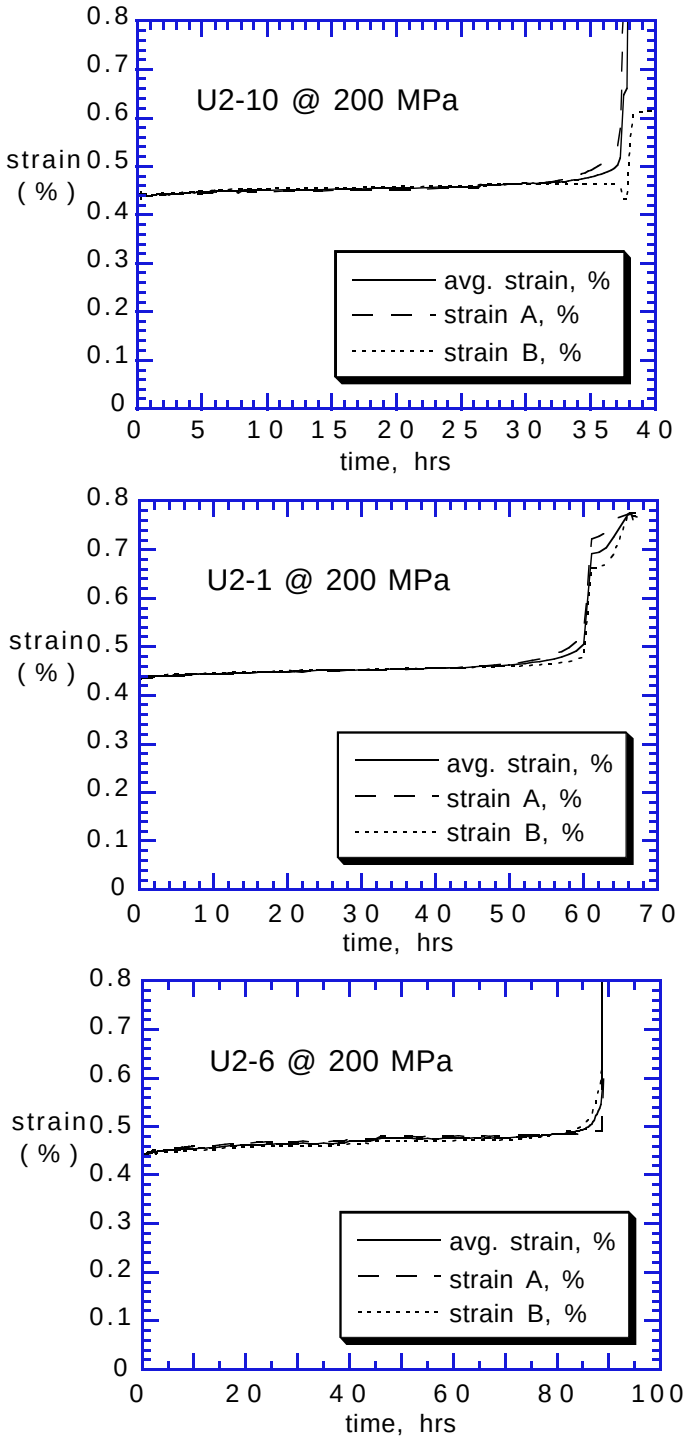

Figure 6. Creep results for 200 MPa constant stress tests of $[0]_2$ E-glass/913-epoxy in 0.01 molar HCl acid bath.

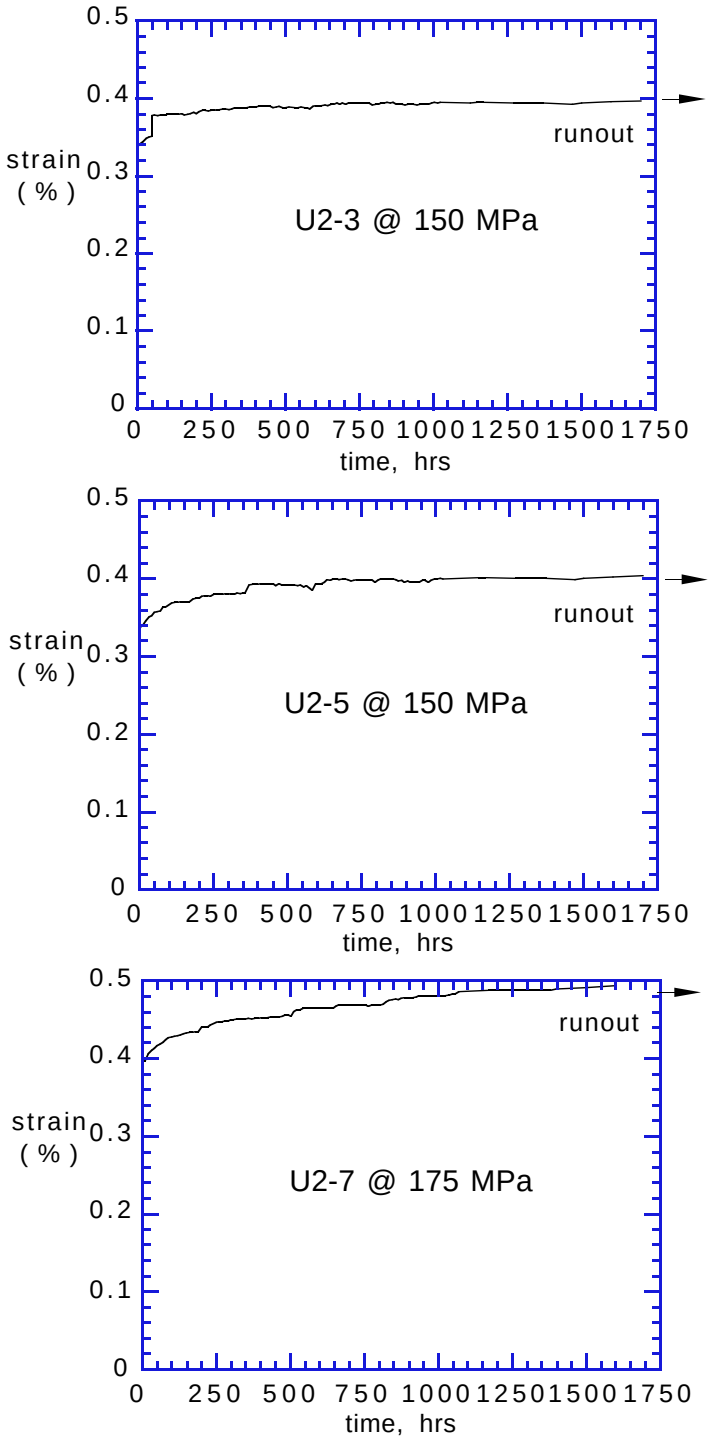

Figure 7. Creep results for constant stress tests of $[0]_2$ E-glass/913-epoxy in 0.01 molar HCl acid bath. Tests were stopped before failure. No cracks had formed.

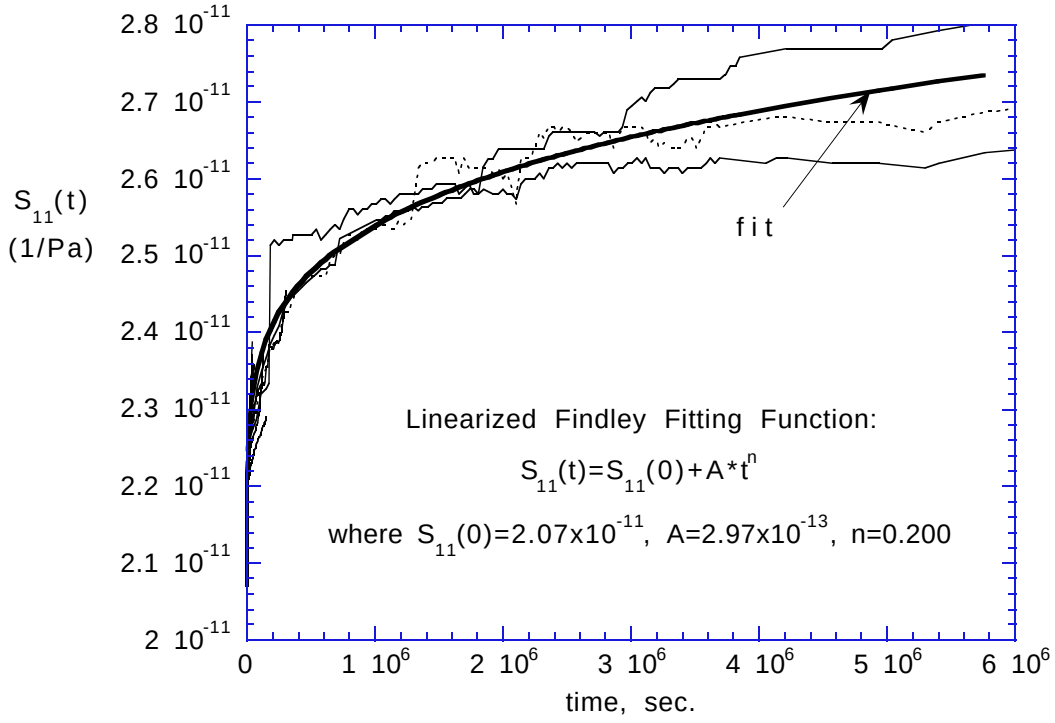

Figure 8. The linearized Findley fitting function is fit to experimentally determined $S_{11}(t)$ compliance vs. time data for unidirectional $[0]_2$ E-glass/913-epoxy immersed in a 0.01 molar hydrochloric acid bath. Heavy line is the fit, light lines are data.

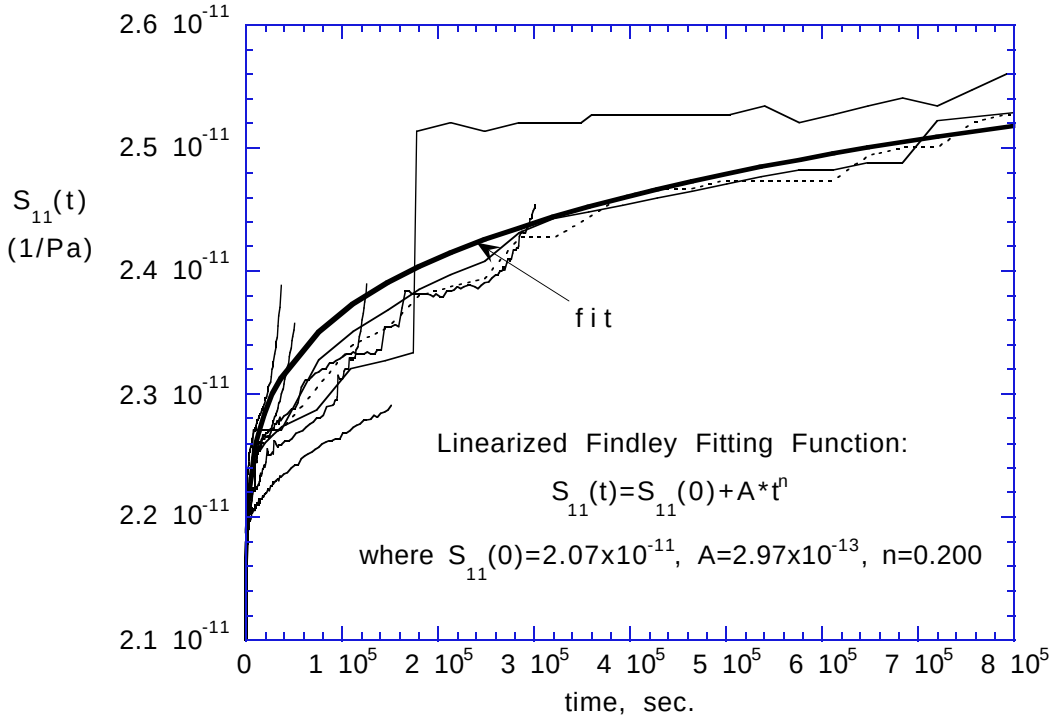

Figure 9. Examination of quality of fit early in the life. Heavy line is the fit, light lines are data. Where data turn upward at the end of their life is compliance change due to accumulation of damage. Damage influences compliance for a significant portion of the life of the highly stressed specimens, but may be ignored when characterizing the low-stress long-life specimens. Hence, only the effect of matrix stress relaxation on compliance is accounted for.

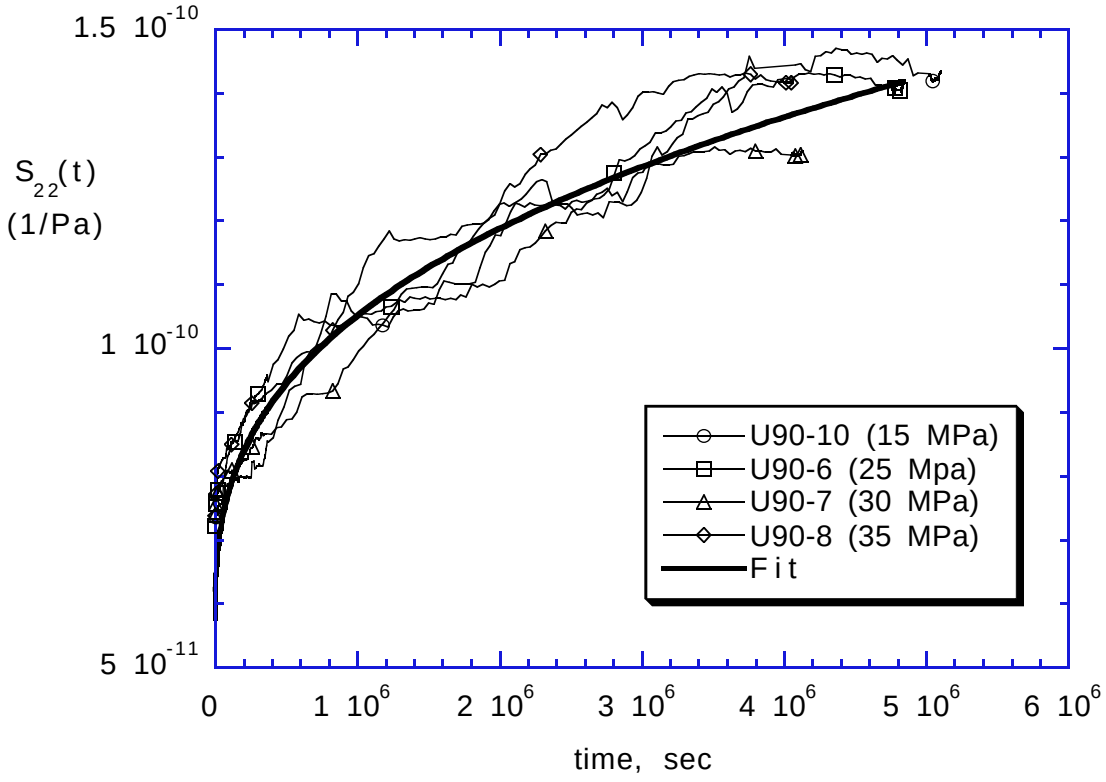

Linearized Findley Fitting Function:

$S_{22}(t)=S_0+A*t^n$

where $S_0=5.62x10^{-11}$, $A=3.629x10^{-13}$, $n=0.355$

Figure 10. Linearized Findley fitting funtion (heavy line) fit to experimentally determined $S_{22}(t)$ (transverse compliance) vs. time data (light lines). No apparent stress dependence.

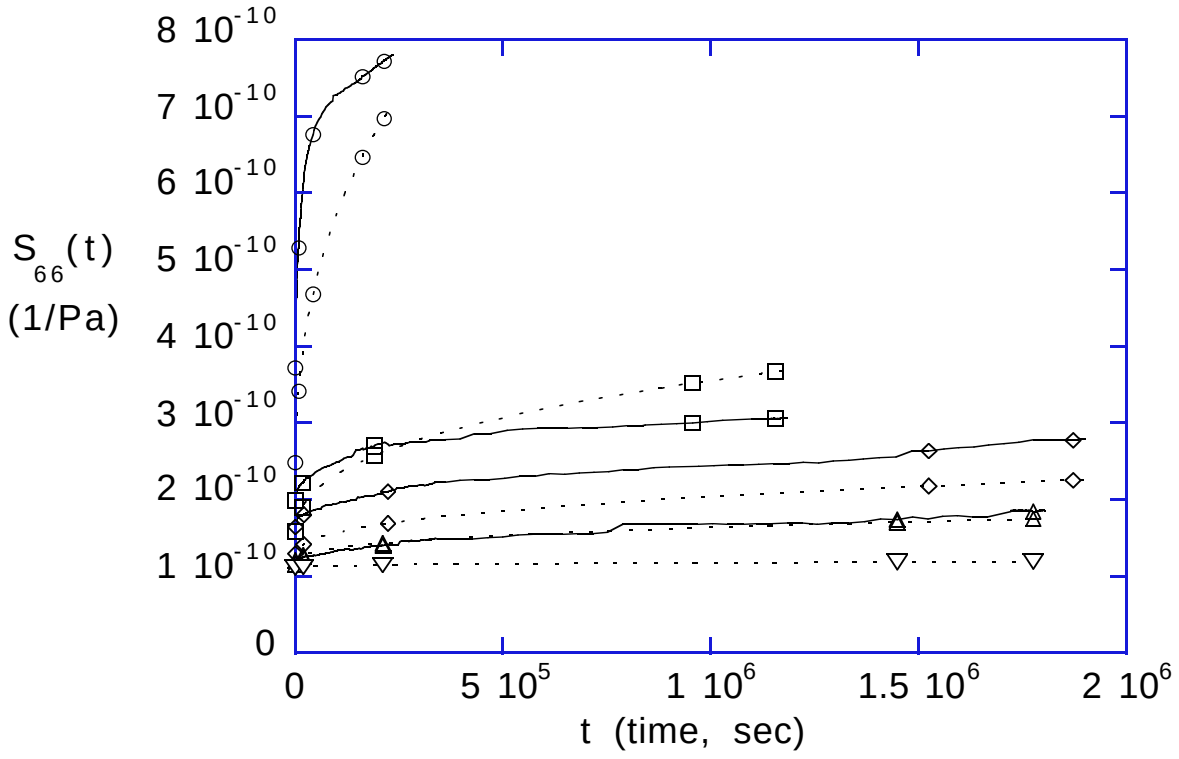

Schapery's fit: $S_{66}(\sigma,t)= S_{66}(0)*(1+g\sigma^2)+m(1+f\sigma^2)t^2$

$g=2.8x10^{-16}$ $m=12.36x10^{-15}$ $f=1.0x10^{-13}$ $n=0.37$

Figure 11. Schapery's quadratic fitting function (dashed lines) is fit to experimentally determined $S_{66}(t)$ (shear compliance) vs. time data (solid lines) from $[+45/-45]_{2S}$ E-glass/913-epoxy tensile creep tests. Stress dependency, σ, is included.

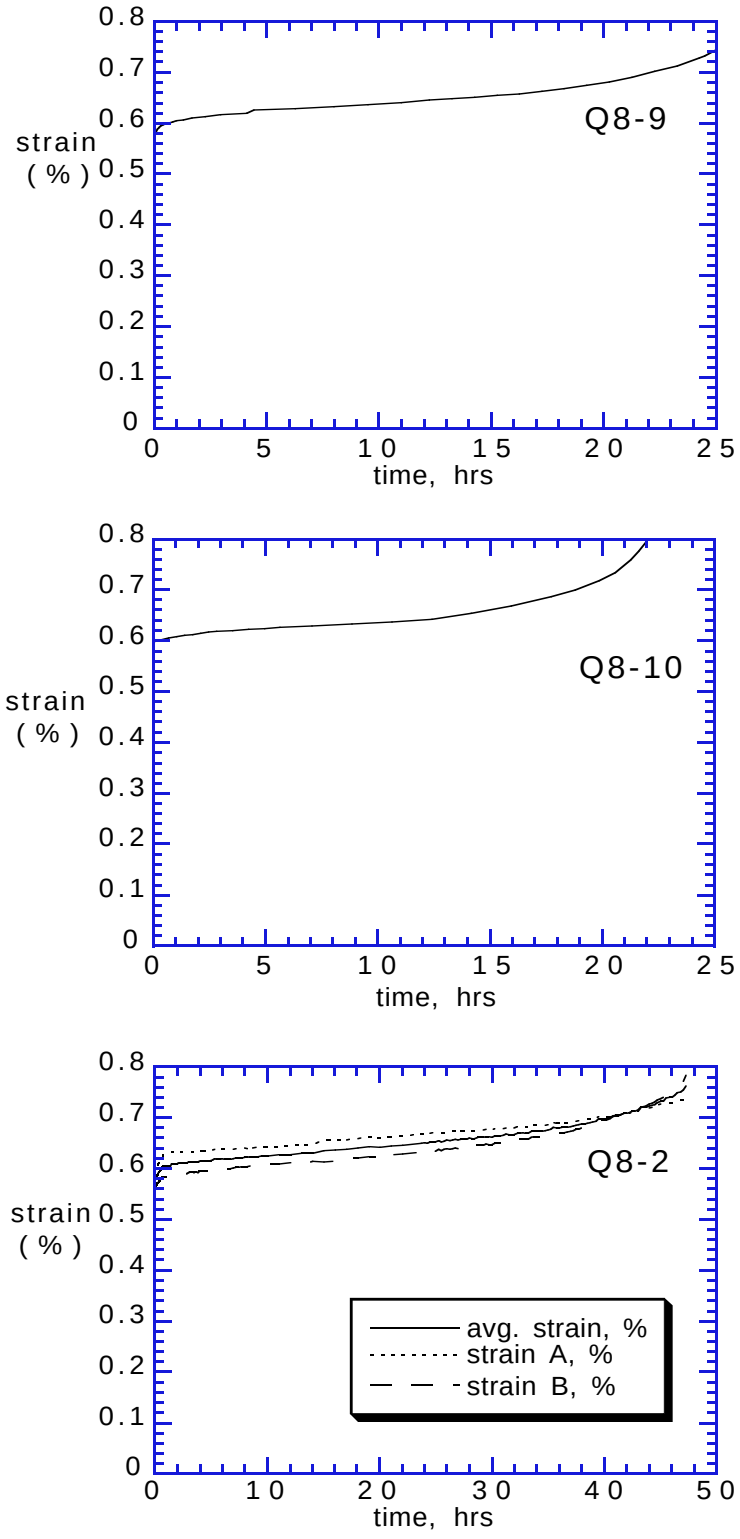

Figure 12. Creep results for 128 MPa constant stress tests of $[0/90/+45/-45]_s$ E-glass/913-epoxy in 0.01 molar HCl acid bath.

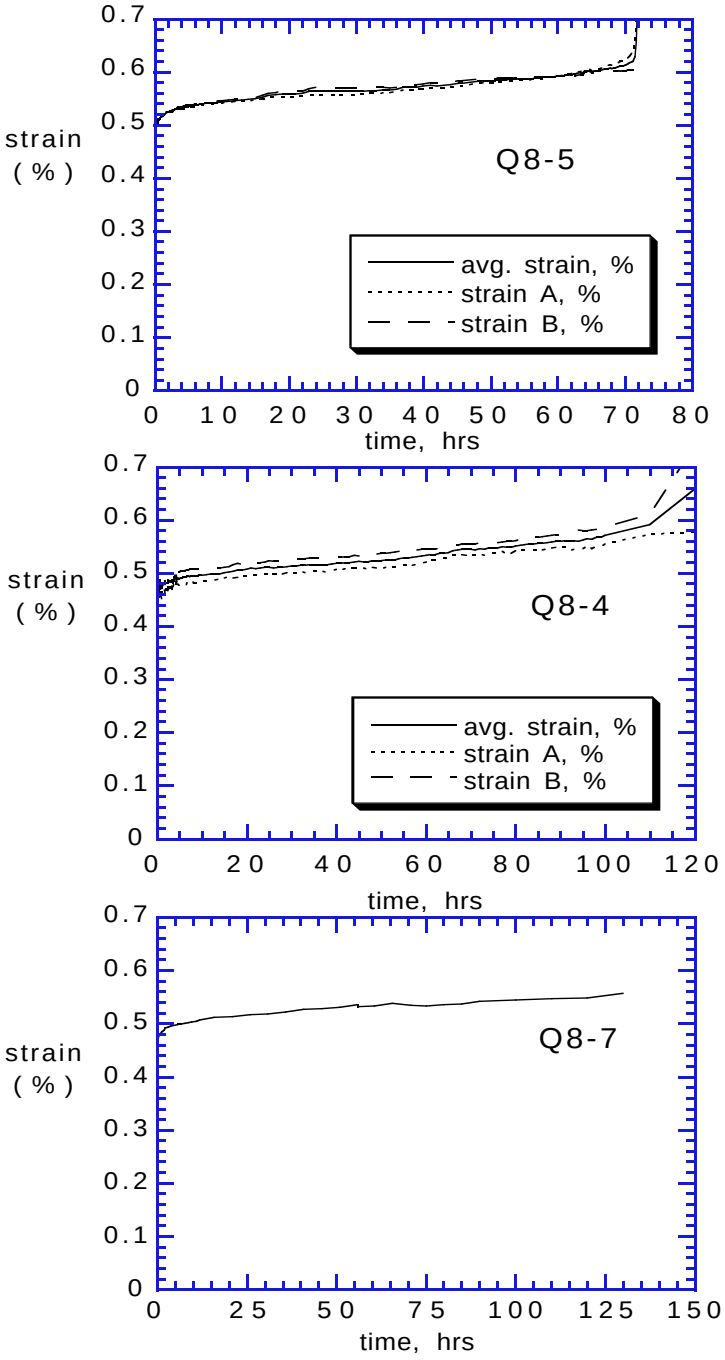

Figure 13. Creep results for 112 MPa constant stress tests of $[0/90/+45/-45]_s$ E-glass/913-epoxy in 0.01 molar HCl acid bath.

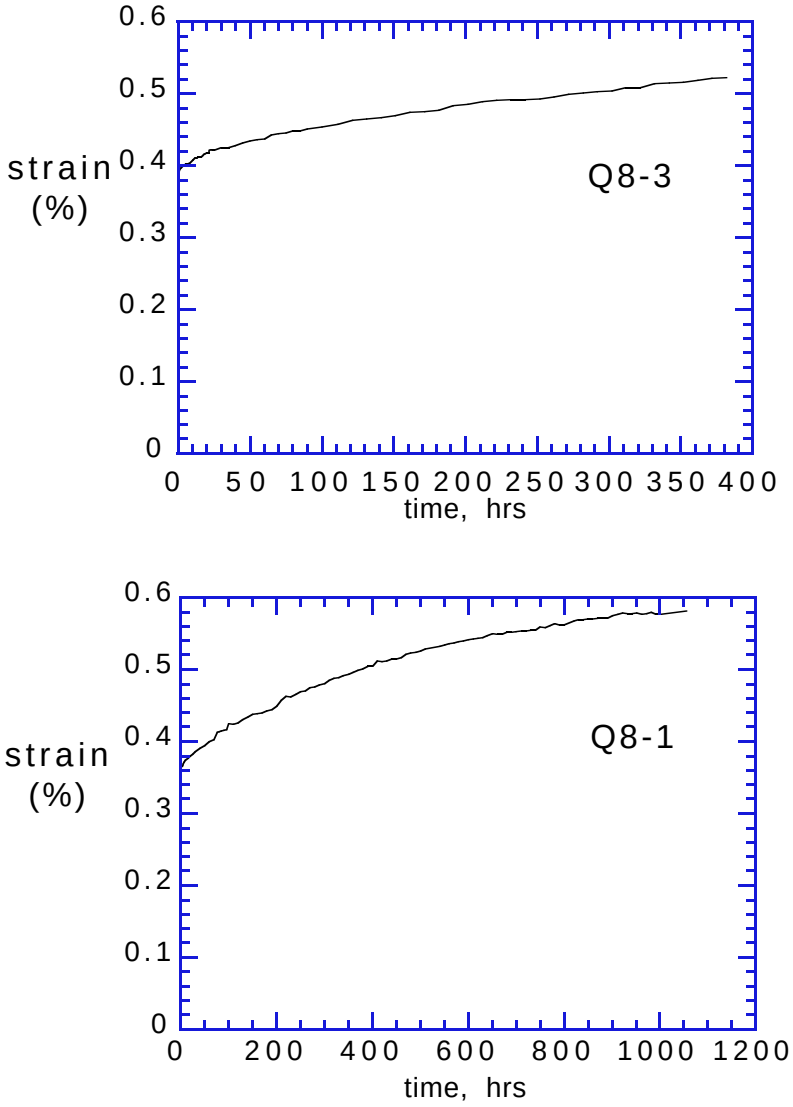

Figure 14. Creep results for 80 MPa constant stress tests of $[0/90/+45/-45]_s$ E-glass/913-epoxy in 0.01 molar HCl acid bath.

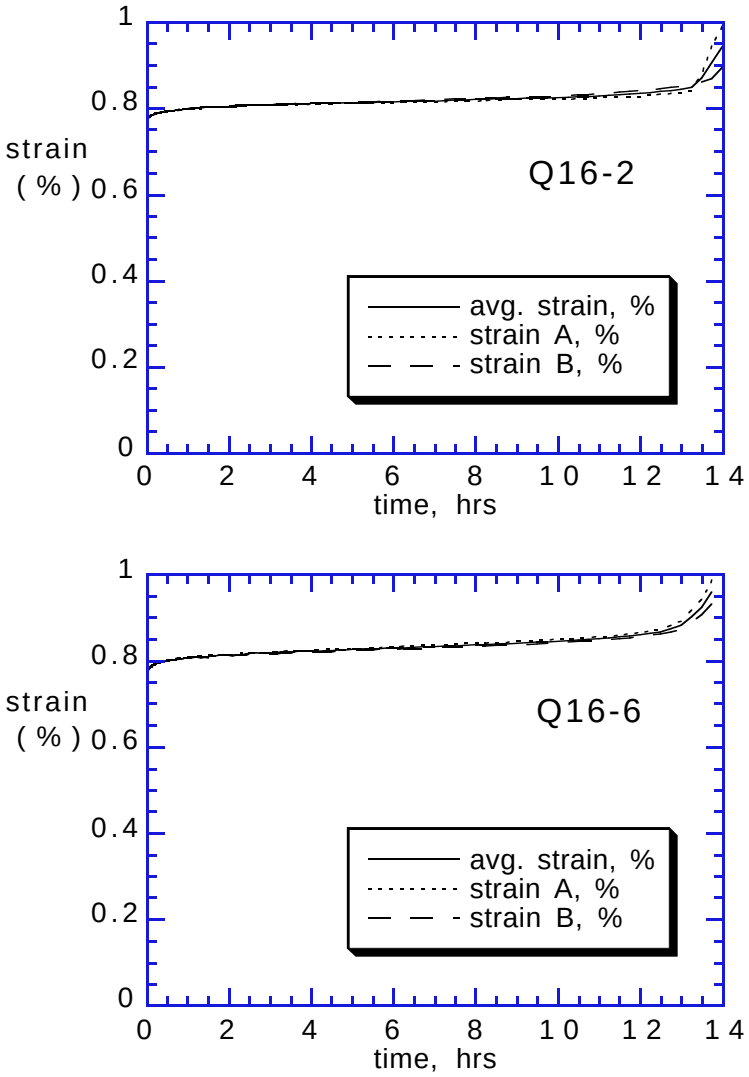

Figure 15. Creep results for 154 MPa constant stress tests of $[0_2/90_2/+45_2/-45_2]_s$ E-glass/913-epoxy in 0.01 molar HCl acid bath.

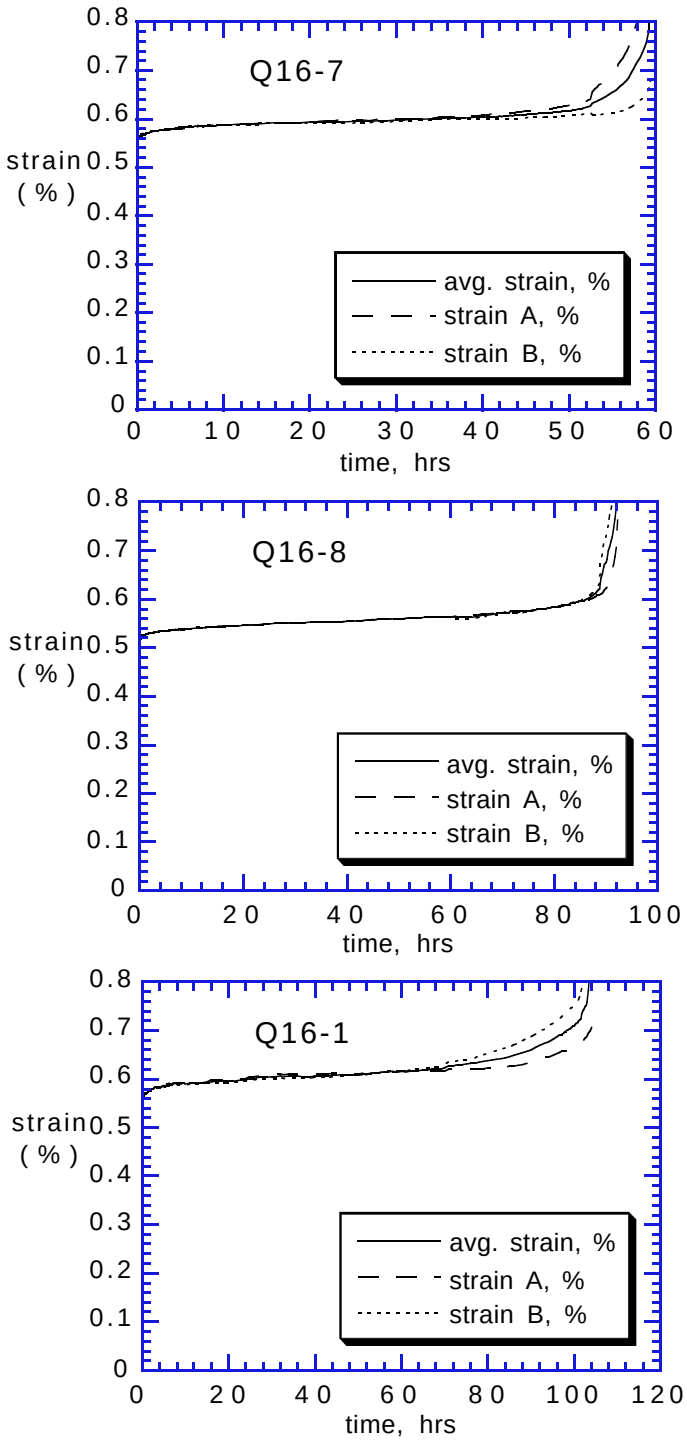

Figure 16. Creep results for 124 MPa constant stress tests of $[0_2/90_2/+45_2/-45_2]_s$ E-glass/913-epoxy in 0.01 molar HCl acid bath.

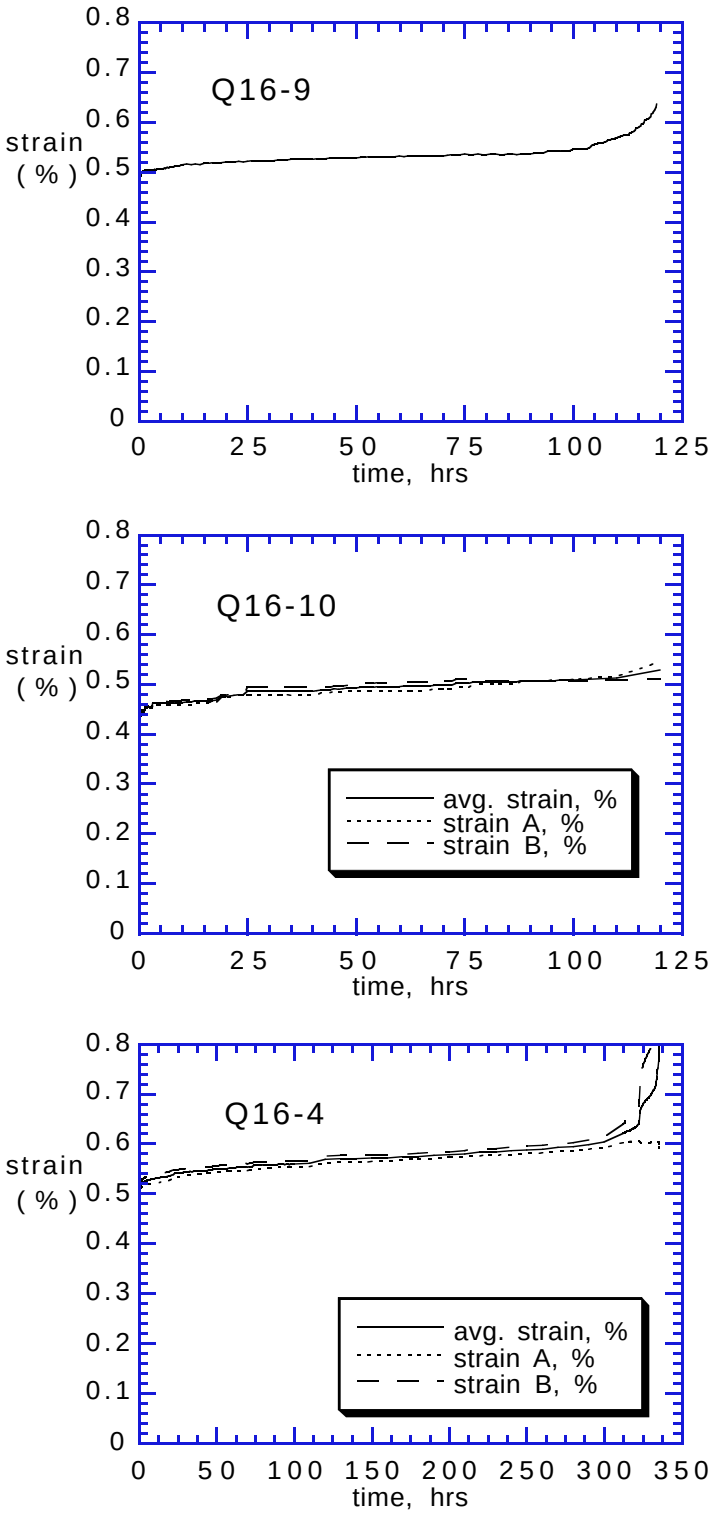

Figure 17. Creep results for 108 MPa constant stress tests of $[0_2/90_2/+45_2/-45_2]_s$ E-glass/913-epoxy in 0.01 molar HCl acid bath.

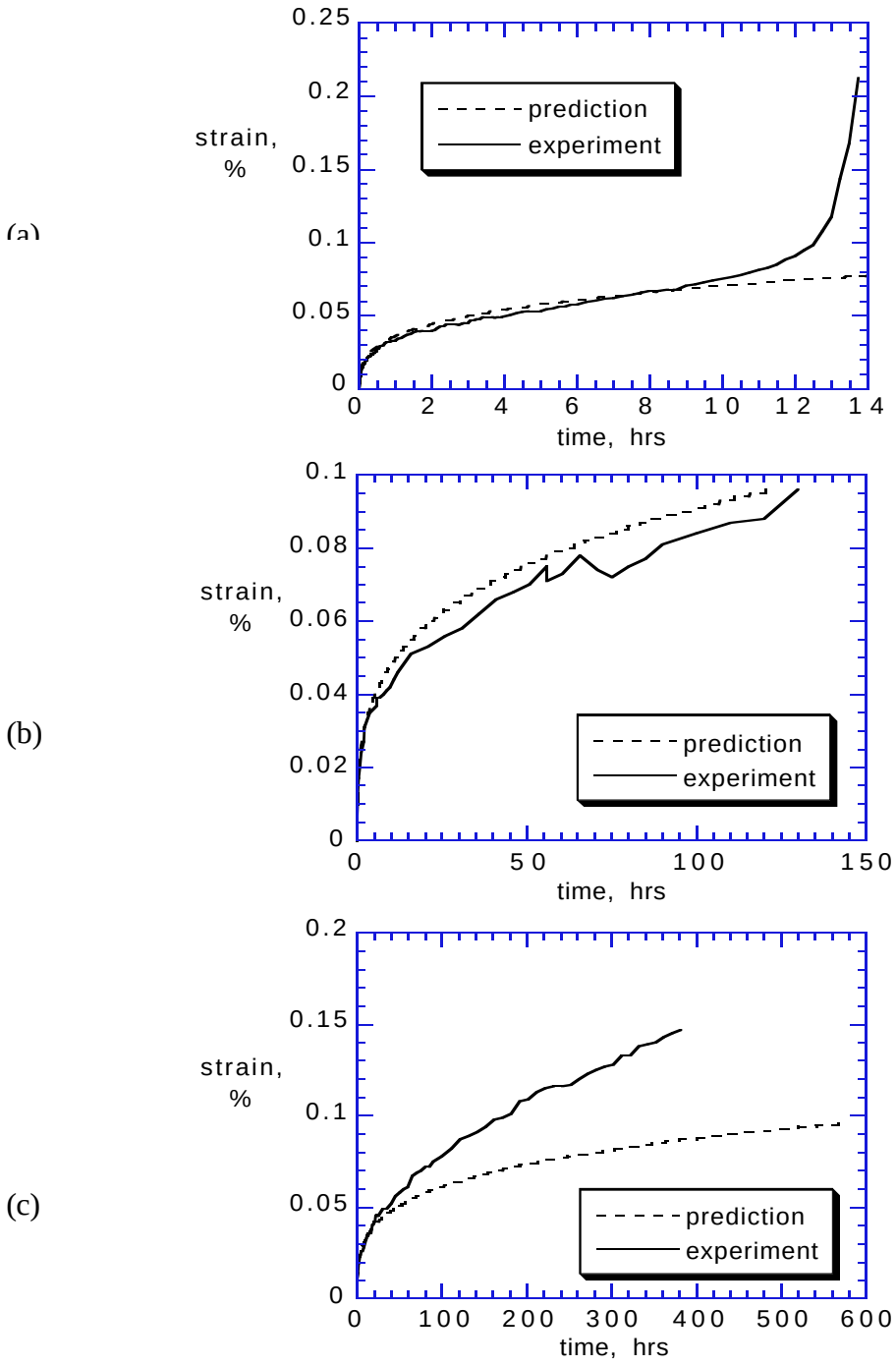

Figure 18. Predicted and experimental creep vs. time response of quasi-isotropic layup. In (a) and (b) agreement is good, until stress-corrosion cracks radically increase strain. In (c) the error is substantial, and is likely because at long times the effects of moisture uptake on compliance and expansion become significant.

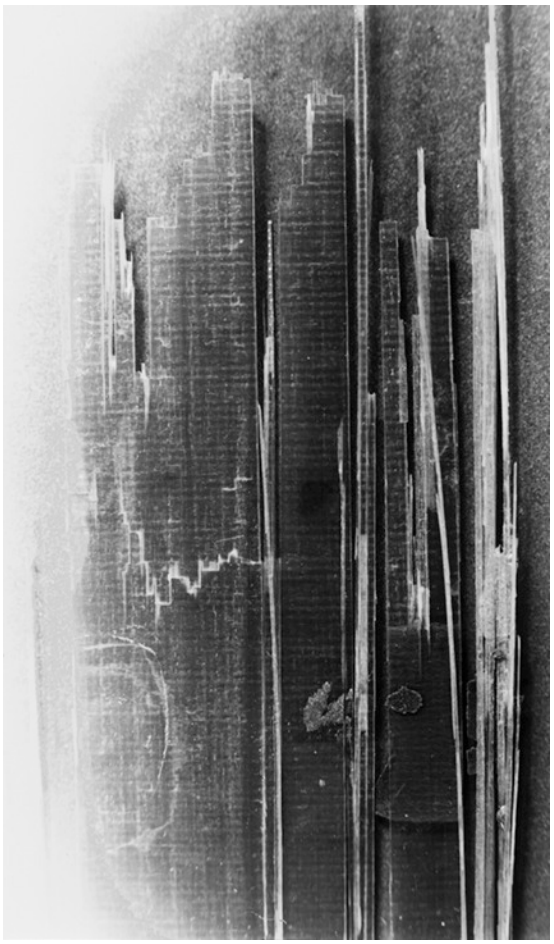

Figure 19. Representative fracture profile of stress-ruptured $[0]_2$ E-Glass/913-epoxy having a higher stress (225 MPa), and shorter life (18.7 hours). The irregular profile is due to a large number of small cracks forming accompanied by splitting which arrests their growth.

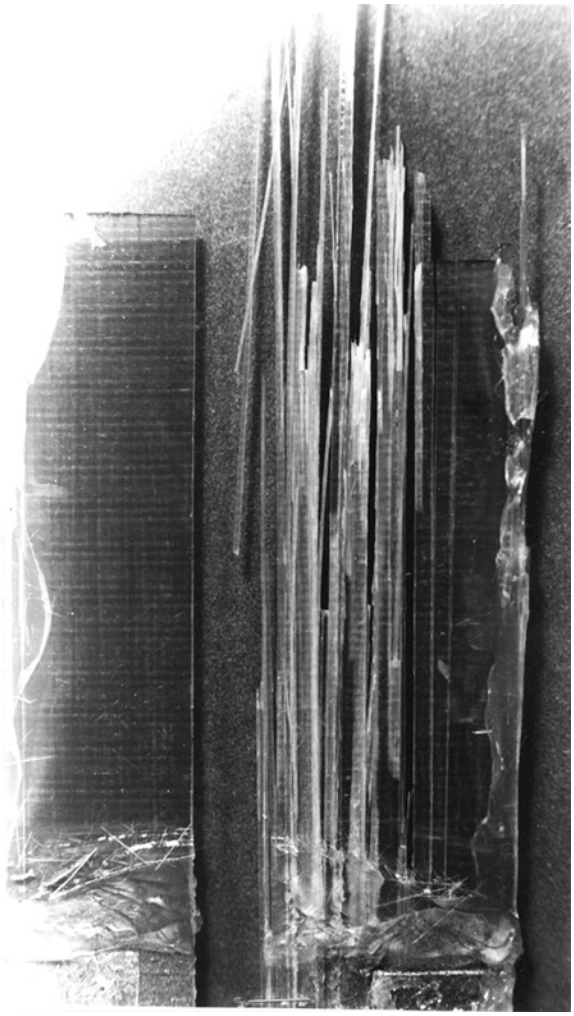

Figure 20. Representative fracture profile of stress-ruptured $[0]_2$ E-Glass/913-epoxy having a lower stress (185 MPa), and longer life (41 hours). The mixed profile is due to two long cracks growing without forming splits, then the highly stressed remaining cross-section fails much like the that of Figure 19. (shows U2-9).

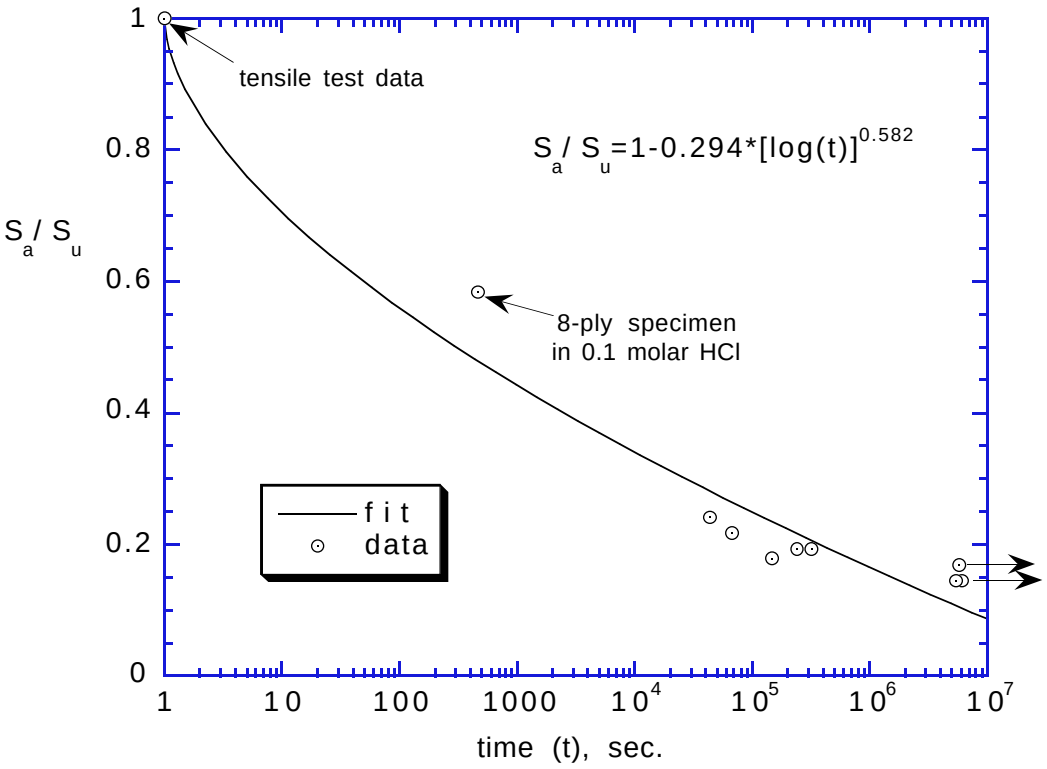

life function: $F_a = \frac{S_a}{S_u} = A + B[log(t)]^p$

fit parameters: A=1 B=-0.294 p=0.583

Figure 21. Life versus time response of E-glass/913 in 0.01 molar HCl. Fit (solid line) to stress-rupture life data (circles).

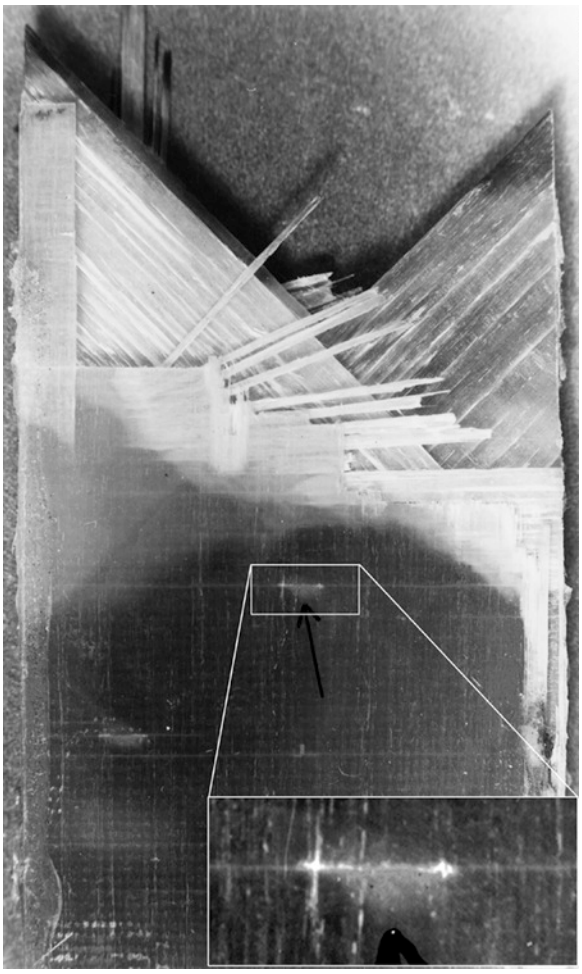

Figure 22. Representative fracture profile of stress-ruptured $[0_2/90_2/+45_2/-45_2]_s$ E-Glass/913-epoxy having a higher stress (154 MPa), and shorter life (13.0 hours). The stress-corrosion cracks grow across much of the laminate, with no attack to the underlying layers, in particular the 45's are intact. There are two prominent stress-corrosion cracks visible below the fracture zone (one is magnified). Width-spanning 90° cracks then appeared, accompanied by an oval delamination at the 0/90 interface around the zone having the 0° crack. There were 90° cracks only where 0° stress-corrosion cracks preexist.

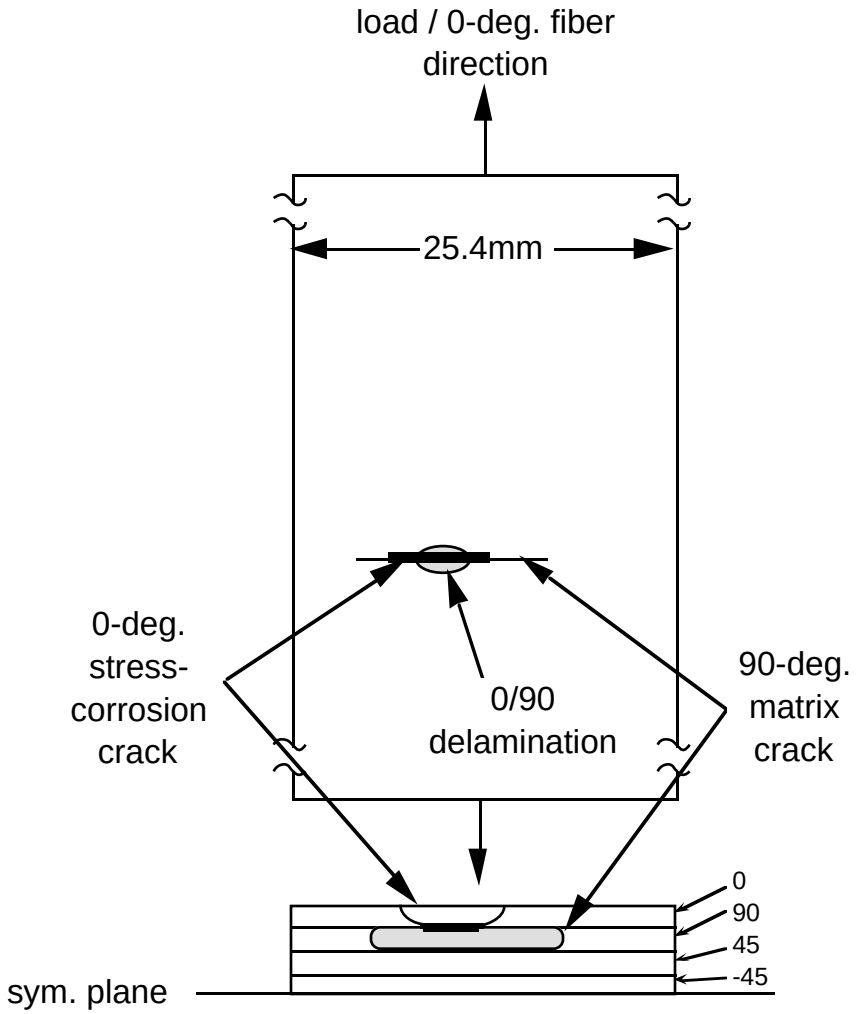

Figure 23. Schematic of the formation of a stress-corrosion crack (thick line) in the surface 0°-ply, and the subsequent appearance of a 0/90 delamination (shaded oval in upper Figure) and a 90°-crack (thin line). This sequence was typical because the loading was below that to initiate 90° matrix cracks.

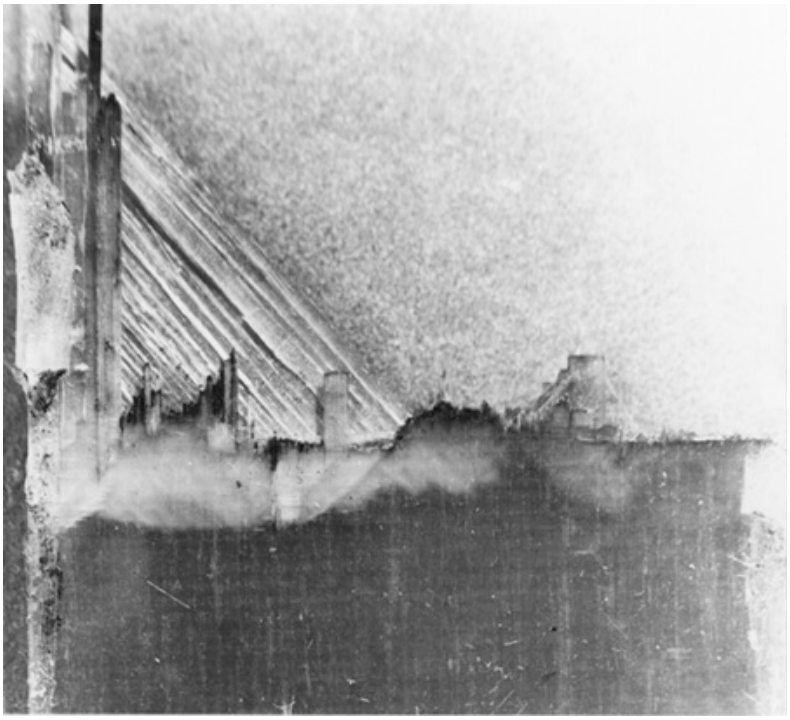

Figure 24. Representative fracture profile of stress-ruptured $[0/90/+45/-45]_s$ E-Glass/913-epoxy having a lower stress (112 MPa), and longer life (130.3 hours). The stress-corrosion cracks grow across much of the laminate, and clean through about 40% of the width. Only a portion of the midplane -45° plies have not fractured. The light area just below the fracture line is a delamination.

Figure 25. Representative fracture profile of stress-ruptured $[0_2/90_2/+45_2/-45_2]_s$ E-Glass/913-epoxy having a lower stress (108 MPa), and shorter life (119 hours). The stress-corrosion cracks grow across about 20% of the laminate, while the 0° plies cracked across much of the width before final separation.

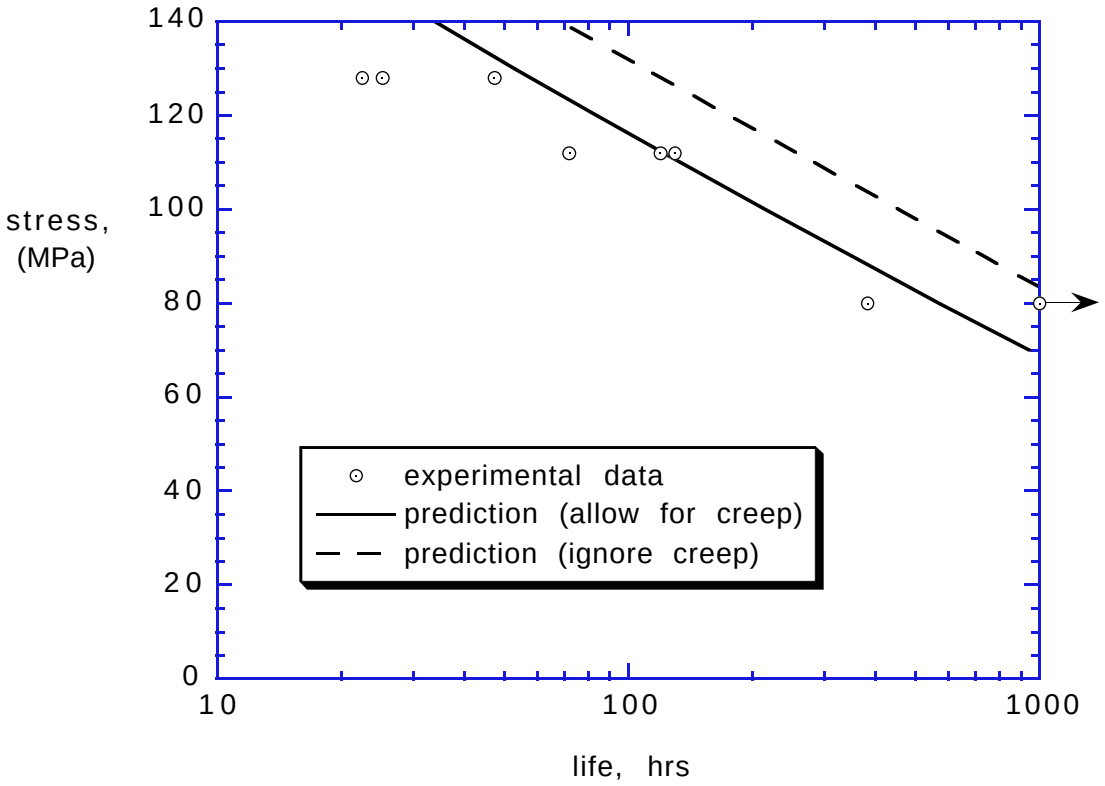

Figure 26. Prediction of the stress-rupture life of a $[0/90/+45/-45]_S$ quasi-isotropic laminate of E-glass/913-epoxy under tension and immersed in an 0.01 molar hydrochloric acid bath. If stress-relaxation (creep) is ignored, life is overpredicted.

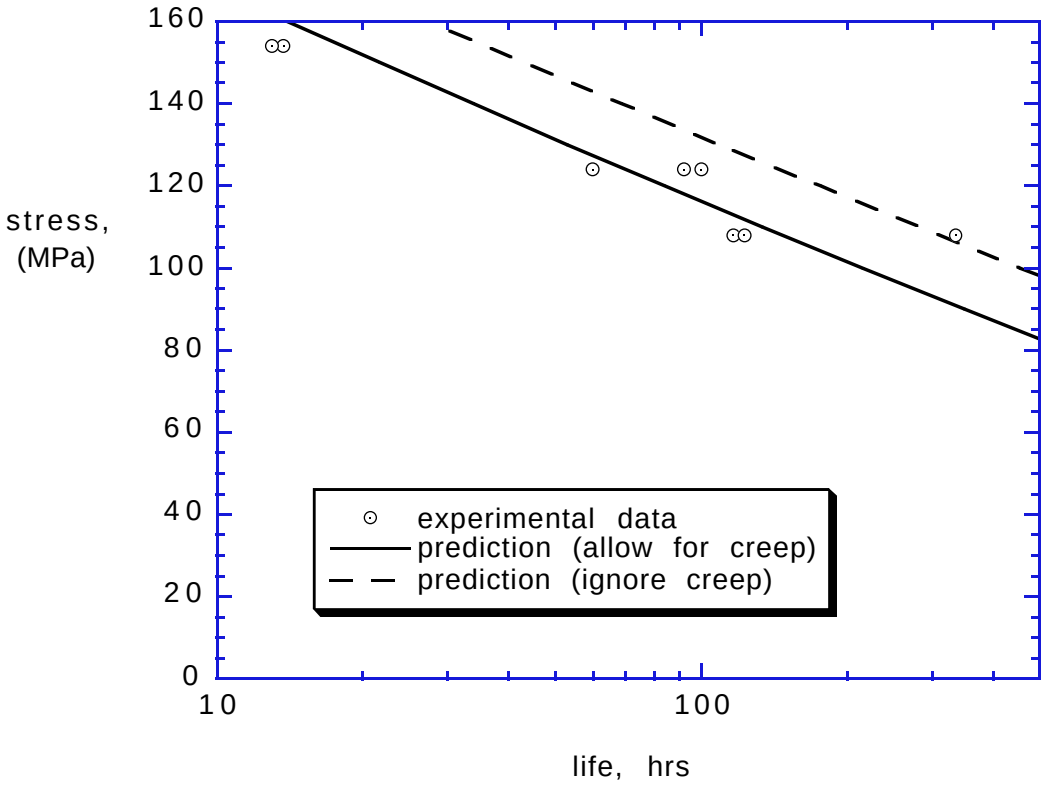

Figure 27. Prediction of the stress-rupture life of a $[0_2/90_2/+45_2/-45_2]_S$ quasi-isotropic laminate of E-glass/913-epoxy under tension and immersed in an 0.01 molar hydrochloric acid bath. If stress-relaxation (creep) is ignored, life is overpredicted.

Appendix. Stress-Rupture Life FORTRAN Code.

```
PROGRAM  LIFE

C     COMPOSITE STRESS-RUPTURE LIFE ANALYSIS

C     J. Andre Lavoie
C     Department of Engineering Science & Mechanics
C     Virginia Polytechnic Institute & State University



      character*40 name(10)
      integer tmax,plies,nomatl,angles,noang,stack
       REAL JVAR, P, tlapse
      double precision matpro,DT,N(3),M(3), PRNSTR(3,151),
     $QBAR,SBAR,ZCOORD,CTE,T,TINV,
     $FR, FA1, FA2, SA1, SA2, SU, TAU1, TAU2, DTAU,
     $A, B, DN, BIGN1, BIGN2, INTGRL, crpstr

       COMMON QBAR(3,3,150),MATPRO(10,12),STACK(150,2),PLIES,SBAR(3,3),
     $   ANGLES(50),ZCOORD(151),CTE(3,150),T(3,3,150),TINV(3,3,150)



C  MATPRO(i,j) contains the material properties used by CLT:
C  (i is the material number, and is usefull for specifying
C   individual laminae for degrading)

C MATPRO(i,1) = E1
C MATPRO(i,2) = E2
C MATPRO(i,3) = G12
C MATPRO(i,4) = Nu12
C MATPRO(i,5) = ply thickness
C MATPRO(i,6) = cte1
C MATPRO(i,7) = cte2
C MATPRO(i,8) = Xt
C MATPRO(i,9) = Xc
C MATPRO(i,10) = Yt
C MATPRO(i,11) = Yc
C MATPRO(i,12) = S



C-----------------------------------------------------------------
C  all results are printed to this file:

      OPEN(unit=6,file='LIFE.out',status='unknown')

C-----------------------------------------------------------------
```

```
C  Initial, undamaged material properties, # of plies, # of materials,
C  and stacking sequence are read from a data file on disk.

      call DATA(plies,nomatl,angles,noang,matpro,name,stack,N,M,DT)

      WRITE(*,*) 'ENTER THE TENSILE FORCE RESULTANT (in N/m):'
      READ(*,*) N(1)
      WRITE(*,*) 'ENTER STEP SIZE (in seconds):'
      READ(*,*) DN

C-----------------------------------------------------------------------
C The initial transverse and shear moduli, E2 and G12, are assumed the
C same for each ply in the stack.

C     E2= MATPRO(1,2)
C     G12= MATPRO(1,3)

      SU= MATPRO(1,8)

C  These constants define the S-N curve of the fibers:

      A= 1.0D0
      B= -0.29425D0
      P= 0.582
      Jvar= 7
      INTGRL= 0.D0


      CALL CLT(nomatl,noang,N,M,DT,PRNSTR,crpstr)
      SA1= PRNSTR(1,1)
C     WRITE(*,*) PRNSTR(1,3), PRNSTR(2,3), PRNSTR(3,3)
      BIGN1= 10**(((SA1/SU-A)/B)**(1./P))
      TAU1= 0.D0
      FA1= SA1/SU

      write(*,100) Sa1,Su,Fa1
  100 format(1x,'initially:'/1x,'Sa=',e10.3/1x,'Su=',e10.3/1x,'Fa=',
     $e10.3///' hit enter to continue')
      read(*,*)

      WRITE(*,150)
  150 FORMAT(' Time (sec)',T25,'Fa',T45,'Fr',T60,'epsX')

      DO 1000 tmax=0,10000000

       tlapse= 1. + tmax*DN

       CALL CREEP(tlapse,MATPRO,PRNSTR,nomatl,noang,N,M,DT,crpstr)

       CALL CLT(nomatl,noang,N,M,DT,PRNSTR,crpstr)
```

```
C     READ(*,*)
      SA2= PRNSTR(1,1)

      BIGN2= 10**(((SA2/SU-A)/B)**(1./P))

      TAU2= (tlapse+DN)/( BIGN2 )

      DTAU= (TAU2-TAU1)/DN

      FA2= SA2/SU

     INTGRL= INTGRL + ( (1-FA1)*Jvar*(TAU1)**(Jvar-1.)*DTAU +
    $      (1-FA2)*Jvar*(TAU2)**(Jvar-1.)*DTAU )/2.D0 * DN

     FR= 1.D0 - INTGRL
     WRITE(*,200) tlapse, FA2, FR, crpstr
     WRITE(6,210) tlapse, FA2, FR, crpstr
 200 FORMAT(T1,E10.3,T20,F7.4,t40,F7.4,t55,e10.3)
 210 FORMAT(1X,E10.3,1X,F7.4,1X,F7.4,E10.3)
     IF(FR .LE. FA2) stop

     SA1= SA2
     BIGN1= BIGN2
     TAU1= TAU2
     FA1= FA2

1000 CONTINUE

     STOP
     END


C  ************** subroutine CREEP  ******************************

      SUBROUTINE CREEP(tlapse,MATPRO,PRNSTR,nomatl,noang,N,M,DT,crpstr)

     INTEGER nomatl,noang
     DOUBLE PRECISION N(3), M(3), DT, MATPRO(10,12), PRNSTR(3,151),
    $              crpstr
     REAL S11o, A1, b1,
    $     S22o, A2, b2,
    $     S66o, g, p, f, q,
    $     tlapse, E1, E2, G12, tau12,tau122



C  These constants define the creep in the 0-degree direction:

     S11o= 2.07e-11
       A1= 2.97e-13
       b1= 0.2
```

```
      E1=1./(S11o + A1*(tlapse)**b1)
       MATPRO(1,1)= E1
       MATPRO(2,1)= E1
       MATPRO(3,1)= E1

C  These constants define the creep in the 90-degree direction:

     S22o= 5.62e-11
       A2= 3.629e-13
       b2= 0.355

       E2= 1./(S22o + A2*(tlapse)**b2)
       MATPRO(2,2)= E2
       MATPRO(1,2)= E2
       MATPRO(3,2)= E2


C  These constants define the shear creep response:

     S66o= 1.1e-10
       g= 1.0e-16
       p= 2.77e-15
       f= 2.23e-14
       q= 0.37

C  It is necessary to cycle G12 and tau12 calculations until there
C  is convergence:

  100   tau12= PRNSTR(3,3)
      tau122= tau12*tau12
       G12= 1./( S66o*(1.+g*tau122) + p*(1+f*tau122)*tlapse**q )
       MATPRO(3,3)= G12
       CALL CLT(nomatl,noang,N,M,DT,PRNSTR,crpstr)

       IF(ABS(tau12-PRNSTR(3,3)) .LT. ABS(0.01*tau12)) RETURN

       GOTO 100


      RETURN
      END

C  ********** subroutine data ******************************

      SUBROUTINE DATA(plies,nomatl,angles,noang,matpro,name,stack,
     $                N,M,DT)

C  variable definitions
C    N(i), M(i)  [dbl]   the force and moment resultants
C    plies       [int]   The number of lamina in the laminate
```

```
C    nomatl      [int]   The number of different lamina materials.
C    matpro(,)   [dbl]   E1, E2, G12, Nu12, thickness, cte1, cte2,
C                        Xt,Xc,Yt,Yc,S
C    name()      [chr]   material names (40 characters max.)
C    stack(,)    [int]   Stacking sequence: matl. #, angle
C    angles()    [int]   the different ply angles expected
C    noang       [int]   the number of different angles to read
C
C  example data file (all unformatted):
C
C  4             this tells the number of angles.
C  0,90,45,-45   there are four angles: 0, 90, 45 and -45.
C  4, 2          four plies, and two materials used, integer
C  30.0e6,.75e6,.37e6,.3,.005,-1e-7,13e-6 E1,E2,G12,Nu12,thick,cte1,cte2
C  110e3,75e3,5e3,13e3,20e3              Xt,Xc,Yt,Yc,S;
C  ..... as many doublerows as matls. used.
C  'T300/5208 graphite/epoxy'
C  'P75/ERL-1962 graphite/epoxy'
C  1,   0        <--
C  2,  90         |---- the stacking sequence consists of
C  1,  45         |     the material #, followed by the ply angle.
C  1, -45 etc.   <--
C  -82.5         difference between the use and cure temp.
C  1E6,0,0,0,0,0  the force and moment resultants


      character*40 name(10)
      integer i,j,plies,nomatl,stack(150,2),angles(50),noang
      double precision matpro(10,12), N(3), M(3), DT
      open(unit=3,file='LIFE.DAT')

      read(3,*) noang
      read(3,*) (angles(i), i=1,noang)
      read(3,*) plies,nomatl
      read(3,*) ((matpro(i,j), j=1,12), i=1,nomatl)
      read(3,*) (name(i), i=1,nomatl)
      read(3,*) ((stack(i,j), j=1,2), i=1,plies)
      read(3,*) DT
      read(3,*) N(1),N(2),N(3),M(1),M(2),M(3)
  700 continue

      return
      end
```

Vita

J. André Lavoie was born in Salem, Massachusetts on July 21, 1962. He did not stay there, but promptly moved to Alaska, courtesy, U.S. Army. After a lengthy 32 months, split between Anchorage and Fairbanks, he moved back to Salem to wait the 12 months for his Dad to return from Viet Nam so he could learn to tie his shoes. Out of necessity, he learned to tie them himself. He credits this early experience in experimental mechanics with setting the stage for an adult career in engineering.

He gained his B.S. degree in Engineering Science and Mechanics from Virginia Polytechnic Institute in 1986, which included one year of Cooperative Education work experience at the Naval Research Lab in Washington D.C. While there, he was involved with fatigue and creep testing of gas turbine engine materials. His Senior project was on computed aided alignment of hydraulic tensile test machines. He eventually found a job with Lockheed Engineering and Sciences Company at NASA Langley Research Center where he worked as a composite materials test engineer for nearly four years. The highlight was involvement in a project to build an IR interferometer test facility for measuring thermal distortion of composite mirrors in a simulated space environment. After much delay, he published the results of his Senior Project in Experimental Techniques and won a 1990 Best Technical Paper Award from the Society for Experimental Mechanics.

By Spring of 1991, he was preparing himself for graduate school. To do so properly, he would need to become as destitute as the other students who were continuing on directly from undergrad. A six month trip around the globe was planned to the hot places of the world. Included on the itinerary were the beautiful islands of Hawaii, New Zealand, Bali, and Koh Pee Pee, Thailand. Time was well spent in big countries like Australia (home of termite mounds, crocodile pies, and Kangaroo curry). India had much better food, whether it was in the states of West Bengal, Uttar Pradesh, or Rajahstan. From Bombay, it was off to Kenya for four wheel driving in Turkana, and to do big game spotting in the Masai Mara. By the time he had returned home to Virginia, he had increased his tally of countries visited to over twenty-five.

A Master of Engineering degree was taken at V.P.I. His project was on the design of a new test method for crush energy absorption of composite plates. He (and his two co-authors) won a Prize for Most Outstanding Paper published in 1995, in the Proceedings of the Institution of Mechanical Engineers, in the area of materials and solid mechanics. He continued study for the Ph.D., which brought with it special opportunities to perform part of his research at the Defence Research Agency in England, visit other research centers in Sweden and Italy, and present some of his work at conferences in Italy, and Portugal. André has no idea where life will take him next, but it will not be alone. He met his then future wife, Chiara from Italy, at Virginia Tech International Club's regularly held Friday coffee hour in the Cranwell International Student Center.

J. André Lavoie